# APPLICATION OF ATOMIC FORCE MICROSCOPY FOR THE STUDY OF CRYSTALLIZATION KINETICS AND MORPHOLOGY OF L- AND D-POLYLACTIDE BLENDS IN SOLUTION CAST THIN FILMS

Yury Yuryev

A Thesis

in

The Department

of

Mechanical and Industrial Engineering

Presented in Partial Fulfilment of the Requirements

for the Degree of Master of Applied Science (Mechanical Engineering) at

Concordia University

Montreal, Quebec, Canada

June 2006

*Your file Votre référence*
*ISBN: 978-0-494-20769-7*
*Our file Notre référence*
*ISBN: 978-0-494-20769-7*

**Abstract**

**Application of Atomic Force Microscopy for the study of crystallization kinetics and morphology of L- and D-polylactide blends in solution cast thin films.**

**Yury Yuryev**

The purpose of this research was to explore the possibility of studying crystallization behavior and morphology of thin solution cast polylactide films using Atomic Force Microscopy. The crystallization of L-/D-polylactide blends was studied and precise measurements of the spherulite growth rates were performed. The changes of crystalline morphology over crystallization temperature was observed and analyzed from the point of view of modern crystallization theory. Also a variety of different experimental techniques was used for the polylactide blends characterization including DSC and FT-IR. Since the crystallization rate of polylactide is very high, a custom superfast cyclic heating and cooling technique was developed to ensure isothermal annealing conditions. The validity of this technique was successfully verified.

DSC analysis showed that L-/D-polylactide blends form a triclinic stereocomplex during casting with a high melting point which suppresses cold crystallization. In this study, a custom technique for the measurement of the isothermal glass transition temperature using elongational measurements was performed on a miniature uniaxial stretching device. It was found that small amounts of residual solvent can significantly decrease the glass transition temperature of polylactide. Significantly

higher nucleation in the solution cast polylactide as compared to bulk polymer was also observed.

Crystallization behavior and morphology of solution cast polylactides containing different amounts of D-polylactide content were studied. It was experimentally proven that while blends of L-/D- polylactide copolymer with D-polylactide demonstrate typical "bell" shaped crystallization temperature dependence, blends of pure L-polylactide with the same D-polylactide have unusually high spherulite growth rates at high temperatures. For all blends, addition of D-polylactide significantly decreased the spherulite growth rate. An extensive kinetic analysis was performed on the experimental data, crystallization regimes were identified and critical nuclei formation energies were determined for the different blends.

Moreover, despite having a higher molecular weight, the pure poly(L-lactide) demonstrates almost twice higher spherulite growth rate than copolymer probably caused by the absence of D-polylactide units in chain thus absence of the steric difficulties for the crystallization. This, in turn, leads to the significantly lower *Kg* values for the Purasorb PL and its blends with Purasorb PD as compared to those of the copolymer in regimes II and III and, respectively, to higher spherulite growth rates. The addition of the D-polylactide not only suppresses the overall crystallization of the blend due to stereocomplexation but also shifts the crystallization maximum to the lower temperature region. From the kinetics analysis, it was found that this is caused by the lowering of the regime II transition temperature.

**Dedications.**

**To my Mom Galina and Dad Vitaly.**

**Acknowledgments.**

I would like to express my most sincere gratitude to Dr. Paula Wood-Adams, my advisor, for her guidance, inspiration and irrefutable help with both science and administrative issues. She was also tireless with the numerous revisions of this document.

I would like to thank Dr. Marie-Claude Heuzey (Ecole Polytechnique), Dr. Charles Dubois (Ecole Polytechnique) and Dr. Josee Brison (Laval University) for their valuable help during this research .

Finally, I want to thank each and every of colleagues and friends Arkadz Fatseyeu, Wang Heng, Ramin Motameddi and Cheng Huang for help, sharing their expertise and just for being nice people to work with.

**Table of contents**

**List of Figures**

## List of Tables

## List of Nomenclature

$A$ – surface area, $m^2$.

$a$ – crystalline cell parameter, m.

$a_0$ – the molecular width, m.

$b$ – crystalline cell parameter, m.

$b_0$ – the thickness of the layer of polymer, m.

$C$ – an adjustable parameter equal to 30°C.

$c$ – crystalline cell parameter, m.

$D$ – thermal diffusivity, $m^2/s$.

$E$ – activation energy, J/mol.

$G_e$ – Gibbs free energy of system, J/mol.

$G$ – spherulite growth rate, m/s.

$G_0$ – lamellae growth constant, m/s.

$\Delta G^*$ – the activation energy barrier for the nuclei growth, J/mol.

$g$ – substrate compaction rate, $m^{-3}$.

$G_I$ – growth rates in regime I, m/s.

$G_{II}$ – growth rates in regime II, m/s.

$G_{III}$ – growth rates in regime III, m/s.

$H$ – enthalpy of system, J/mol.

$\Delta H$ – the heat of fusion, $J/ m^{-3}$.

$i$ – the primary nucleation rate, $s^{-1} \cdot m^{-3}$.

$K_{g(I)}$ – the nucleation constant in regime I, $K^{-2}$.

$K_{g(II)}$ – the nucleation constant in regime II, $K^{-2}$.

$K_{g(III)}$ – the nucleation constant in regime III, $K^{-2}$.

$k_b$ – the Boltzman constant equal to $1.380\ 6505 \cdot 10^{-23}$ J/K.

$k'$ – temperature dependent dimensionless parameter in Perez-Cardenas equation.

$k(T)$ – crystallization rate constant.

$L$ – sample size, m.

$m$ – order of the crystallization in Avrami equation.

$m'$ – temperature dependent dimensionless parameter in Perez-Cardenas equation.

$N$ – rate of nucleation, $s^{-1} \cdot m^{-3}$.

$n$ – spherulite growth regime constant.

$n_0$ – characteristic constant of the polymer and nucleating agent system.

$n_s$ – the mean number of stems placed in adjacent niche to the newly nucleated stem.

$Q_D^*$ – the activation energy for steady-state reptation, , J/ $m^{-3}$.

$q$ – cooling rate, K/s.

$R$ – universal gas constant equal to $8.314472\ J \cdot K^{-1} \cdot mol^{-1}$.

$r$ – radius of nuclei, m.

$S$ – entropy of system, J/mol·K.

$S_R$ – reference angle coordinate, m.

$T_f$ – fictive temperature, K

$T_g$ – glass transition temperature, °C.

$T_m$ – melting temperature, °C.

$T^0_m$ – equilibrium melt temperature, °C.

$T_c$ – isothermal crystallization temperature, °C.

$t$ – time, seconds.

$U^*$ – activation energy barrier for the transportation of polymer molecules from the melt to the crystal surface, J/mol.

$V_0$ – total volume of polymer, $m^3$.

$X$ – degree of crystallinity.

$X_R$ – reference X axis coordinate, m.

$X_{pc}(t)$ – mass fractions of polymer crystallized by primary crystallization.

$X_{sc}(t)$ – mass fractions of polymer crystallized by secondary crystallization.

$Y_R$ – reference Y axis coordinate, m.

$\beta$ – stretch parameter.

$\gamma$ – specific surface energy, $J/m^2$.

$\Theta$ – scan angle correction, degree.

$\theta$ – contact angle, degree.

$\Xi$ – the overall weight fraction of polymer that has crystallized at the moment of termination of primary crystallization.

$\rho_c$ – crystalline density of polymer, $kg/m^3$.

$\rho_l$ – liquid density of polymer, $kg/m^3$.

$\tau$ – crystallization time, seconds.

$\tau_{1/2}$ – the half time of crystallization, sec.

$\tau_n$ – characteristic constant of the polymer and nucleating agent system.

$\sigma$ – the crystal growth face surface energy, $J/m^{-2}$.

$\sigma_e$ – the crystal fold surface energy, $J/m^{-2}$.

# 1. Introduction

## 1.1. Polylactide (PLA), a new environmentally friendly polymer

At the present time, polymeric materials used for packaging are becoming one of the most important sources for environmental concern. Only in the USA, municipal solid waste (MSW) consisting of polymeric materials has increased from 390000 tons in 1960 to 24.7 million tons in 2000. These huge amounts of waste totaled less than 1 percent of the overall waste in 1960 and increased their share to 10.7 percent in 2000. Of that, almost 50 percent were containers and packaging materials. Only 5.4 percent of the MSW produced by plastic manufacturing was recovered in 2000. This is a very slight 0.2% improvement as compared to 1995[1].

It is apparent that the recycling rate for used packaging remains at the same level and the environmental impact on nature is increasing. Also it is important that the main source for plastics is natural oil that has limited reserves. As it is estimated by the U .S. Geological Survey National Center, the world's known reserves of oil are about 1.103 trillion barrels and potentially can reach 1.802 trillion barrels. At current levels of consumption this resource will be depleted in 45 to 73 years[2]. That is why substitution of conventional plastics by new biodegradable materials from renewable sources becomes a more and more important concern not only from point of view of its environmental effects but also because of the limited nature of natural reserves of oil.

One of the most promising new materials for packaging applications is polylactide (PLA), which is synthesized from lactic acid[3]. Lactic acid is produced by the

fermentation of corn and other plant material and is therefore a renewable resource. Studies of degradability of PLA showed that PLA degradation does not produce any toxic by-products and totally decays in a period of 20 days[4] to 3 years[5] depending on conditions. At the same time, PLA combines good processability and packaging properties. Polymerization technology for this new polymer is well developed already and several companies including international companies like Cargill Polymers LLC, PURAC, Biomer and many others have started semi-industrial commercial production of PLA. Industry representatives indicate that current production of PLA in the United States is about US$ 300,000,000 per year and continues to grow[6].

Since PLA is a relatively new material, it provides an extensive field for research. Especially interesting directions of research include crystallinity development, mechanical properties and surface structure of PLA films under different conditions, their aging and degradation. For packaging purposes studies of barrier properties and methods of their improvement are also very important. Perfection of properties of PLA films will accelerate large-scale production of new packaging materials and allow the substitution of conventional plastics from nonrenewable resources by nature friendly materials.

In this work we studied the crystallization behavior of polylactic acids of different composition and their blends, development of the crystalline structure and morphology in the solution cast thin films of polylactides over the time using different research techniques. Most attention in this work had been focused on the implementation of Atomic Force Microscopy (AFM) for quantitative analysis of the crystalline structure. The study also included Differential Scanning Calorimetry (DSC) and Fourier Transform Infrared (FTIR) analysis of PLA. Implementation of elongational measurements of the

polylactide films to reveal influence of the residual solvent on glass transition temperature ($T_g$) was also attempted.

### 1.2. Molecular structure of the polymers

Polymer molecules consist of repeating combinations of the functional groups bonded in linear or branched chains. These groups are called *repeat units.* Many properties of the polymers demonstrate continuation of the behavior of repeat units at the limit of high molecular weights. This is true for mechanical properties, melting point and some other properties of the polymers.

Some organic compounds being chemically identical differ in spatial arrangement of the atoms and represent mirror images of each other. Since this difference is most obviously observed in the direction of polarized light rotation these substances are called optical isomers or *enantiomers*. Optical isomerism is intrinsic to the subject of our studies – polylactide and its monomer lactic acid which has two optical isomers (Fig.1.1, 1.2). Since two molecules that are chemically identical but optically different can not be superimposed this leads to significant difference in many properties. For the optically active polymers *meso* and *racemic* group placements are distinguished. These terms are related to the optical orientation of the adjoining repeat units. Meso placement corresponds to the same position of the two neighboring optically active centers while racemic placement assumes that they are opposite.

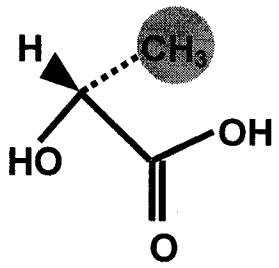


Fig.1.1 L (-) Lactic Acid

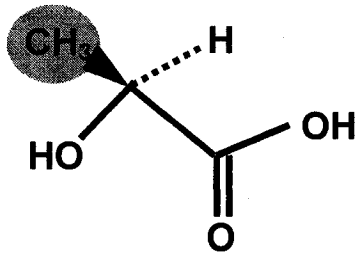


Fig.1.2. D (+) Lactic Acid

A similar phenomenon among repeat units of a polymer chain when groups of the same polymer have different spatial arrangements is called *tacticity.* Depending on group arrangement, polymers can be isotactic, syndiotactic or atactic (Fig. 1.3).

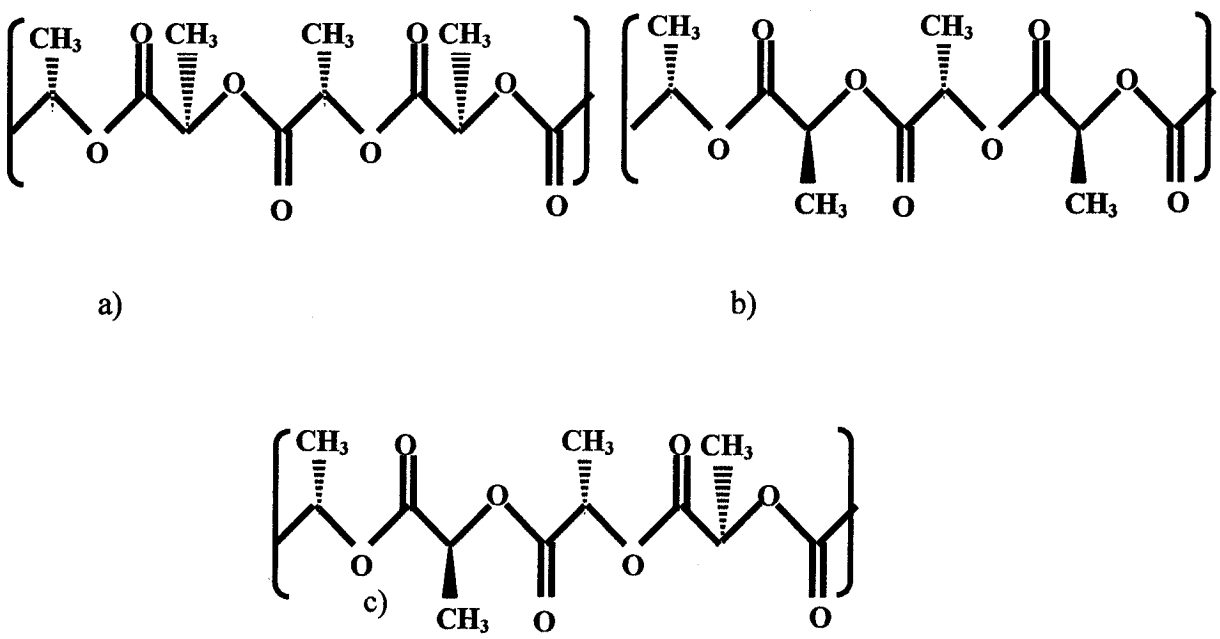


Fig.1.3. Isotactic (a), syndiotactic (b) and atactic (c) group arrangement schematics for polylactide linkage.

Tacticity results in significantly different physical and mechanical properties. Isotactic and syndiotactic polymers can crystallize due to the regularity of the chain while atactic polymers are usually amorphous and can crystallize to some degree only if their side groups very small or very polar[7]. The unit cells and melting temperatures of isotactic and syndiotactic crystallized polymers are not the same. Knowledge of polymer molecular structure provides great opportunities for engineering polymers with desired properties.

### 1.3. Crystalline structures of polymers

Crystallization is a process of phase transformation of polymer from the disordered amorphous state to an ordered crystalline phase. Polymer crystal structures have some similarities to those of inorganic substances such as crystallographic symmetry groups. Unlike metals, the crystalline density of polymers depends on many factors including the temperature of crystallization and crystalline density changes along crystalline structure. Another significant difference from inorganic substances is the long chain nature of polymer molecules. This fact strongly affects the crystallization process and polymers never reach a fully crystalline state due to spatial limitations and entanglements. Variation in polymer chain regularities makes it possible for polymers having optically active isomers to crystallize in the form of a *stereocomplex* like for the case of polylactide. Stereocomplexation is a specific form of crystallization, which involves polymer chains consisting mostly of different enantiomers. The

stereocomplexation leads to quite different crystalline symmetry and more dense chain packaging. This results in crystalline structures having significantly different physical properties[8].

Typical crystallinity of semicrystalline polymers is in range of 30 – 70 % and in some cases can reach 90-93 %. Crystalline phase can be up to 12% denser than the amorphous phase[9]. Several methods are used for determining crystallinity in polymers. The most common techniques are calometric methods, e. g. Differential Scanning Calorimetry (DSC), densimetry methods and X-Ray Difractometry (XRD).

There are several models that explain crystallinity phenomena in long-chained polymers. One of them is *the fringed micelles model*[7] (Fig. 1.4.) According to this model each long polymer chain wanders from one crystallite to another and binds them together. This model explains leathery behavior of olefin polymers and polymer behavior in fibers. This model predicts especially well the difference in properties of low molecular weight waxes and high molecular weight polyethylene.

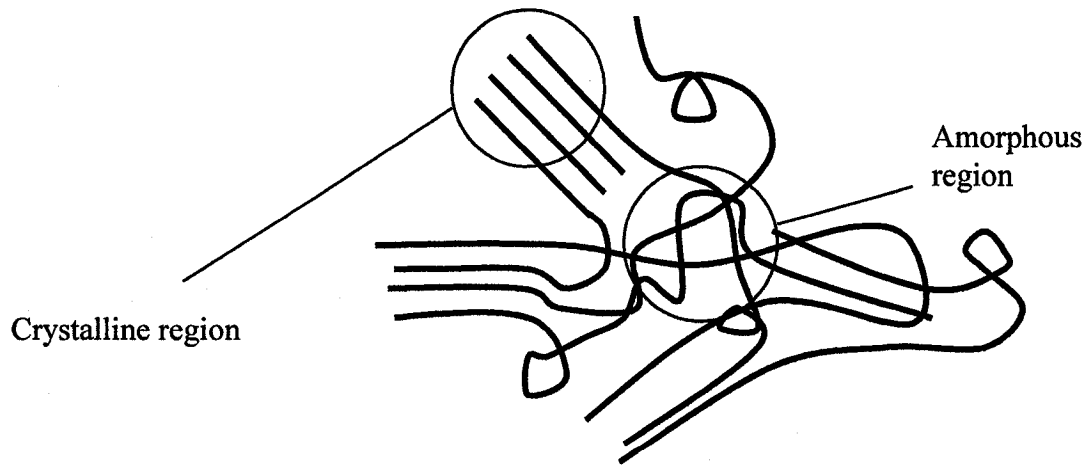


Fig.1.4. The fringed micelle model.

After 1957 when the first single polyethylene crystals were prepared by Keller[7] it became clear that the fringed micelle model can not explain polymer crystallization phenomena properly and *the folded chain model* was developed (Fig.1.5). This model considers polymer crystals as consisting of polymer chains folded many times with adjacent reentry. It was also found that not only homopolymers but also block copolymers could form single crystals. In this case the lamellae consist of similar polymer chain segments while rest of the chain is placed outside of the lamellae and forming amorphous material.

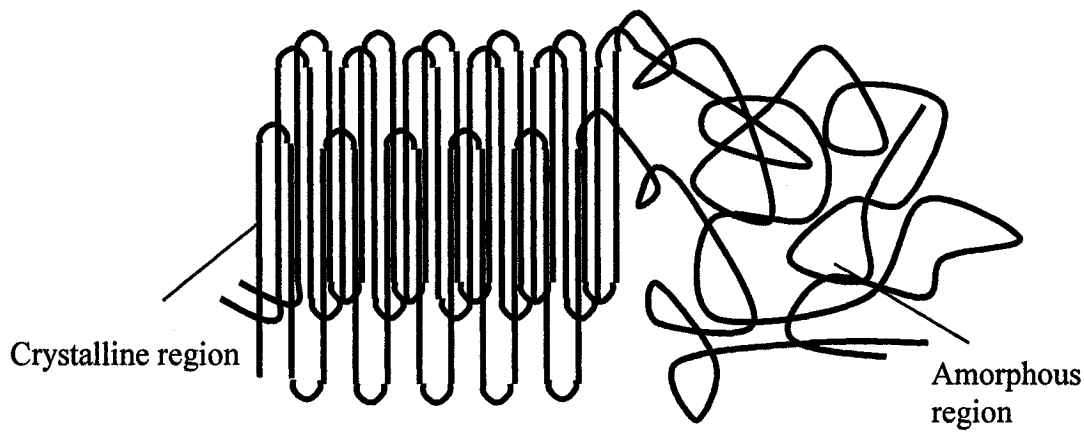


Fig.1.5. The folded chain model

The folded chain model satisfactory explains morphology of polymer single crystals and the formation of some peculiar crystalline structures, e. g. chair-like pyramidal crystals. Two types of the collapsed chair-like pyramidal single polyethylene crystal are shown in Fig. 1.6. The thickness of the crystal lamella is approximately 10 nm.

The most up to date *switchboard model* differs from the folded chain model only in its different approach to polymer chain reentry. The switchboard model assumes more

or less random reentry of the folded polymer chain, while the folded chain model assumes that reentry is ordered[7]. It is assumed that real crystalline structures in polymer are formed according to both the folded chain and the switchboard models.

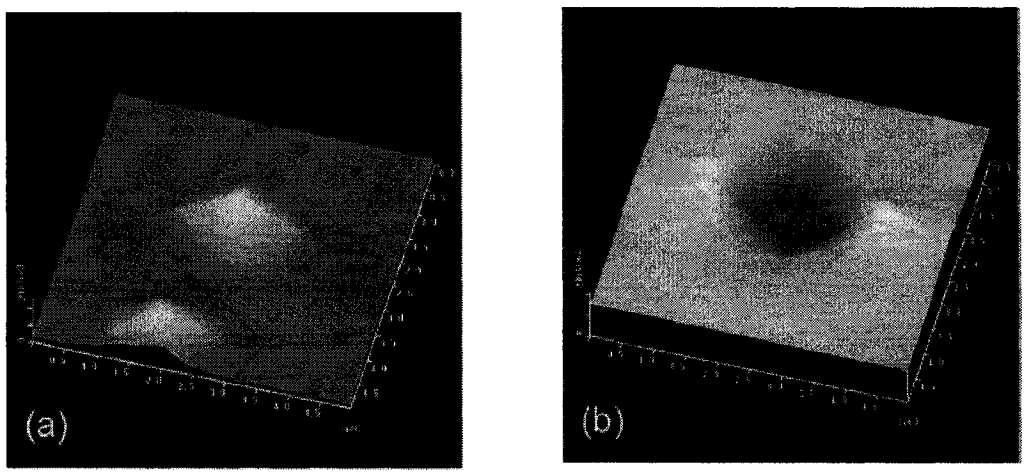


Fig.1.6. Atomic Force Microscopy topographic images of polyethylene single crystals grown from dilute xylene solution: convex hollow pyramidal type (a) and concave hollow pyramidal type (b)[10].

### 1.4. Basic properties of polylactide

Polylactide (PLA) is biodegradable aliphatic polyester of lactic acid. Fermentation of dextrose yields two optically active enantiomers, D (-) and L (+) lactic acids[9] (Fig.1.1 and 1.2). Like the majority of polymers, the properties of PLA such as melting point, crystallinity and mechanical strength are defined by the molecular weight and its

distribution and specifically for PLA by the polymer chains microstructure namely the arrangement of the L- and D- lactide repeat units.

The bulk properties of PLA depend strongly on compounding and processing conditions. The proportion of D- and L-lactides and the thermal history of the sample determine its morphology which can be almost amorphous or up to 70% crystalline[1]. Typically, polylactides containing more than 93 % of L-lactic acid are semi-crystalline and the ability of PLA to crystallize decreases with increasing D-lactide content. The glass transition temperature is also influenced by the D-/L- lactide ratio and the polymer molecular weight. The glass transition temperature of PLA ($T_g$) ranges from 50° C to 80 °C and the melting temperature ($T_m$) ranges from 130°C to 190 °C[11]. This results in PLA polymers having a wide range of hardness and stiffness. PLA can be processed using most industrial techniques like injection molding, sheet extrusion, blow molding, and thermoforming and film forming[8]. Polylactide has a relatively low density of about 1.25 g/cm[9]. They are also transparent in all range of visible light, at least as 120 microns thick films.

The mechanical properties of polylactides strongly depend on their crystallinity and their mechanical and thermal history. The tensile yield strength of a semi-crystalline PLA can vary between 65 and 84 MPa, Young's modulus between 2.11 GPa and 2.87 GPA and elongation at break between 5.5 and 96.9% depending on a wide set of parameters[1]. These values are typical for plastics used for packaging applications but inferior to the most durable packaging materials (Fig 1.7.)[12].

The carbon dioxide permeability for PLA films is in the range of $1.99 - 4.18 \cdot 10^{-17}$ $Kg \cdot m / m^2 \cdot s \cdot Pa$ and significantly increases with increasing temperature. The $CO_2$

permeability coefficients for PLA polymers are lower than the reported value for polystyrene (1.55 x $10^{-16}$ Kg·m / $m^2$·s·Pa) but higher than those for PET (3.17 x $10^{-18}$

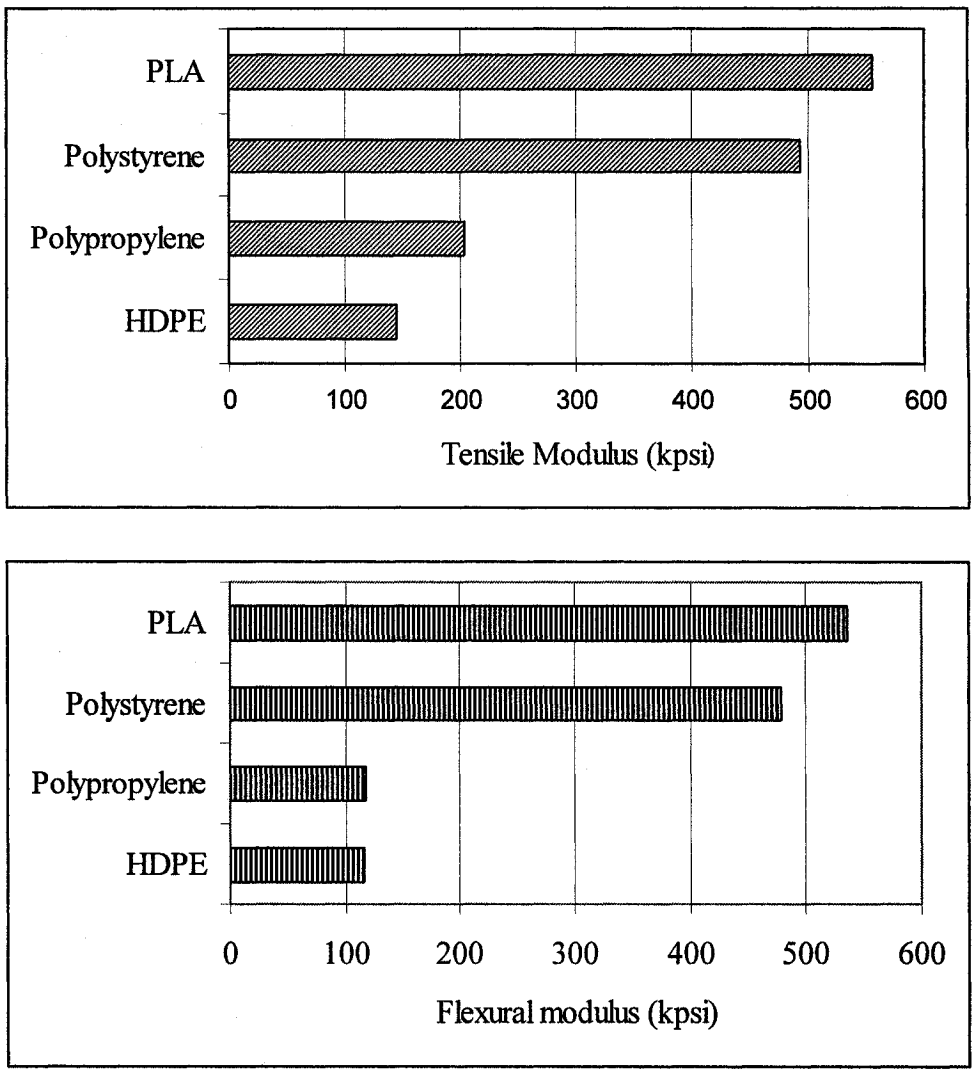


Fig. 1.7. Comparison of the mechanical properties of the PLA with some common polymer[12].

Kg·m / $m^2$·s·Pa). The oxygen permeability coefficients of PLA are about 20 times lower than the values published for polystyrene at 25°C: 2.7 · $10^{-17}$ Kg·m / $m^2$·s·Pa . However

they are higher than the oxygen permeability coefficient for PET: $1.88 \cdot 10^{-19}$ Kg·m / $m^2 \cdot s \cdot Pa$. The water permeability coefficients of PLA films are within the range 1.48 – $2.20 \cdot 10^{-14}$ Kg·m / $m^2 \cdot s \cdot Pa^1$ and more than 10 times higher than those of PET and almost 100 times higher than for high-density polyethylene so methods of improvement of this parameter should be considered. All this shows that polylactide is a very promising polymer for industry.

### 1.5. Stereocomplex formation between L- and D- polylactide

Since lactic acid is optically active (Fig.1 and 2.) a blend of L- and D-polylactides is able to crystallize in the form of a *stereocomplex*. This type of the crystallization is called *racemic crystallization.* Racemic crystallization in polylactides has become the object of much attention in the past several years and many studies have been carried out.

Both L- and D-lactide are able to crystallize individually in an orthorhombic crystalline form whereas it was found that L-lactide and D-lactide repeat units together form stereocomplex crystals of a triclinic crystalline form that is the lowest crystallographic symmetry possible (Table 1.1). This crystallization takes place under the side by side packing mechanism and therefore the stereocomplex has a significantly higher density and melting point. The stereocomplex can also have a dramatic influence on the rheological behavior of polymer blends because of its significantly higher melting point as compared to the orthorhombic crystals. In fact the formation of the stereocomplex can causes *gelation* at normal melt temperature[13]. This stereocomplexation

strongly influences the crystallization behavior of L- and D-polylactide blends and their spherulitic morphology.

This sort of stereocomplexation is known for some other polymers such as poly (γ-benzyl glutamate), poly (α-methyl-α-ethyl-β-propiollactone)[14]. The stereocomplex formation depends on many factors including the blending ratio of the enantiomers, their molecular weights, the optical purity and the nature of the solvent for solution cast films as considered here. Conditions that yield maximum amount of stereocomplex are low molecular weights for both L- and D- polymers and equimolar blend composition. But it was noted that stereocomplexation occurs even when as little as 10 wt% of poly (D-lactide) is present. In this case the stereocomplex particles can act as a nucleating agent for the formation of orthorhombic crystals[15].

Table 1.1. Crystalline structures of the pure polylactide enantiomers and L-/D-lactide stereocomplex[16,17].

| | Pure L- or D- polylactide | L-/D-stereocomplex |
|---|---|---|
| Crystalline form | Orthorombic | Triclinic |
| Lattice dimension | a=1.07 nm<br>b=0.645 nm<br>c=2.78 nm | a=0.916 nm<br>b=0.916 nm<br>c=0.87 nm |
| Lattice angle | α = 90°<br>β = 90°<br>γ= 90° | α = 98°<br>β =69.5°<br>γ= 121.2° |
| Conformation | 10/3 helix | 3/1 helix |
| Melting point | 130 –185 C° | 230 – 279 C° |

Usually commercial PLA's contain repeat units of both enantiomers. In this case for stereocomplex formation the presence of sufficiently long sequences of both the L-lactide and D-lactide units are essential[18].

### 1.6. Mechanism of spherulite formation

While crystallization from dilute solution yields single polymer crystals usually having two-dimensional symmetry, bulk crystallization leads to the formation of spherically shaped crystalline aggregates called spherulites. Spherulites consist of lamellar plates of equal thickness. Typically the thickness of the lamellae ranges from 20 to 80 Å depending on the nature of the polymer chain[7].

The crystallization process starts at certain locations called *nuclei*. There is little information about the nature of the nuclei. It is known that in many cases impurities in the bulk polymer can cause nucleation, and that the size of the non-growing nuclei is about 10 nm. The stability of each nucleus is determined by thermodynamic conditions and it may or may not develop into crystalline lamellae depending on its size and the thermodynamic conditions. During crystallization from melt, the first structure that forms is a single lamella that starts to crystallize from an unstable nucleus in the form of a platelet growing at both ends. Further development of the crystalline structure takes place through *induced nucleation*. This appears in form of subsidiary lamellae branching out from the middle of the founding lamella[19].

Further branching of the lamellae leads to the formation of sheaf-like crystalline structures and finally spherulites. Since it takes time to develop a spherulite from the sheaf, typically they can obtain the shape of a sphere only starting from a certain size.

There are two main types of spherulites. (Fig. 1.8). Type I spherulites are formed by lamellae radially growing from a center nucleus at approximately equal rates in all directions. The type I spherulite therefore has spherical symmetry. The type II spherulite is formed through extensive branching of the central single lamella until a spherical shape is reached. This type of spherulite has planar symmetry[20].

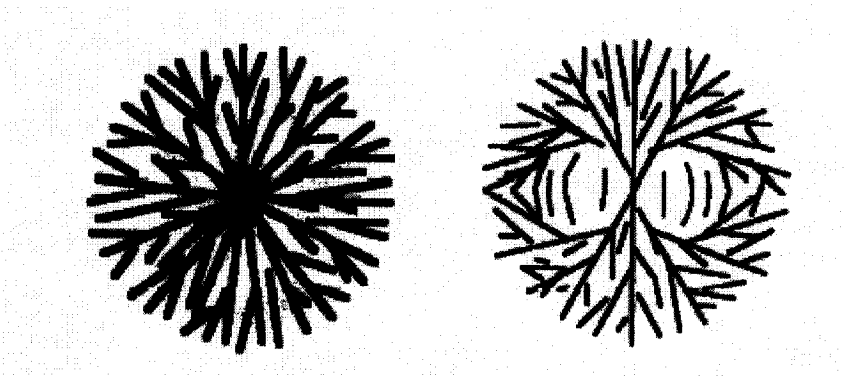

Fig. 1.8. Sketch of two possible growth morphologies with planar (at right) and spherical (at left) symmetry.

Usually there is no clear difference between type I and type II spherulites and both types can be present at the same time in the same polymer. It is known that type II spherulites are usually formed during crystallization at higher temperatures. Starting from a certain temperature the polymer crystallizes in the form of axialites that are an extreme case of the type II spherulite. Molecular weight also affects polymer crystallization behavior; crystallization rate is faster in low molecular weight polymers. The spherulitic morphology is very typical for polymer crystallization. Block copolymers also can form

spherulites but their development proceeds by a different mechanism because the crystallization process is constrained by the structure of the polymer chains. Usually the amorphous phase in crystallized block polymers is enriched by one of the functional groups of the chain[21]. Crystallization in polymer blends is more complicated and the polymer miscibility, their molecular weights and other factors determine spherulite formation[22].

### 1.7. Crystallization kinetics - general assumptions

During crystallization, a polymer undergoes a phase transformation and amorphous material transforms into crystalline structures. Since this process develops over time and depends on temperature, the crystallization process can be considered as a thermodynamic phenomenon and the following general kinetic equation can be applied[23]:

$$X = X(t,T) \qquad [1.1]$$

where $X$ is a measure of the extent or degree of crystallization, $t$ is the time elapsed from the onset of crystallization and $T$ is the absolute temperature.

Typically during cooling of a liquid polymer below its melting point, crystallizing particles, in the form of spherulites or axialites, randomly appear in the polymer and grow with time. The degree of crystallization X is defined by the following equation:

$$X = \frac{\text{mass of crystalliz ed particles}}{\text{total mass of polymer}} = \frac{\rho_c \sum_0^n V_i(t)}{\rho_l V_0} \qquad [1.2]$$

where $\rho_c$ is the crystalline density, $\rho_l$ is liquid polymer density and $V_i$ is volume of each of n crystalline structures in the total polymer volume $V_0$.

At the microscopic level, the crystalline structures in polymers are not evenly distributed and crystalline density varies along different directions in the spherulite. Therefore the *degree of crystallization* which was defined above should be distinguished from the *degree of crystallinity,* as they may not be corresponding precisely to each other. Most crystallization theories assume that crystallization in polymers follows *the additivity principle*. It means that the rate of crystallization is a function of temperature and relative amount of the polymer that is already crystallized and therefore does not depend on the sample's thermal history (Fig.1.9). The gradient of the line shown in this graph represents the maximum rate of crystallization. The time $\tau_i$ is the incubation time which represents the time required for the nuclei to reach the supercritical state.

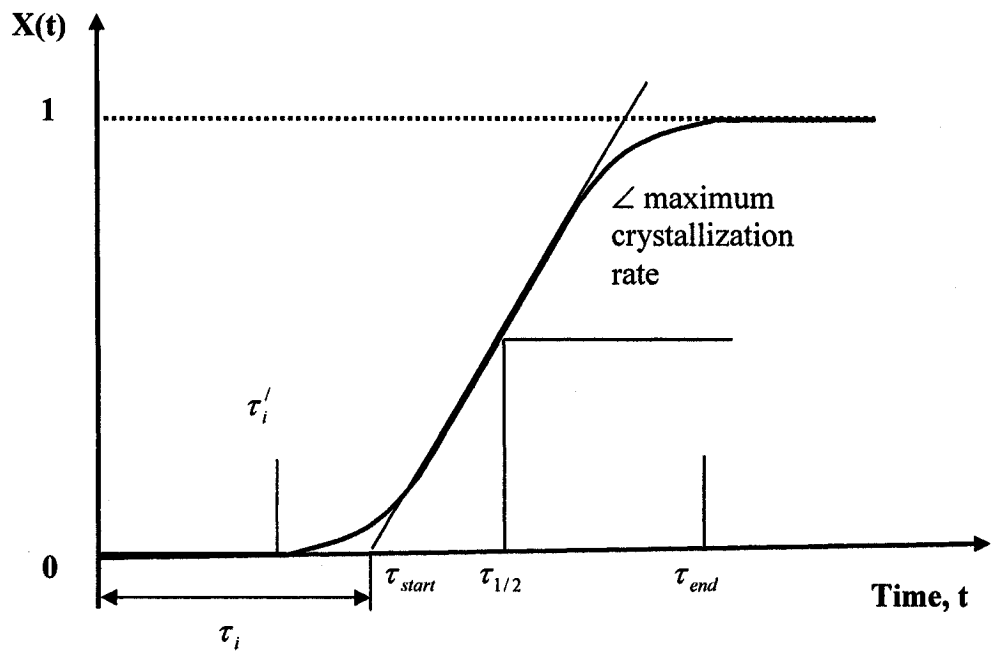


Fig.1.9. A schematic of the development of crystallinity over time in polymers.

### 1.8. Thermodynamics of crystallization

The driving forces for polymer crystallization are induced by the surplus of free energy in the system. The unstable state of the system causes transportation of the polymer chains from the liquid melt or solution to the solid crystalline state. This process increases the level of order in the system and brings it to new stable state.

Turnbull and Fisher[24] adapted the J. W. Gibbs equation for the nucleation process in polymers. They showed that when the free energy of the system becomes negative, the energy barrier becomes surmountable and phase transformation starts. This transformation starts with the formation of the nuclei that will grow in size according to the associated free energy. For ideal conditions when crystallization takes place without any chemical changes and volume constraint the Gibbs free energy of the system, G is given by:

$$G=H-TS \qquad [1.3]$$

In this case the temperature change only and the change in Gibbs free energy drives the crystallization process:

$$\Delta G=\Delta H-T\Delta S \qquad [1.4]$$

where $\Delta H$ is the change in enthalpy and can be considered equal to the latent heat of melting and $\Delta S$ is change of the entropy between the crystalline state and the melt or solution. To understand crystallization in polymers, nucleation and crystal growth should be considered as independent phenomena.

## 1.9. Nucleation and crystal growth in homogeneous polymer systems

Above the equilibrium melting temperature the value of ΔG, defined in equation [4], increases monotonically with increasing temperature. Below the equilibrium melting temperature this function has a maximum, defined by:

$$\frac{d(\Delta G)}{dr} = 0 \qquad [1.5]$$

where r is the radius of the nuclei[25].

This maximum value, denoted as ΔG*, can be regarded as being the activation energy barrier which has to be overcome in order to form a stable nucleus which will grow. On a molecularly smooth crystal surface, a new layer can only be grown after secondary nucleation, a process similar to primary nucleation, but with a somewhat lower free energy barrier since the surface area that must be newly created is smaller. The change in free energy of the growing crystal can be described by[26]:

$$\Delta G'' = \Delta G_c + \sum \gamma A \qquad [1.6]$$

where $\Delta G_c$ is the change of the free energy of phase change and γ represents the specific surface energy, $A$ is the corresponding surface area and the summation is carried out over all crystal surfaces.

There are three physical mechanisms for polymer nucleation:

1. Spontaneous homogeneous nucleation that occurs (rarely) in a supercooled homogeneous melt;

2. Orientation induced nucleation caused by alignment of macromolecules and spontaneous crystallization;
3. Heterogeneous nucleation on the surface of a foreign phase.

Heterogeneous nucleation always occurs at lower supercooling than homogeneous nucleation. Thus the heterogeneities with whose surfaces the nucleation is concerned are frequently referred to as nucleation catalysts or nucleating agents[46]. Solvent residue, impurities and intentionally introduced phases can all act as nucleating agents for most polymer systems.

### 1.10. Isothermal crystallization

An isothermal crystallization is carried out by rapidly cooling a polymer liquid from above its melting temperature to the crystallization temperature, $T_c$, and holding it at that temperature until crystallization is completed. The study of isothermal crystallization is usually carried out under the following four assumptions[23]:

1. That the rate of change of temperature during the cooling is relatively slow compared to the thermal diffusion time through the sample:

$$dT/dt < DT/L^2 \qquad [1.7]$$

where $D$ is thermal diffusivity and $L$ is sample size.

2. That the release rate of latent heat of crystallization is at least two orders less than the heat transfer rate with surroundings.

3. That the ratio of $\rho_c/\rho_l$, where $\rho_c$ and $\rho_l$ are the densities of the crystalline phase is constant.

## 1.11. Using the Atomic Force Microscope for crystallinity studies with polylactide films

Since it is known that the morphology of the crystalline and amorphous areas is one of the most important factors determining polymer properties it is necessary to be able to observe crystalline morphology in polymers. There are numerous techniques suitable for crystallinity studies, such as Raman spectroscopy and X-ray diffraction that have been successfully employed for film studies. Unfortunately these techniques do not provide certain information on crystalline morphology such as growth rate. Also the atomic force microscopic technique could provide new data on film surface features not available with other techniques. With reference to PLA films, it is possible to determine the level of crystallinity using Raman spectroscopy but an image of the film surface is not produced.

The atomic force microscope (AFM) is one of the most powerful methods for studying material surfaces. For exploring the surface, the AFM uses a tiny sensor in the shape of a pyramid (less than 2 μm high) that is attached to the free end of a flexible cantilever. The contact area of the probe is extremely small and therefore when the tip is near a surface it is affected by a variety of forces that cause deflection of the cantilever. These forces are very different in nature and range from $10^{-11}$ to $10^{-6}$ N[27]. The deflections of the cantilever are described by Hook's law, thus interaction force between tip and surface can be measured. The tip's displacement is magnified by an optical laser system (Fig.1.10.).

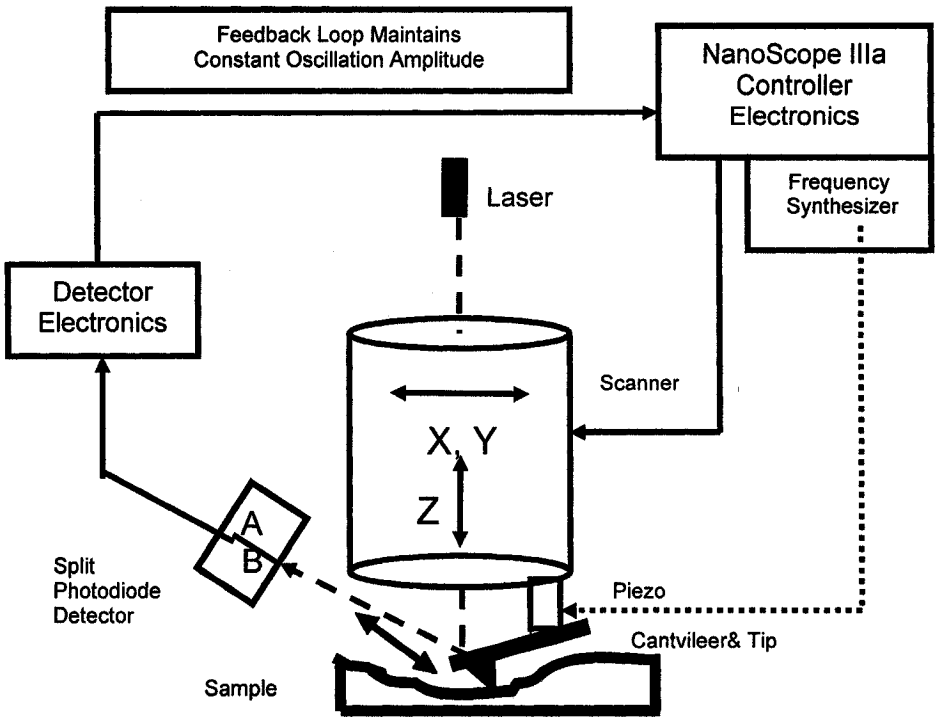


Fig.1.10. Schematic of tapping mode Atomic Force Microscopy.

This approach allows detecting displacements of up to 0.1 Å and its accuracy is restricted only by thermal noise[28]. To image a surface the probe is moved by an extremely precise piezoelectric device in the plane parallel to the surface. Due to its small size the probe has a very high (up to the hundreds of kilohertz) resonance frequency, and scanning proceeds at very high speed. Unlike many methods, tapping mode AFM does not require particular conditions for imaging such as vacuum or conductive coating and can be operated at room temperature. Depending on the tip-cantilever movement pattern contact and non-contact modes of the AFM are distinguished. Over the last years, the new tapping mode of AFM that combines advantages of both methods has been developed (Fig. 1.11.).

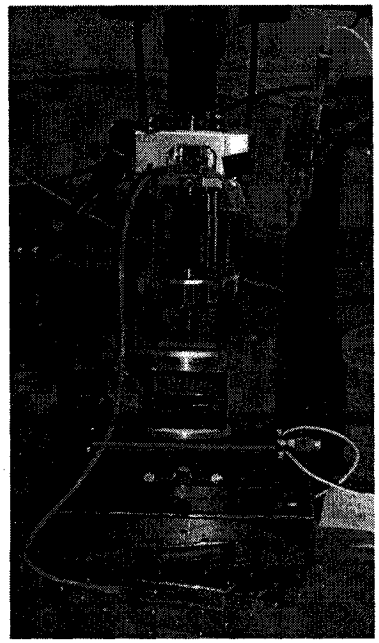

Fig. 1.11. Digital Instrument's Nanoscope IIIa device.

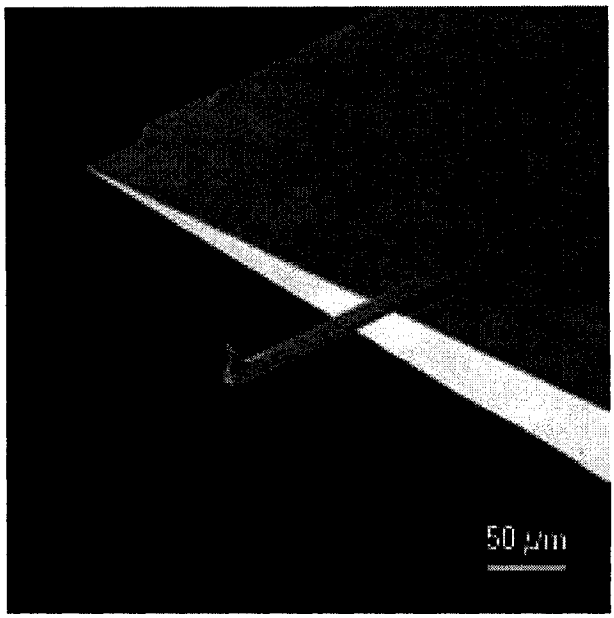


Fig.1.12. SEM image of NSC15 silicon cantilever. Image by MikroMash company.

When operated in tapping mode, the cantilever (Fig. 1.12) is moved to and from the surface by a supplementary piezo-element at its resonant frequency and touches (taps) the surface for only a very small portion of its oscillation cycle thus does not make alterations on the surface. At the same time, tapping mode AFM provides a wide range of data about the surface. The phase and amplitude images provide very important information on the surface structure and properties that can not be obtained by other modes. Phase images provide information on magnitude of the repulsive and attractive forces in specific point on the surface of the sample and potentially give possibility to distinguish crystalline and amorphous areas with very high resolution. It is believed also that phase image contrast reflects many important surface properties such as stiffness and viscoelasticity.

Atomic force microscopy provides great opportunities to study surface structures. It allows direct non-destructive imaging of the surface structure, and provides information that could not be obtained with previous techniques. For example, much information can be obtained by measuring lateral forces on the cantilever. Many devices also allow the measurement of torsion forces on the cantilever. In many cases, drag force measurements gives important additional information on surface structures and allow imaging of crystalline and amorphous areas of a surface. Moreover the AFM can even image the hardness of sample's surface by pressing the tip into each scan point. By using the AFM technique it is possible to study patterns of orientation and to disclose mechanisms of crystallization.

It is clear that AFM has at least one apparent disadvantage. It has a very small working area that is usually limited to one tenth of a millimeter. Taking into account that crystal structures in polymers can be much larger, it calls into question the possibility of utilization of the AFM for investigation of crystalline and amorphous structures. Investigations have showed that in some cases crystalline structures in PLA could have a typical size up to 300 micrometers[29]. In films, the typical crystalline structure size will be much less than in cast melt polymers. It also should be noted that there are some other effects concerned with the size and the shape of the tip that complicate imaging such as broadening and aspect ratio. It is also very important that the AFM technique allows monitoring of not only the crystalline structure but also the amorphous areas of the surface[30]. In this work, the AFM will be used to image the crystalline and amorphous regions of polylactide films. Different types of AFM images will be considered to characterize the distribution, growth kinetics and morphology of the crystallites.

## 1.12. Objectives

It is known that temperature is one of the most influential factors in the crystallization process. That is why one of the most important parts of this research is the study of the effect of temperature on crystalline growth rate and spherulite morphology in solution cast polylactide films. Significant attention will be paid to the studies of the influence of the stereocomplex on spherulite morphology and growth rate.

As PLA films are characterized by dynamic evolution of the crystalline network it would be very interesting to employ the AFM technique for its imaging followed by image processing in order to obtain quantitative assessment of the spherulite growth to trace its changes under different conditions.

The experimental methodology of the research includes:

1. Development of the appropriate technique for obtaining thin, uniform films from polylactide solutions.
2. Development of an adequate approach for isothermal film annealing.
3. Adapting Atomic Force Microscopy for the spherulite growth studies in different D- and L-polylactide compositions.
4. Characterization of different composition of polylactide using advanced techniques such as FT-IR, GPC, and DSC.
5. Studies of the influence of the residual solvent on polylactide glass transition temperature using custom elongation measurements.

The obtained experimental data will be analyzed to understand crystalline morphology of different polylactide compositions, their crystallization kinetics and influence of the stereocomplexation on overall crystallinity.

# 2. Literature review

## 2.1. Modern theory of crystallization

Crystallization is one of the most important phenomena in polymers and differs from the crystallization of the inorganic substances in many ways. This is caused by long-chain nature of the polymers and spatial restrictions for the polymer crystallization. The basic principles of the crystallization in polymers have been formulated by Natta and Corradini as follows[31]:

1. *The equivalence postulate* assumes that all repeat units in the crystal occupy geometrically equivalent positions relative to the chain axis.

2. *The minimum energy postulate* suggests that the chain conformation in crystal is arranged in a way by which the minimal potential energy state is reached.

3. *The packing postulate* says that polymer lattice keeps as much as possible symmetry compared to the isolated chain.

These postulates are used for explanations of the crystallization behavior in polymers and to create a basis for theoretical modeling of crystallization. Studies of the crystallization phenomenon are complicated by many factors such as miscibility of blends, entanglement and optical isomers. The nucleation phenomenon is relatively rarely observed in the crystallization of the inorganic substances. This fact makes modeling of the polymer crystallization using traditional approaches very difficult. All abovementioned is the reason for existence of many theories of the crystallization that are controversial in many important approaches.

## 2.2. Glass transition temperature as a kinetic phenomenon

The glass transition phenomenon is one of the most significant properties of polymers. During cooling from the equilibrium liquid-like state, polymers continuously change their properties toward a non- equilibrium solid state where it reaches a kinetically frozen configuration. This change does not occur abruptly at a certain temperature like in case of inorganic substances but over a range of several degrees of temperature called the *glass transition region.* The glass transition is considered as a second-order phase transition or a kinetic phenomenon[32].

For the second order transition a discontinuity of the second derivatives of the Gibbs free energy with respect to the temperature (the temperature slope of the specific heat and of the specific volume) is expected. In real polymers such discontinuities are *smoothed out* depending on the heating/cooling rate[33].

In the process of cooling from above the glass transition temperature any temperature change is instantaneously followed by a change in chain conformation to reach the equilibrium configuration. Near the $T_g$ and at lower temperatures the molecular mobility decreases enough to freeze the structure relaxation towards the corresponding equilibrium status preserving the configuration belonging to higher temperatures. As a consequence, the glass transition temperature is strongly dependent on the thermal scanning rate and the polymer in the glassy state becomes a metastable solid depending on the thermal history. That is why the glass transition is mainly accepted as a kinetic phenomenon[34]. Experimental observations of this phenomenon are presented on Fig 2.1 for polystyrene. The data show a monotonic decrease of $T_g$ with decreasing cooling rate.

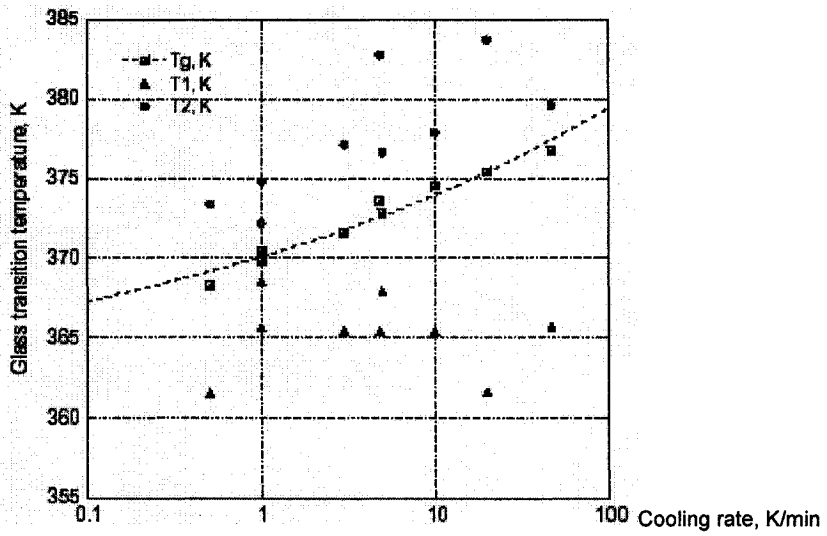


Fig. 2.1. Polystyrene glass transition temperature as function of cooling rate[35].

The investigation of the dependence of the glass transition temperature on cooling rate has been carried out by a number of scientists. Ritland[36], starting from Tool's equation suggested a linear relation between the fictive temperature $T_f$ (the temperature at which the non equilibrium value of the macroscopic property would be the equilibrium one) and the logarithm of the cooling rate $q$:

$$\partial[\ln(q)] = \partial T_f / E \qquad [2.1]$$

where $E$ is the activation energy.

Moynihan et al.[37] extended the analysis to polymers that exhibit a spectrum of relaxation times showing that in the case of a temperature independent spectrum or thermorheologically simple materials the reciprocal of the fictive temperature, $T_f$, is linear with respect to the logarithm of the cooling rate $q$:

$$\partial[\ln(q)] = -E \cdot \partial[1/T_f] \qquad [2.2]$$

More recently, Halpern and Bisquert[38] pointed out that not only the activation energy $E$ plays a role but also does the form of the relaxation spectrum. For the more general cases, where the distribution of the relaxation modes is accounted by the stretch parameter, $\beta$, they proposed:

$$\partial[\ln(q)] = -\beta E \cdot \partial[1/T_f] \qquad [2.3]$$

The equilibrium properties of polymers can be estimated on assumptions made by Gibbs and Di Marcio[39].

### 2.3. Avrami theory for isothermal crystallization and its consequences

Johnson, Mehl[40] and Avrami[41] considered the kinetics of the new phase formation using a constant nucleation rate for the modeling. This simplification diminishes the impact of the fact that the volume of the amorphous material gradually decreases. Avrami's model employs fictitious nuclei that virtually exist in the already transformed phase. From the mathematical point of view this assumption allows us to conveniently determine the amount of the crystallized polymer and to make further correction by subtracting the amount of crystalline phase from fictitious nuclei.

The mathematical model for first order isothermal crystallization satisfying the conditions described in section 1.10, can be written in the following form[42]:

$$\frac{dX}{dt} = k(T)(1 - X) \qquad [2.4]$$

where $k(T)$ is crystallization rate constant and $X$ is crystallization rate.

The same crystallization rate can be expressed as a summation of the general functions for nucleation and growth[43]:

$$\frac{dX}{dt} = f_1(T,X) + f_2(T,X) \qquad [2.5]$$

For *m*th order crystallization the kinetic equation can be expressed as:

$$\frac{dX}{dt} = mkt^{m-1}(1-X) \qquad [2.6]$$

The general solution yields the final Avrami equation:

$$X = 1 - \exp\left[-k(T)t^m\right] \qquad [2.7]$$

where $m$ is a dimensionless parameter called the Avrami exponent.

Many studies were made on the validation of the Avrami equation for real crystallization processes. As result it was found that Avrami exponent is influenced by the nucleation type[44], molecular weight[45] and secondary crystallization[46]. There is evidence that Avrami exponent also slightly depends on temperature[47]. It was found that the Avrami exponent is uniquely related to the nucleation rate and crystalline growth morphology and should be an integer for certain specific crystalline shapes. For real crystallization processes, the Avrami exponent is also affected by parameters that are not constant during crystallization. There are four main causes for this phenomenon: (1) changes in morphology during crystallization, (2) changes in lamellae growth rate, where a decrease in growth rate decreases m, (3) changes in the true nucleation rate, where a decrease of this value decreases m and (4) variations of the $\rho_l/\rho_c$ ratio.

Hoshino et al.[48] reported values for m ranging from $m$=4 to $m$<2 for crystallization of isotactic polypropylene. Typically the highest m value is achieved for spherulitic crystallization. For polylactide crystallization in the range of 110 – 150 ° C, the Avrami exponent usually is about 4, decreasing to 3 for high temperature crystalization[14] (Fig. 2.2). This is consistent with observed crystalline morphologies and seems to be typical for the crystallization of aliphatic polyesters.

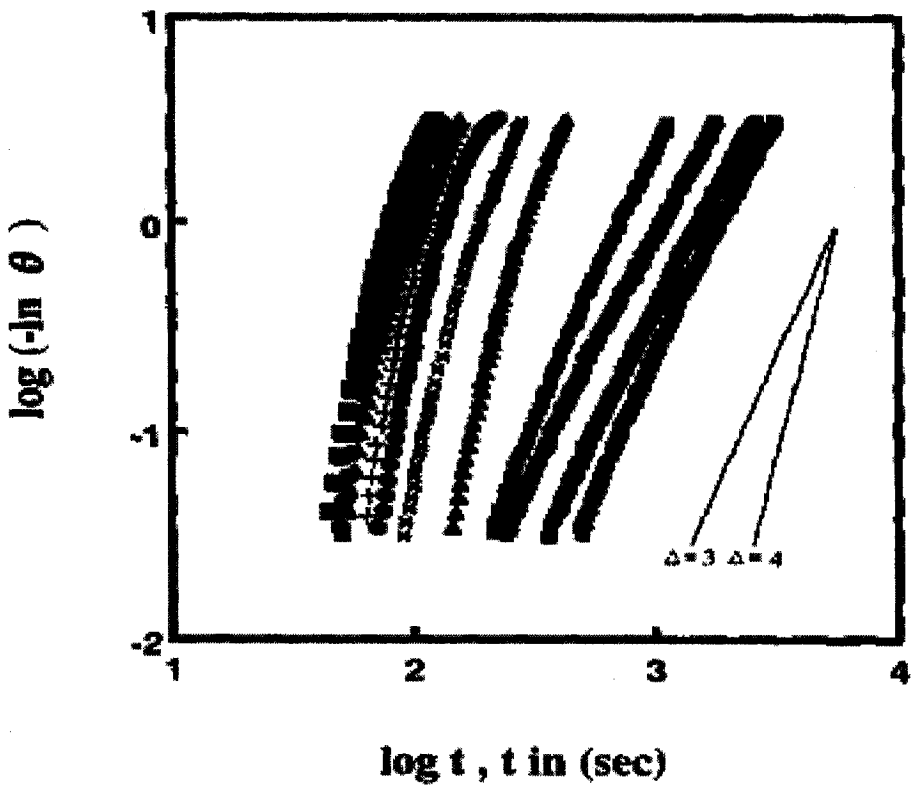


Fig. 2.2. Avrami plot for isothermal crystallization of the polylactide at different crystallization temperatures. The lines indicate the gradients of 3 and 4[51].

The simple Avrami model was developed further by Perez-Cardenas[49] who introduced a model that considers crystallization as result of primary crystallization and secondary crystallization proceeding simultaneously:

$$X(t) = X_{pc}(t) + X_{sc}(t), \qquad [2.8]$$

where $X_{pc}(t)$ and $X_{sc}(t)$ are mass fractions of polymer crystallized by primary and secondary crystallizations respectively. The factor $\xi$ in this theory represents the overall weight fraction of polymer that has crystallized at the moment of termination of primary crystallization:

$$1 - X(t) = \exp(-k\tau^m - k'\tau^{m'}\left[mk(1-\xi)\int \exp(k\tau^m + k'\tau^{m'})\tau^{m-1}d\tau + 1\right] \qquad [2.9.]$$

$$1 - X(t) = (1-\xi)\exp(k'^{*}t^{m'})\exp(-k't^{m'}) \qquad [2.10]$$

for X(t) < ξ and

for X(t) > ξ

where k′ and $m'$ are temperature dependent parameters. As result there are five parameters to achieve better explanation of the crystallization process.

### 2.4. Nucleation kinetics and crystallization thermodynamics

The importance of understanding of the nucleation processes in polymers comes from the fact that nucleation affects not only initial crystallization. Unlike crystallization in inorganic systems nucleation is a significant part of crystallization during the entire process. Hoffman et al.[50] expressed the rate of nucleation in polymers as follows:

$$N = \exp\left(-\frac{U^*}{R(T - T_g - C)}\right)\exp\left(-\frac{\Delta G^*}{k_b T} f(\theta)\right) \qquad [2.11]$$

Here:

$$f(T) = \frac{2T}{T_m^0 + T} \qquad [2.12]$$

$$\Delta G^* = \frac{\beta \sigma_e \sigma^2 T_m^{0\,2}}{(\Delta H f(T))^2 \Delta T^2}, \qquad [2.13]$$

$$f(\theta) = \frac{(2+\cos(\theta))(1-\cos(\theta))^2}{4}, \qquad [2.14]$$

where $\sigma$ is the crystal growth face surface energy, $\sigma_e$ is the crystal fold surface energy, $\Delta H$ is the heat of fusion per unit volume, $\Delta T$ is the supercooling, $\beta$ = 32 is a geometrical constant, $R$ is the gas constant, $k_b$ is the Boltzmann constant, $T_g$ is the glass transition temperature, $U^*$ is the activation energy barrier for the transportation of polymer molecules from the melt to the crystal surface. $T_g - C$ is called the Gibbs-di Marcio equilibrium glass transition temperature and is an adjustable parameter with the value of $C$ being about 30° C. For homogeneous nucleation, the function $f(\theta)$ assumes a value of 1 ($\theta$ = 180°). For heterogeneous nucleation, 0 <$f(\theta)$ < 1. The function $f(T)$ is an approximate correction factor which is needed to take into account the changes of the heat of fusion with supercooling.

For polylactide, the values of $U^*$ are estimated to range from 3500 to 5700 J/mol depending on molecular weight[51]. Sufficient information on the lamellae structure of polylactide is not available. Myiata and Masuko attempted to estimate the thickness of the layer $b$ and found its value equal to 0.53 nm[52]. The heat of fusion from DSC measurements[51] is found be $\Delta H$ = 174 x $10^6$ J/m$^3$. These data are sufficient for the estimation of the lateral surface energy $\sigma$ = 0.0092 J·m$^{-2}$ using the Thomas-Stavely equation[50]:

$$\sigma = 0.1\Delta H_f b \qquad [2.15]$$

This value is independent of molecular weight. The crystal fold surface energy $\sigma_e$ can be estimated from the product of $\sigma\sigma_e$ calculated for polylactide as a function of molecular weight by Vasanthakumari and Pennings[53]. The value of $\sigma_e$ is dependent on the molecular weight of the polymer and ranges from $63x10^{-3}$ to $107x10^{-3}$ $J \cdot m^{-2}$ increasing with increasing molecular weight. This means that lamellae are predominantly composed of loose-loop folds[51].

At constant crystallization temperature the number of active nuclei rapidly increases with time and reaches some asymptotic value when saturation is achieved. Both the nucleation limit and the saturation time in polymers is strongly temperature dependant (Fig. 2.3).

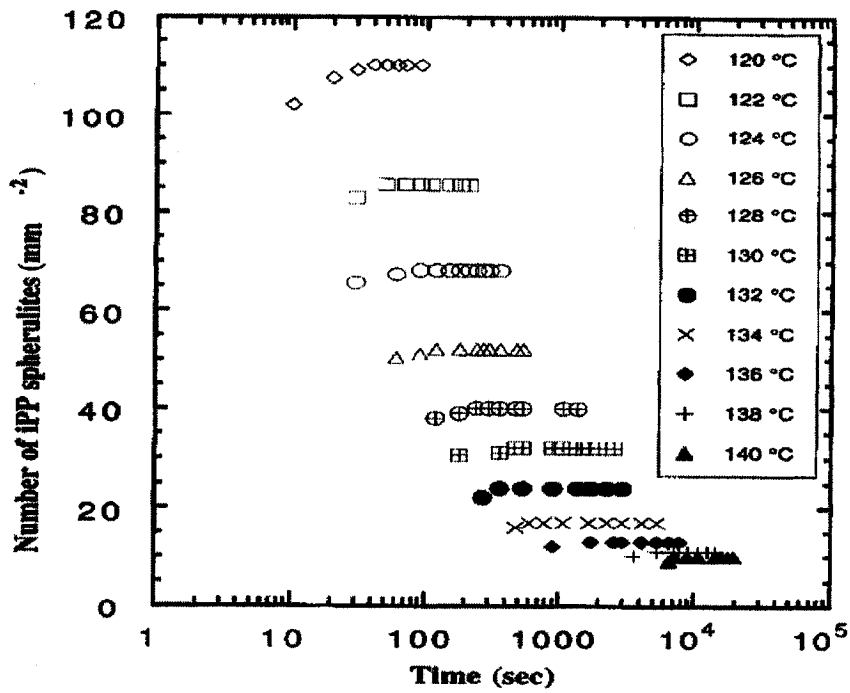


Fig. 2.3. Spherulite concentration in isotactic polystyrene as a function of time and crystallization temperature[23].

The number of active nuclei can be approximated using an exponential equation[54]:

$$n(t,T) = n_0(T)\left[1-\exp(-\frac{t}{\tau_n}(T))\right], \qquad [2.16]$$

where $n_0$ and $\tau_n$, are characteristic constants of the polymer and nucleating agent system. The true nucleation rate, $N$, is related to the observed nucleation rate, $dn/dt$, through the following relationship[55]:

$$N = \frac{dn/dt}{1-X} \qquad [2.17]$$

An important consequence from the molecular theory of the nucleation is that in pure, monodisperse polymers the spherulite radius always increases in direct proportion to time (Fig. 2.4). The volume of individual spherulite particles will increase with time according to:

$$[V(t,T)]_i = \alpha_i[r(t,T)]_i^{m-1} = \alpha_i[G(T)t]_i^{m-1}, \qquad [2.18]$$

where $r(t, T)$ is the spherulite radius.

The spherulite growth rate can be expressed as[56]:

$$G = G_0 \exp\left(-\frac{U^*}{R(T-T_g-C_2)}\right)\exp\left(-\frac{nb\sigma\sigma_e T^0 m}{k_b T(\Delta Hf(T))\Delta T}\right), \qquad [2.19]$$

where $G_0$ is lamellae growth constant and $n$ can assume two values of 4 or 2 depending on the spherulite growth regime.

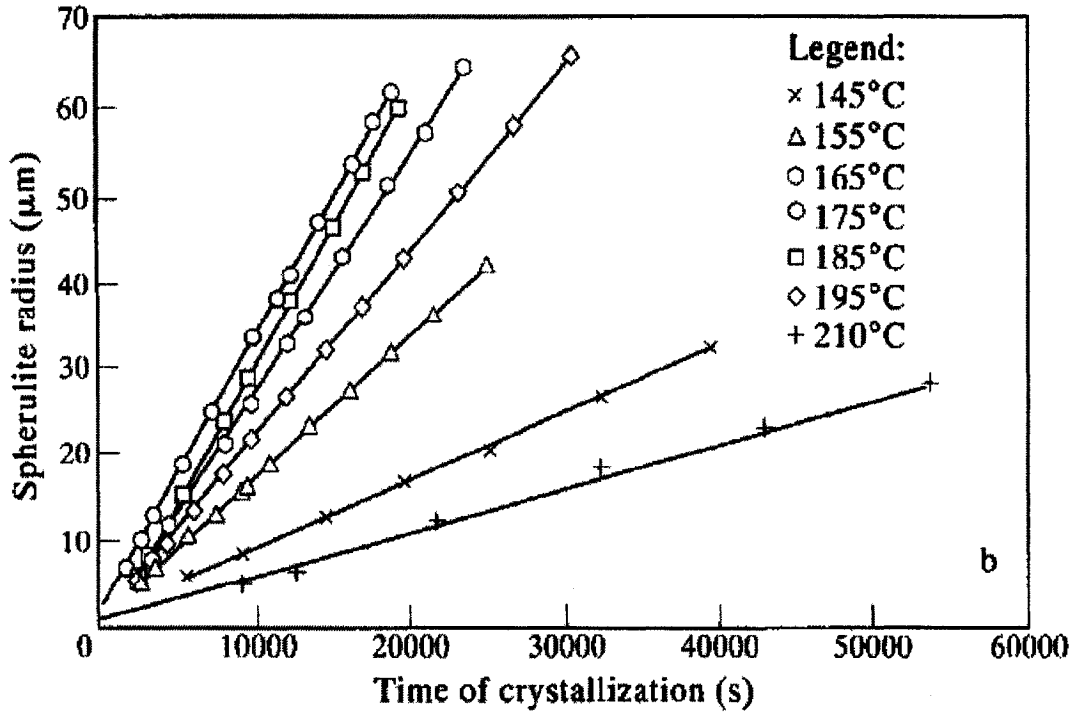


Fig. 2.4. Spherulite size versus time depending on temperature for the isothermal crystallization of the isotactic polystyrene[23].

The overall crystallization rate trend vs. temperature trend is a bell-shaped curve. This is consistent with Equation [2.19]. The spherulite growth rate is very low at high temperatures and increases as undercooling increases; it reaches a maximum and then gradually decreases. This crystallization behavior is typical for the overwhelming majority of pure non-blended polymers. Measurements of spherulite growth rate are usually made using a polarized microscope equipped with hot stage. Together with image analysis software this gives resolution of about 0.3 μm[57].

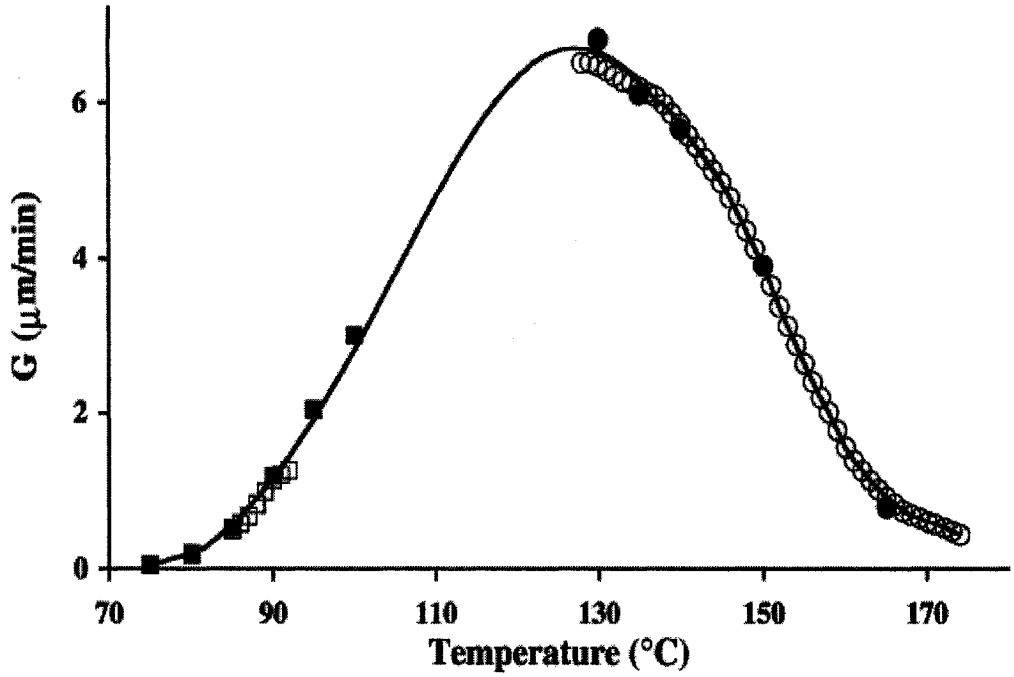


Fig. 2.5. Spherulite growth rates of poly (L-lactide) measured by various techniques: (○) cooling at 1°C/min after self-nucleation; (●) isothermal crystallization after cooling from the melt; (□) heating at 1°C/min after self-nucleation and quenching; (■) isothermal crystallization after self-nucleation and quenching[58].

## 2.5. Ozawa theory for non-isothermal crystallization

Ozawa[59] proposed a further development of the Avrami theory for the kinetics of continuous cooling or heating crystallization of polymers. His approach involved modifying the Avrami equation to include transformation processes under nonisothermal conditions at constant rate of temperature change:

$$1 - X = \exp\left(\frac{-k(T)}{|dT/dt|^n}\right) \qquad [2.20]$$

where *k(T)* is the cooling function of the process, a kinetic parameter which takes into account the geometry and change in nucleation and growth rate, and *n* is the Ozawa exponent which has some relation to the Avrami exponent but is not the same value. Equation [2.20] can be rewritten in following form:

$$\ln[-\ln(1-X)] = \ln[k(T)] + n\ln\left(\frac{1}{|dT/dt|}\right) \qquad [2.21]$$

Obviously a plot of ln[- ln(1 - X)] versus ln $|(dT/dt)^{-1}|$ should yield a straight line having *n* as slope and *k(T)* as the intercept. A more complex and precise expression for the Ozawa model includes the Nakamura equation[60]:

$$1-X = \exp\left\{-\left[\int_0^t K(T)dt\right]^n\right\} \qquad [2.22]$$

For isothermal conditions, this equation reduces to the Avrami equation. The Ozawa model has been successfully used for description of the crystallization of poly (ethylene terephtalate), polypropylene, and polyamide 6[61].

The Ozawa equation is applicable only if there are no secondary crystallization or morphology changes and the cooling rate is relatively low. The curvature of the non-linear parts (Fig. 2.6) is positive showing that at higher cooling rates the true crystallinity is higher than predicted by the Ozawa model at any moment of crystallization time. This approach is not applicable to the studies of crystallization behavior of polylactides which demonstrate significant influence of secondary crystallization. The relationship between isothermal and non-isothermal transformation rates is still not studied in details. However

an ability to predict non-isothermal transformation kinetics using isothermal transformation data would certainly be advantageous in the polymer processing industry.

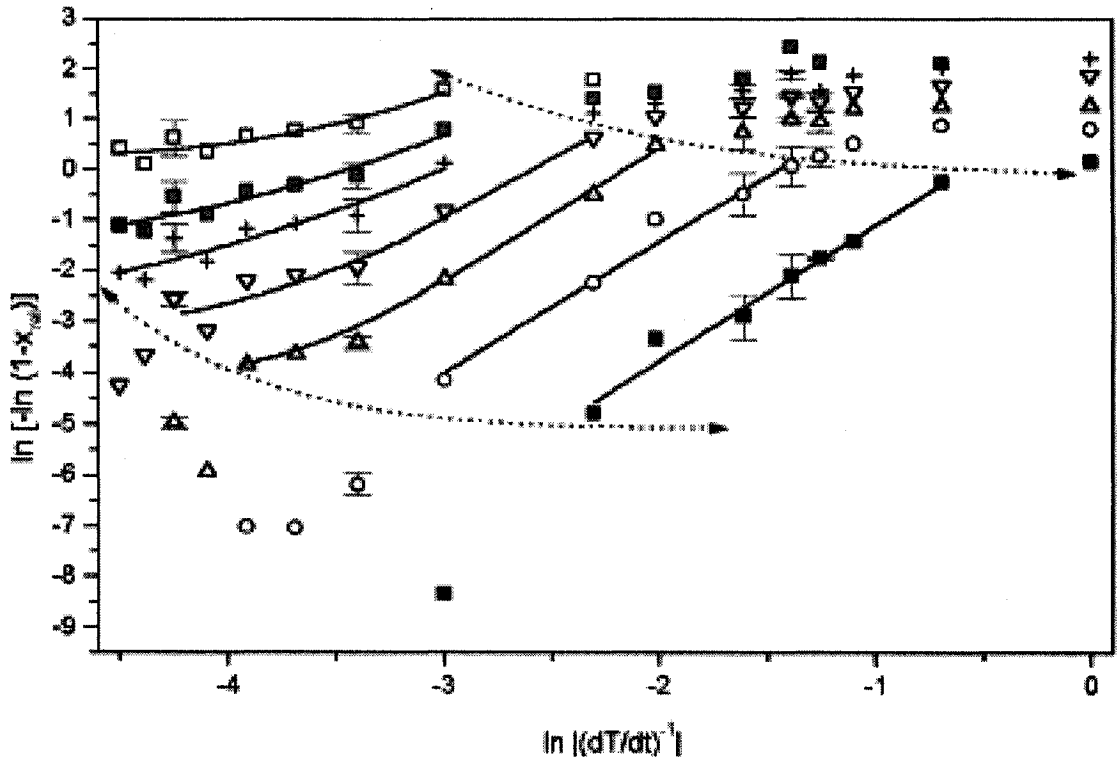


Fig. 2.6. Ozawa plot for non-isothermal crystallization at different temperatures for poly (ethylene terephtalate) :(□) 140, (●) 160, (+) 170, (∇) 180, (Δ) 190, (○) 200 and (■) 210 ° C. The data between doted lines corresponds to the conditions of unconstrained spherulite growth[61].

## 2.6. Three regimes of crystallization kinetics

Hoffman[62] defined three regimes of crystallization kinetics which differ in terms of the rate at which chains form the crystalline structure:

*Regime I. (Low temperatures)* This regime is characterized by very rapid crystallization and the growth rate is defined by:

$$G_{III} = b_0 i n_s a_0 \qquad [2.23]$$

Where $n_s$ is the mean number of stems placed in adjacent niche to the newly nucleated stem and $a_0$ is the molecular width. Thus chains preferably make few folds and enter the amorphous phase rather than undergo adjacent reentry. Then it can reenter the same lamella or switch to the next lamella.

*Regime II. (Intermediate temperatures)* In this regime, the rate of nucleation is larger than the rate of crystallization. As result multiple surface nucleations occur. To reach this state larger undercooling is necessary but the microkinetics of the crystallization remains the same and the polymer chain folds back and forth creating adjacent reentry.

$$G_{II} = \sqrt{b(2ig)} \qquad [2.24]$$

Where b is the layer thickness, $i$ is the primary nucleation rate, and $g$ is the substrate compaction rate.

*Regime III. (High temperatures)* In this case each surface nucleus completes an entire crystalline structure. After the beginning of crystallization, the polymer chain is laid in the crystal through the reptation mechanism and the growth rate in regime I can be expressed as:

$$G_I = \left(\frac{C_1}{n}\right)\exp\left(\frac{Q_D^*}{RT}\right)\exp\left(-\frac{K_{g(I)}}{T(\Delta T)}\right) \qquad [2.25]$$

Where $C_I$ is a preexponential factor for regime III, $n$ is the number of chain elements, $Q_D^*$ is the activation energy for steady-state reptation, $K_{g(I)}$ is the nucleation constant. Regimes III and II differ not only kinetically but also morphologically. In regime III axialites are usually observed while in regime II normal spherulites are observed. As the temperature is lowered from regime III to I the substrate completion rate per chain decreases but more chains crystallize simultaneously.

### 2.7. Crystallization behavior of polylactide

At this moment it is known that three structural modifications of polylactide crystals exist. They are characterized by different helix conformations and cell symmetries that develop upon different thermal and/or mechanical treatments. The α form grows from melt or cold crystallization and from solution-spinning processes at low drawing temperatures and/or low hotdraw ratios[63]. De Sanctis and Kovacs[64] first determined the chain conformation of α phase to be a left-handed $10_3$ helix, that packs into an orthorhombic unit cell with parameters a = 1.06 nm, b = 1.737 nm, and c = 2.88 nm. A few more recent analyses report slightly different parameters for the unit cell of this form. Extra 00l reflections have also been observed in the XRD experiments, suggesting some deviation from a pure $10_3$ helix conformation[63].

The β modification that was first observed by Eling et al.[65], develops upon mechanical stretching of the more stable α form or from the solution-spinning processes

conducted at high temperatures and/or high hot-draw ratios[66]. The crystal structure of the β modification has not been solved yet. Hoogsten et al. suggested an orthorhombic unit cell with a = 1.031 nm, b = 1.821 nm, and c = 0.900 nm, and a chain conformation with lefthanded $3_1$ helices. Instead, Brizzolara et al. proposed an orthorhombic unit cell with two parallel chains[67].

Very recent studies conducted by Puggiali et al. show that the β phase is an α frustrated structure of three three-fold helices in a trigonal unit cell of parameters a = b = 1.052 nm, c = 0.88 nm which is able to accommodate the random up-down orientation of neighbor chains associated with rapid crystallization conditions[66].

A third crystal modification of PLLA, the γ form, has been recently reported to develop upon epitaxial crystallization on hexamethylbenzene substrate, and has two antiparallel helices packed in an orthorhombic unit cell with a = 0.995 nm, b = 0.625 nm, and c = 0.88 nm[68].

The crystallization kinetics from melt for poly (L-lactide) has also been analyzed by a number of research groups. Isothermal bulk crystallization rates were determined over a wide temperature range, 70 to 165 °C[69]. The maximum in crystallization rate was observed around 100 °C, and the most peculiar behavior was a discontinuity in the kinetics around 110–120 °C (Fig. 2.7). This discontinuity has been correlated to a transition in spherulitic growth regimes II to III that was observed in the same temperature range[70] although other explanations of the unusual crystallization behavior of PLLA exist as well.

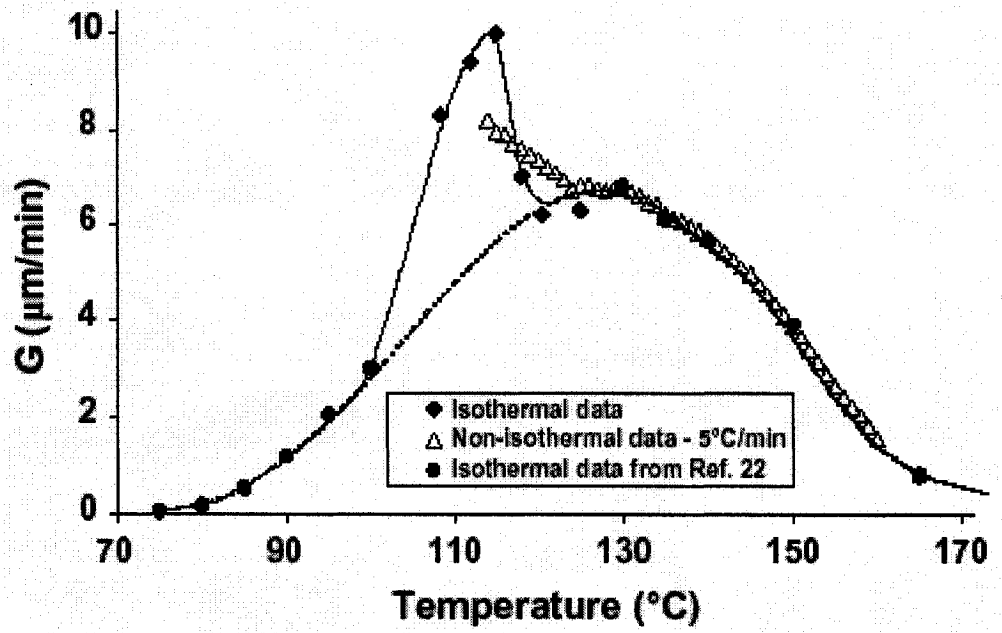


Fig. 2.7. Spherulite growth rates of poly (L-lactide) measured in isothermal and non-isothermal conditions[71].

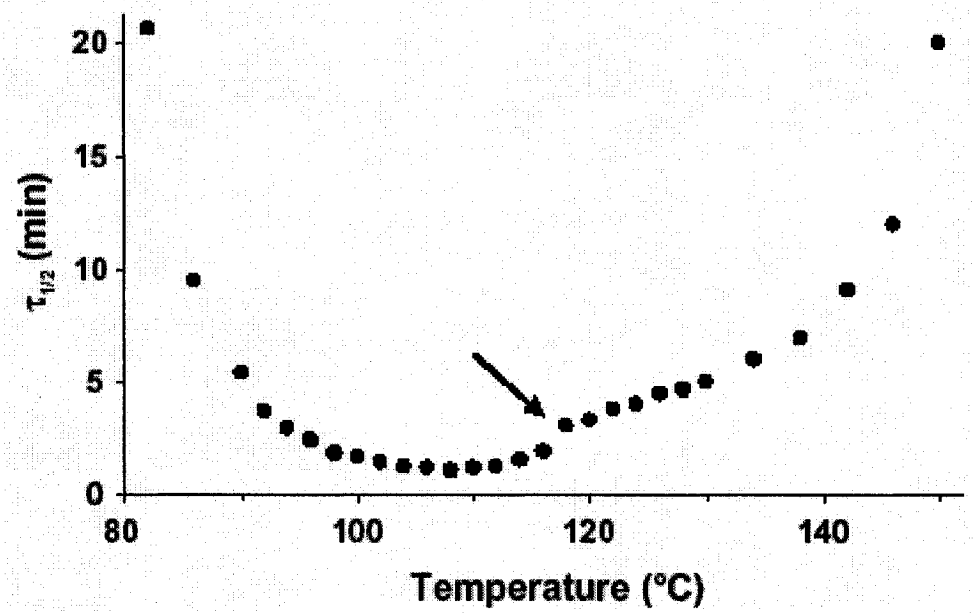


Fig. 2.8. Half-time of crystallization of poly (L-lactide) as a function of the isothermal crystallization temperature[71].

The half time of crystallization ($\tau_{1/2}$) of poly (L-lactic acid), measured under isothermal conditions after cooling from the melt, is reported in Fig. 2.8 as a function of temperature ($T_c$). As typical for polymers, the crystallization of PLLA is slow in the temperature ranges close to the melting point and the glass transition. In addition, the $\tau_{1/2}$ vs. $T_c$ plot presents a broad minimum around 108 °C and a discontinuity around 116–118 °C, indicated by the arrow in Fig. 2.8.

As shown in Fig. 2.8, below 120 °C the crystallization rate of PLLA is very high, due both to the high rate of spherulite growth and to the large nucleation density in this temperature range. A high number of simultaneously growing spherulites at a high rate corresponds to a large amount of heat evolved. The rapid development of latent heat may cause some local heating and create some thermal gradients within the sample, such that the phase transition occurs at temperatures that do not correspond to those detected by the instrumentation. This produces an increase in the experimental uncertainty associated with the experimental determination of $G$, both in isothermal and non-isothermal conditions. The error associated with non-isothermal measurements is higher, since the temperature is continuously reduced, and the cooling power of the hot stage may not be able to balance the latent heat rapidly developed during crystallization, perhaps giving a cooling rate lower than expected. This explains the discrepancy below 120 °C in growth rate values obtained during cooling at 5 °C/min as compared to data measured in isothermal conditions.

The morphology of the growing spherulites seems to vary in the whole explored temperature range, even during the very rapid increase of linear growth rate below 120 °C. Similarly, spherulites grown isothermally at various temperatures do not show any

noteworthy morphological difference, at least for the resolution power of optical microscopy, indicating that the abrupt increase in crystallization rate cannot be ascribed to changes in morphology occurring during growth at different temperatures. Crystalline structure analysis has also shown the effects of temperature on the nucleation rate of PLLA spherulites. Besides the large spherulites, smaller spherulites start to appear as the temperature is decreased. They have different sizes, being nucleated at various temperatures during cooling. However, the increase in nucleation density with decreasing temperature, commonly reported for polymers, is continuous, and does not display a rapid acceleration with temperature. Hence, the discontinuity in crystallization rate of PLLA below 120 °C has to be mainly ascribed to a drastic variation in crystal growth rate, and is not affected by abrupt changes in nucleation behavior. The sudden change in crystallization rate may be due to growth in a different crystal modification, which might be favored at temperatures below 120 °C[71]. The discontinuity in crystallization rate of PLLA reported above has been sometimes correlated with a transition in crystallization regime, observed in the same temperature range[72]. This issue will be addressed further in this work.

## 2.8. Stereocomplexation in L-/D-polylactide blends and its influence on polymer rheology and crystalline morphology

The formation of the stereocomplex from equimolar blends of poly (L-lactide) and poly (D-lactide) was first reported by Ikada et al[73]. Further research showed that nonequimolar blends can exhibit both homopolymer and stereocomplex crystallization[74]. For the last two decades stereocomplexation phenomena between two polylactide enantiomers has been studied by many researchers from the point of view of conditions that are advantageous for stereocomplex formation. Studies of asymmetric blends showed that stereocomplexation can occur even with less than 10 wt% poly (D-lactide) present in a blend[74]. It was found that stereocomplex formation is affected by numerous factors including blending ratio, molecular weight and optical purity of the enantiomers in the blend. Experimental conditions such as temperature and time after blending, blending mode and nature of the solvent also influence stereocomplex formation. For the exclusive stereocomplex formation low molecular weight and presence of the sufficiently long sequences of both L-lactide and D-lactide units are important[75]. Interesting to note that stereocomplexation can occur even in polymer blends of copolymers containing long sequences of the L- and D-lactides. Such kind of stereocomplexation was observed in blends of polyglycolide and L- and D-copolymers. For all kinds of polylactide systems there is critical sequence length of 15 isotactic units for stereocomplexation to occur.

It was found that for solution cast blends the most important factor for stereocomplexation is the molecular weight of the polymer. Stereocomplex crystallites are predominantly formed in blends of low molecular weight polymers. Blends of high

molecular weight polymers yield mostly mixtures of the L- and D- lactide homocrystallites[76]. Supposedly two main factors prevent stereocomplexation in high molecular weight blends. First, as concentration of the solution increases during casting, microscopic phase separation occurs. Thus, racemic crystallization is surpressed in phases that are rich in one of the enantiomers and homocrystallization prevails. Second, some researches indicate that racemic crystallization proceeds at slower rate than homocrystallization. The molecular weight also strongly affects stereocomplexation and this influence is much stronger than for homocrystallization. At normal drying conditions crystallites in films cast from blends of polylactides with molecular weight higher than 60 000 consist mostly of homopolymers[77].

The studies of crystallization from well mixed concentrated solutions of equimolar blends of L- and D-lactides showed that stereocomplexation proceeds more readily when good mixing conditions exist. This results in *gelation* since the formed crystallites of the stereocomplex act as three-dimensional crosslinkers[75]. (Fig. 2.9). This phenomenon is especially important for solution cast polymers because the lowest critical concentration for crystallization is lower for the stereocomplex than for homo-crystallites. Mechanical properties of the polymer are mostly defined by tie chains between crystalline structures; numerous tie chains in the 3D gelation structure yield better mechanical properties of the blends.

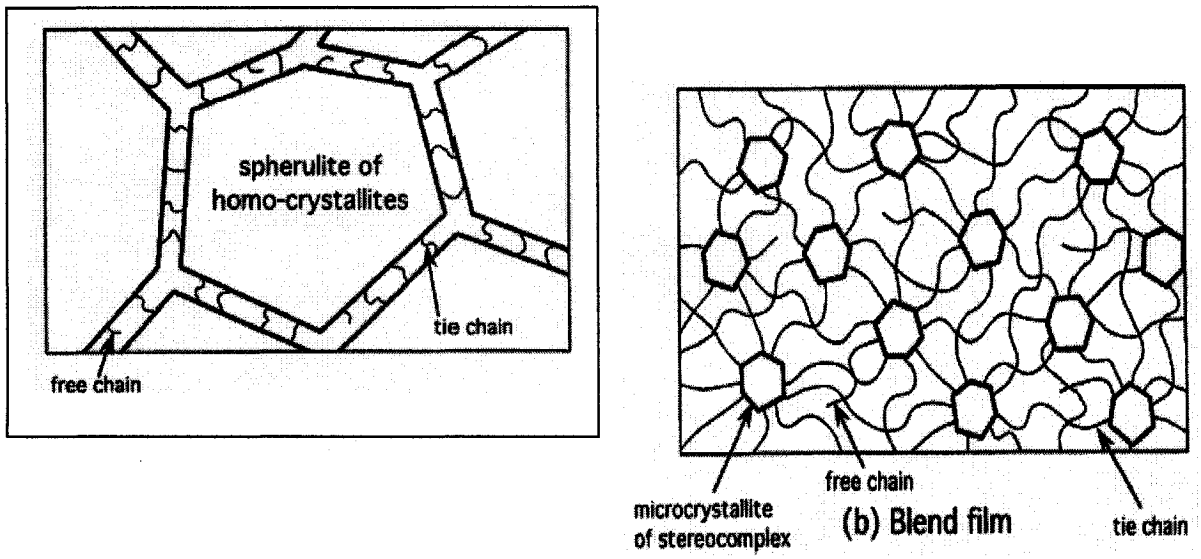


Fig. 2.9. The speculated crystalline structure of the polylactide for: a) non-blended film and b) L-/D-polylactide blend containing stereocomplex[75].

The studies have revealed that L-/D-polylactide blends with rich content of stereocomplex have significantly better tensile properties than polymer containing only homopolymers[75]. The most important effect on morphology of polymer is that while L- and D-polylactides form spherulites of large size on their own, even a small amount of streocomplex decreases their size. The suppressed spherulite formation in L-/D-polylactide blends may be attributed to the 3D gelation. This can be an explanation for better properties of the blended film since stereocomplexation suppresses formation of the large spherulites that give poor mechanical properties[78] (Fig. 2.10). The data presented in Fig. 2.11 shows that the polymer blend containing the highest concentration of the stereocomplex has better properties.

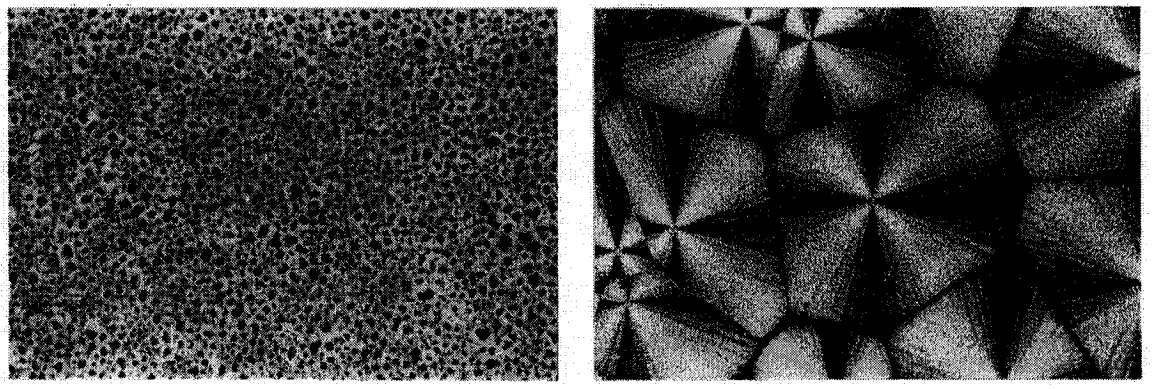


Fig. 2.10. Polarizing microscope photographs of equimolar L-/D-polylactide blend (left) and pure L-polylactide crystallized at the same conditions[75].

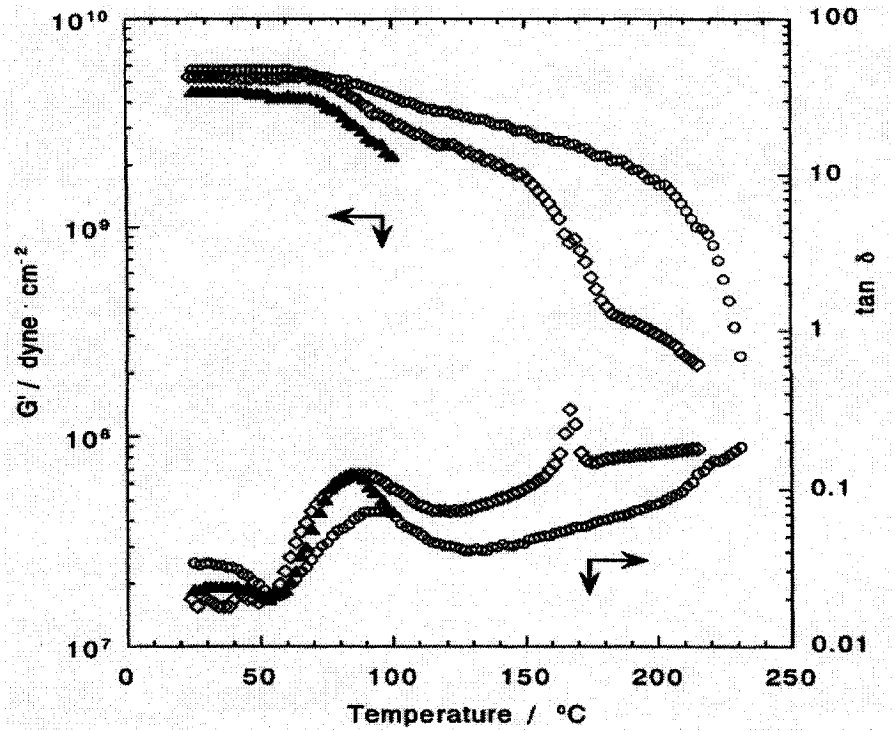


Fig. 2.11. Storage modulus (G′) and loss tangent (tan δ) for equimolar blend of PLLA and PDLA (○), for 1:3 blend of PDLA and PLLA (◊) and non blended PLLA (▲)[75].

## 2.9. Different approaches to crystalline morphology characterization: dilatometry, DSC, polarized optical microscopy and AFM

Many measurement techniques have been developed for the characterization of polymer crystallinity. They implement different polymer properties and phenomena for crystallinity characterization.

*Dilatometry* is a technique based on measuring changes of sample volume with temperature. Since the crystalline phase is up to 12 % denser than the amorphous one, the sample undergoes significant changes in volume during crystallization. The changes in volume are measured by a mercury filled capillary[79]. The dilatometery method has been well known for more than half a century. The experimental setup for the dilatometry is rather simple but results lack precision especially when crystallization proceeds quickly. Dilatometry data also can not give reliable information about crystallization mechanism[41].

*Differential scanning calorimetry (DSC)* is a technique based on measuring of the change in heat capacity of a material under controlled temperature conditions. DSC measures either the thermal energy difference required to keep the sample and reference at the same temperature conditions or the heat flux generated between the sample and reference. DSC can be used for isothermal crystallization kinetic studies. The sensitivity of the DSC technique has been greatly improved over the last decades. The use of computer software has significantly increased the versatility of the DSC technique. Many studies have proved that DSC is a very advanced technique for the characterization of polymer crystallization.

Hay et al.[80] reviewed the development of the use of DSC to study polymer crystallization kinetics. There are three approaches used to perform DSC analysis. First, the sample is cooled under a controlled rate from above the melting temperature. Second, the sample is quenched from above its melting temperature then heated under a controlled rate assuming that no crystallization takes place during the quench cooling. Third, the sample is rapidly cooled from above its melting temperature to the certain temperature and then the crystallization is measured under isothermal conditions.

The isothermal method assumes that no crystallization happens before the sample reaches the final temperature. This can usually be achieved since crystallization requires an induction time to start. There is an uncertainty in the analysis of the data and the determination of the zero time. Problems increase with decreasing of the isothermal crystallization temperature. DSC measures the rate of evolution of the enthalpy of crystallization *dH/dt* as a function of time. The rate curves can be processed by integration to determine the relative extent of crystallization as a function of time:

$$(X_h)_t / X_\infty = \frac{\int_0^t (dH_t / dt)dt}{\int_0^\infty (dH_t / dt)dt} \qquad [2.26]$$

Ozawa[59] and Harnisch and Muschik[81] developed methods for the study of non-isothermal crystallization kinetics by DSC. Recently isothermal crystallization studies of polymer blends by DSC have been reported. However, like other methods, such as dilatometry, nucleation and spherulitic growth rates can not be determined separately by DSC.

*Polarizing microscopy* is based on the study of the microstructure of objects using their interactions with polarized light. The principle of this very popular technique is based on the phenomenon that a birefringent specimen will split the incident plane of polarized light into two components. An unperturbed amorphous polymer is non-birefringent while crystalline structures are highly birefringent. This allows us to optically distinguish crystalline structures.

The hot-stage is a device coupled with the polarized microscope in which the temperature is controlled. As nucleation and spherulite growth are very temperature dependent, a precise temperature control is necessary. Advanced hot-stages can provide thermostatic control with ±0.03 °C precision, and temperature program rates up to 20 °C/min. One of the objections to the study of thin films of crystallizing polymers is that thermal degradation can lead to erroneous results. There are methods that can be used to minimize this effect such as surrounding the polymer with silicone oil of a suitably high viscosity or measuring the polymer sample under a nitrogen environment.

The advantage of hot-stage polarizing microscopy is that nucleation and growth rate can be easily studied allowing the rates of transformation to be measured independently. The use of this method is however limited to cases where nucleation and spherulite growth can be resolved optically. The details of the birefringent structure are themselves of considerable importance in providing information on morphology. This method is widely used to study the crystallization of polymer blends and their mechanisms[82], most previous reports of optical microscopy using a hot-stage were limited to measurements of individual spherulitic growth and growth in the early stages

of crystallization because the measurement of overall crystallization is not easy. A computer with digital image processing is the tool to solve the problem.

Since its invention in 1986, applications of *Atomic Force Microscopy (AFM)* to the study of soft, organic materials have spread rapidly[83]. Classes of organic materials for which new information was obtained by AFM range from rigid polymers to soft biological molecules and lipids, from highly ordered polymer single crystals to amorphous and liquid-crystalline materials, from molecular monolayers to bulk material, from thin films to fibrillar structures, and from pure compounds to multicomponent composite materials[84]. AFM recently proved its versatility in a large number of morphological studies on polymers[85, 86]. AFM provides the possibility to examine semi-crystalline structures down to the level of lamellar and even molecular organization[87, 88]. In addition, the high resolution and non-destructivity of AFM offer a unique possibility for the repetitive examination of individual elements of the semi-crystalline structure. Such imaging performed on a single polymer spherulite during its isothermal crystallization and subsequent reheating to higher temperatures was first reported by Ivanov et al[89]. The main technical difficulty of these measurements consists in the fact that typical ambient AFM setups preclude heating samples in situ and an advanced hot-stage device is needed.

Application of the AFM technique to molecular films of organic materials includes characterization of their structure on a micrometer, submicrometer and nanometer scales. Heights, depths, roughness, in-plane molecular ordering, defects and in-plane orientation of molecules can be measured. AFM allows making modification of molecular films including hole-making, formation of texture patterns, drawing figures on

a submicrometre level and cleaning surfaces. These advantages of the AFM technique to make reliable observations of ordered molecular films from organic compounds, including small molecules, polymers and lipids made it a very popular means for materials characterization.

Recent applications have extended the range of AFM applications to measurements of forces between surfaces, surface stability, wear, adhesion and elasticity[90]. The sensitivity of the AFM technique to weak surface forces and local mechanical properties on a nanometre scale makes it valuable for study of the surface properties of polymeric materials. Various modifications of the AFM technique were built and used extensively for probing different surface properties including lateral (friction) force microscopy, magnetic force microscopy, electrostatic force microscopy[91]. Among the intensively studied local surface properties are surface viscosity, stiffness and elasticity of composite organic films and forces of interaction between surfaces at nanoscale distances. The AFM tip was also used for structural modification of the surfaces on a submicrometre scale sometimes called surface nanolithography.

Numerous examples of AFM studies had been reviewed by Magonov and Cantow[92]. A partial list of polymeric substances studied by AFM includes: polyethylene[93], cellulose[94], Kevlar and polyimide fibres[95]; ion-containing polymers[96]; latex dispersions of polymers[97]; polyimide droplets[98]; films of mixed polyethylene and polypropylene[99]; ethyleneepropylene copolymers[100]; block polymers[101], single crystals of linear and cyclic alkanes[102]; fluorinecontaining polymers[103]; polystyrene and crystalline polycarbonates[91].

## 3. Experimental methodologies

### 3.1. Materials and chemicals

Dichloromethane was chosen as solvent for solution casting because of its ability to dissolve even high molecular weight polylactides and its high volatility. Dichloromethane of 99.5 % purity was supplied by ACROS. The characteristics of the polymers, used in experiments are listed in Table 3.1.

Table 3.1. Data on polylactides samples.

| | L 9000 | Purasorb PD | Purasorb PL |
|---|---|---|---|
| Manufacturer | Biomer | PURAC | PURAC |
| Country of origin | Germany | Netherlands | Netherlands |
| Composition | L-polylactide with 2 % D-content | Pure D-polylactide | Pure L-polylactide |
| Molecular weight $M_n$ | 220 000 | 350 000 | 350 000 |
| $M_n / M_w$ | – | 2.0 – 3.2 | 2.0 – 3.2 |
| Melting temperature $T_m$, °C | 171 | 181 | 181 |
| Glass transition temperature $T_g$, °C | 57 | 59 | 59 |

### 3.2. Sample preparation for elongational measurements

The solution cast films were prepared from a 2 wt. % poly (D, L-lactide) solution in dichloromethane by casting in a flat bottomed Pyrex glass vessel. Since the partial pressure of dichloromethane under ambient conditions is high, a controlled evaporation of the solvent through a porous barrier over 2 days was performed, allowing us to obtain uniform and clear films with an average thickness of 70 μm. The thickness of the films was controlled by the volume of solution used for film casting.

For Experiment 1, freshly cast and up to 24 hours old film samples were used. In Experiment 2, samples were dried at room temperature for 28 days under conditions that allow solvent to evaporate freely. In Experiment 3, samples were dried for 44 days under ambient conditions and for 48 hours at 41° C immediately before the test. This temperature is slightly higher than the boiling point of dichloromethane under normal atmospheric pressure.

Hot pressed samples were prepared from the same L9000 poly (D, L-lactide) pellets in a Carver press at 185 °C and 4 MPa, in the form of films with average thicknesses of 160 μm. For pressing, a custom made brass mold was used. The cooling of the pressed samples was performed under a constant pressure of 1 MPa and a high cooling rate was maintained to reach low polymer crystallinity. These samples were used as references of samples free from solvent.

### 3.3. FT-IR analyses

The residual solvent content was analyzed by FT-IR spectrometry (ThermoNicolet Nexus 670 FT-IR spectrometer) using a reference dichloromethane IR spectrum from the Aldrich spectral library and the spectrometer's analytical software. For the highest possible sensitivity, a sampling rate equal to 256 $s^{-1}$ was selected for all FT-IR analysis.

### 3. 4. Elongational experiments

Uniaxial film stretching was carried out by a miniature screw driven stretching device that was constructed along the lines of that used by Hild et al[104]. This device has maximum stretching capability of 95-100 % elongation using 52 mm by 2 mm film samples (Fig. 3.1.). For the elongational experiments with this stretching device, a wide range of the film thicknesses can be used.

Isothermal heating was performed in the heating chamber of the Physica Modular Compact Rheometer MCR 500 with ±0.1 °C accuracy. All samples were kept in the sealed heating chamber for 15 minutes prior to test to ensure thermal equilibrium. Stretching was performed at strain rates less than 0.005 $s^{-1}$. Polylactide has a very low elongation to break of 2.7 %[105] at temperatures below its glass transition. When the polymer surpasses its glass transition temperature it is possible to stretch the sample more than 140 %. In order to evaluate maximum elongation, the sample's length was measured before and after stretching with 1 % accuracy. At temperatures close to the glass

transition, the polymer lacks elasticity and even small inhomogenieties in thickness can cause 'necking'. In this case, the measured elongation until break is lower than the true polymer elongational properties. For this reason, several measurements were performed at each temperature to ensure higher reliability of the results.

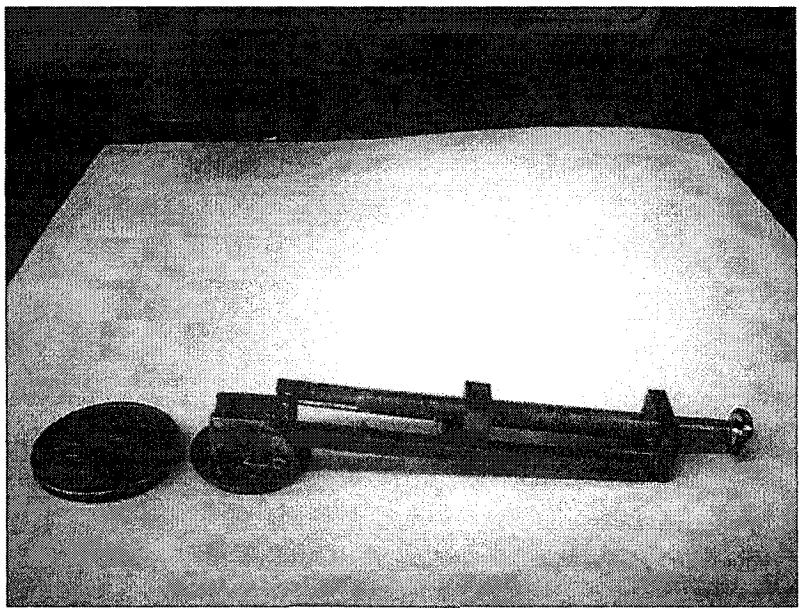

Fig. 3.1. The miniature stretching device.

It was considered that the sample reached the glass transition temperature when it could be stretched at least 90 %. Usually samples capable of stretching 90 % or more showed very little or no strain whitening and this fact indicates that the sample has surely reached the glass transition temperature.

### 3.5. DSC analyses

DSC measurements were performed using a Thermal Analyst 2100 device at 5 K/min. Sample weight ranging 6 to 8 mg was used for each analysis. Glass transition temperatures and curve extremums were determined using the DSC analytical software.

### 3.6. AFM analyses

For polymer surface morphology studies, a Digital Instrument Nanoscope IIIa Atomic Force Microscope was used in Tapping Mode. For the surface probing, aluminium coated NSC-15 silicon tips made by MikroMash were used. These probes have a 125 μm cantilever and a tip curvature of about 20 nm (Fig. 1.12). The average spring constant for the cantilever was about 40 N/m. Typical scanning parameters are given in Table 3.2. All analyses were performed using v.5.12 Nanoscope software.

Table 3.2. AFM imaging conditions.

| Parameter | Value |
|---|---|
| Scan rate | 0.12 – 1.0 Hz |
| Scan size | 5 – 100 μm |
| Gain offset | 0.9 – 0.95 |
| Integral gain | 0.55 – 1.6 |
| Proportional gain | 0.42 – 0.85 |
| Resonance frequency | 272 – 326 kHz |

### 3.7. Sample preparation for the crystal growth kinetics and morphology studies

For the main experiments, three different polylactides were used. Their basic properties are described in Section 3.1. In order to reveal the surface crystalline morphology using AFM, polylactide films much thinner than those used for the elongational experiments were necessary. Polymer films were cast on a glass surface using the following procedure. A drop of a 0.1 wt. % polylactide solution in dichloromethane was placed on a 120 μm thick glass substrate. Evaporation of the solvent was performed in an environment allowing a controlled evaporation rate in order to reach full solvent removal in 2 – 3 hours. The thickness of the film was determined by profiling a groove (Fig.3.2) made by a sharp stainless steel razor. The resulting film thickness was about 500-600 nm according to cross-section analysis of AFM images. (Fig. 3.3).

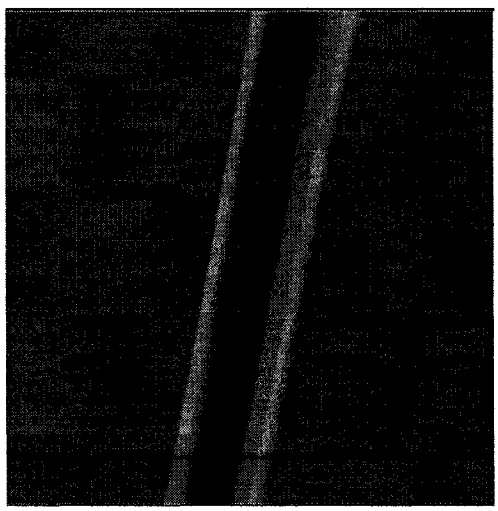

Fig.3.2. AFM height image of the groove made on surface of the solution cast film. The scan size is 100 μm.

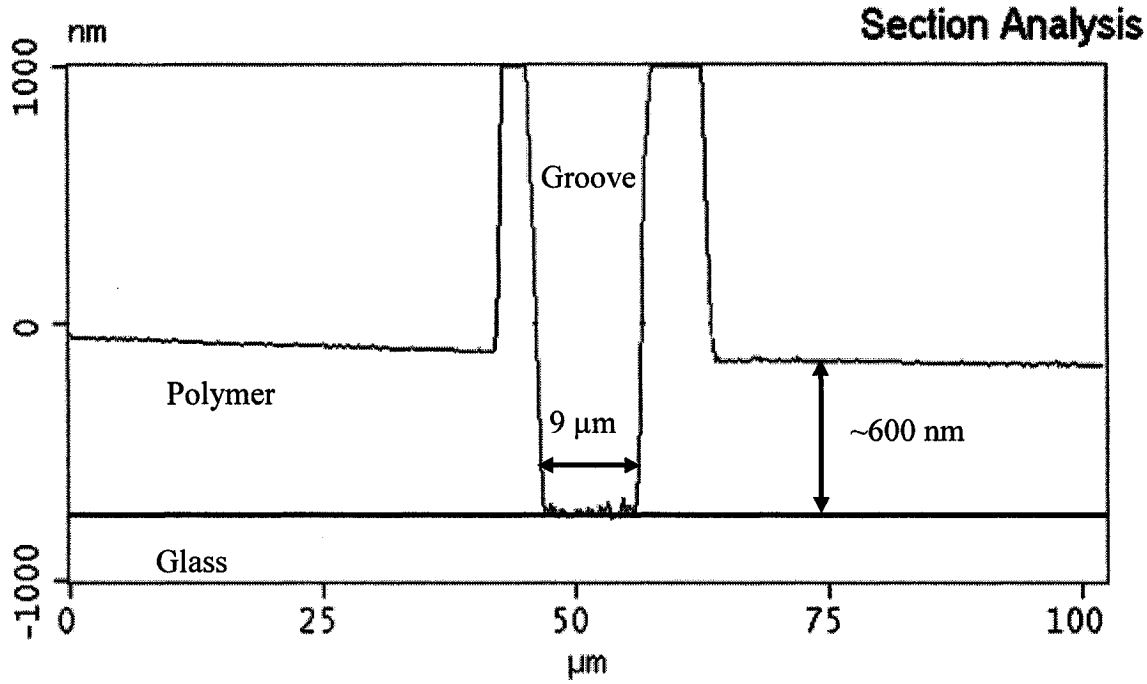


Fig. 3.3. Example of cross sectional analysis.

The apparent inclination of the polymer surface is caused by the non-proportional X (nm) and Y(µm) scales in this figure. The real non-uniformity of the polymer surface for this casting technique is very low.

To eliminate excess nucleation in the solution cast films, samples were premelted for 3 minutes at a temperature approximately 10 K higher than the melting point. All thermal treatments were performed in the heating chamber of the Physica Modular Compact Rheometer MCR 500 with ± 0.1 °C accuracy. For thermal treatment samples were placed on an aluminium pan allowing better heat distribution. To freeze the amorphous structure, the samples were quenched in air. Due to a very small sample size, cooling rates up to 3000 K/min can be achieved under ambient cooling conditions. The aluminium pan acts as a heat dissipating radiator thus increasing the cooling rate.

Similarly, the sample heating rate was very high due to the high thermal capacity of the heating chamber and the small sample size. This allows maintaining conditions close to isothermal. It was found during experiments that temperature deviations caused by sample insertion into the chamber are less than 1 K and the temperature control system compensates for this deviation in approximately 40 seconds.

It is known that humidity could influence many properties of polymers. Since all experiments were carried out at room conditions all series were done same day to minimize influence of humidity.

### 3.8. Sample alignment technique

Since the thermal treatment and imaging of the samples were done in different devices a technique that allows repeated imaging of the same area of sample surface is necessary. This problem is complicated by that fact that the sample surface is many thousand times bigger than the imaging area. There are many techniques that allow imaging repeatedly the same area such as that described by Ivanov et al[89]. All of these techniques involve the use of specialized materials and equipment. For this reason, a simple and reliable technique was developed.

This alignment technique is based on mechanical marking of the samples using a sharp razor. Step by step description of the sample alignment technique is given below:

1. Two grooves are made on the surface of the sample using a regular sharp razor. They intersect each other in the middle region of the sample at approximately 90°.

2. The sample is placed in the AFM setup so that the intersection point of the grooves is exactly placed on the left lower corner of the video monitor and the grooves follow the screen sides. This can easily be done using the AFM screw driven positioning device.

3. Next the area of interest is identified and a reference AFM image is taken. Typically a 50 μm size scan is enough for alignment purposes.

4. After the cantilever is disengaged the reference coordinates, $X_R$, $Y_R$, $S_R$ are taken from the screen. $X_R$ is distance from the end of cantilever to the left side of the screen, $Y_R$ is the distance from the end of cantilever to the bottom edge of the monitor and $S_R$ is the maximum deviation of the groove from the vertical position. (These coordinates are shown in Appendix I).

5. The area of interest is studied starting from the previously defined reference point.

6. Now the sample can be withdrawn from the AFM and subjected to the thermal treatment as planned. After the thermal treatment, the sample is returned to AFM and positioned as it was described in step 2. Since it is very difficult to place the sample manually while maintaining the same angular position of the substrate, the reference deviation, $S_R$, is used to calculate necessary correction of the scan angle, Θ, calculated as follows:

$$\Theta = \arctan\left(\frac{S_R - S_R^{new}}{195}\right) \qquad [3.1]$$

where $S_R^{new}$ is the deviation for the second reference scan explained in step 7. This calculated value is put into the AFM scan angle settings and thus corrected for by the AFM software.

7. The cantilever is placed over the sample so that its end is positioned with respect of the reference coordinates and a second reference image is taken, with a scan size the same as that of the first reference image.

8. Typically even after a deep thermal treatment the second reference image contains many surface features that remained unchanged. Next the difference between the position of second reference scan and the first reference scan is measured in both X and Y directions and these values are put into the AFM scan offset. It was found that this manual positioning allows placing the cantilever with 5 μm precision, therefore a 50 μm scan is enough to recognize all features. The software correction of the cantilever position makes possible positioning with the deviation of less than 1 μm. A detailed schematic of the sample alignment procedure is given in Appendix 1.

The sample alignment procedure described above is suitable for most samples as long as the groove remains unchanged after thermal treatments. This technique was successfully used for thermal treatments of thin films including polymer melting. In those experiments the grooves remained unchanged due to the strong surface tension forces in the liquid thin polymer films.

## 4. Results and discussion

### 4.1. Residual solvent content analysis using FT-IR spectroscopy

It is well known that even a small amount of residual solvent can significantly decrease the glass transition temperature due to the plasticizing effect. This effect is related to the facilitation of the movement of the polymer chains when surrounded by low molecular weight additives. Therefore special attention was paid to the determination of its content in the polymer under consideration. Dichloromethane was used as solvent in this research due to its good dissolving properties and high volatility. This solvent is one of the most popular ones for poly (D, L-lactide) dissolution used in pharmacological studies and numerous researches gave a clear idea concerning solvent removal techniques and its content analysis.

In research, we used FT-IR analysis to control solvent residue content. According to Doelker[106] solvent removal from a polymer is a two-stage process: the first is a boundary layer phenomena depending on solvent volatility and equilibrium vapor pressure; the second which is much slower, is determined by the solvent's diffusion coefficient in the polymer. Clearly in the case under consideration, it is the second stage that limits the solvent removal process. It was shown by Newman and Nunn[107] that an additional vacuum treatment may have no positive effect on the drying process; therefore vacuum drying was not used in this research. Nevertheless long term drying at ambient conditions for more than 1 month was used to ensure the sample's purity.

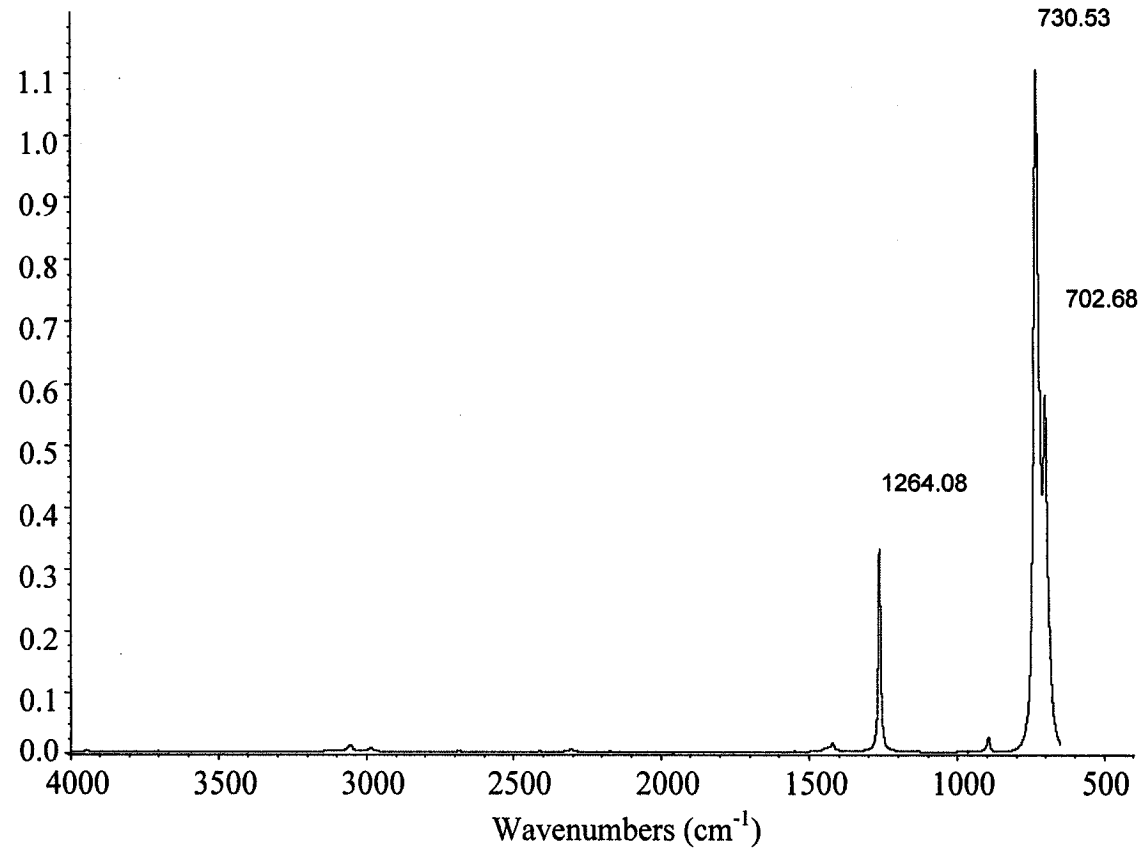


Fig.4.1. Reference absorbance spectrum of dichloromethane from the Aldrich spectral library.

The IR spectrum from the Aldrich spectral library is shown on Fig. 4.1. Based on this spectrum it was expected that solvent residue should give peaks in the 700 – 706 $cm^{-1}$ and 730 - 737 $cm^{-1}$ regions that can be easily distinguished. Spectra of the cast films were compared with those of the hot pressed sample in order to reveal dichloromethane residue.

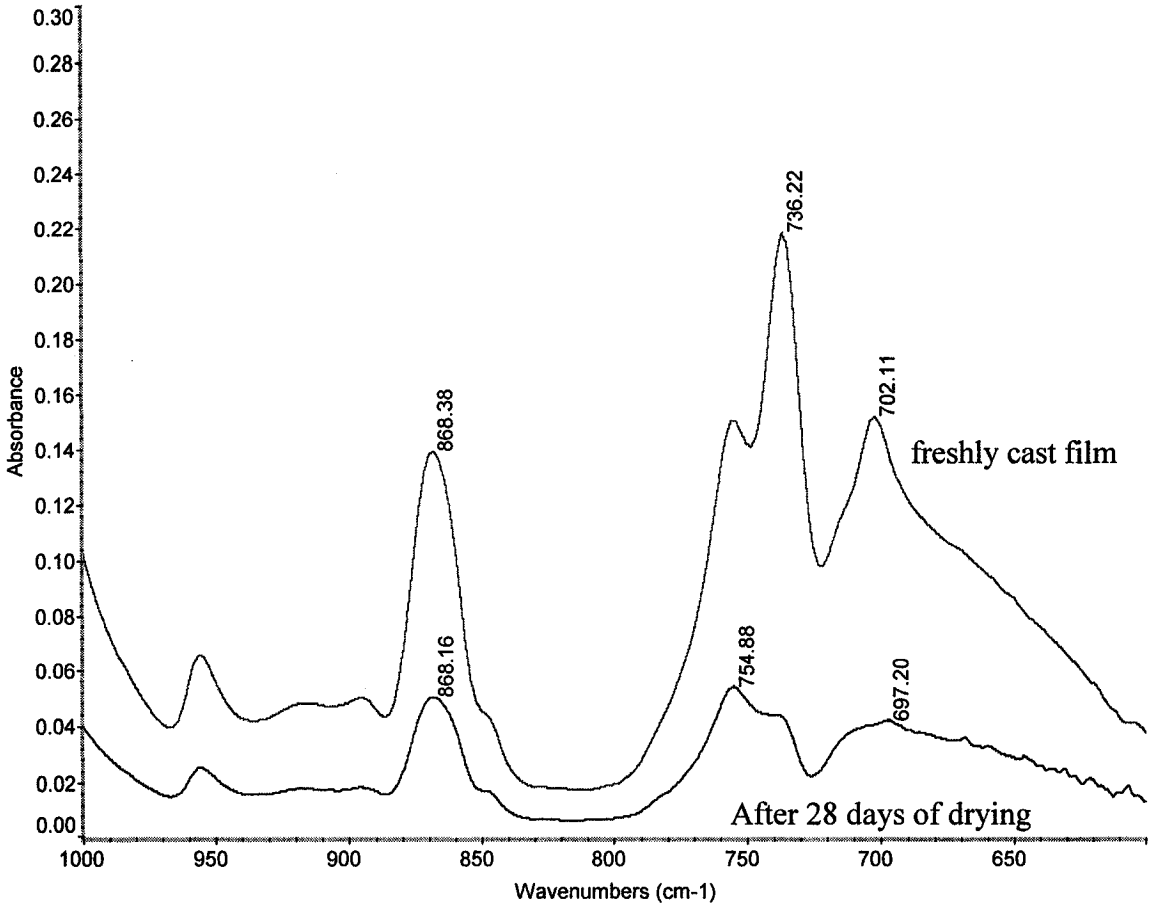


Fig. 4.2. The absorbance FT-IR spectrum of freshly cast and dried L 9000 poly (D, L-lactide) films.

Two small peaks at 736 $cm^{-1}$ and 702 $cm^{-1}$ clearly indicate presence of some residual solvent in freshly cast film. The smallest reference peak at 1268.08 $cm^{-1}$ is masked by a strong polymer peak at 1179 $cm^{-1}$ and is not distinguishable at all.

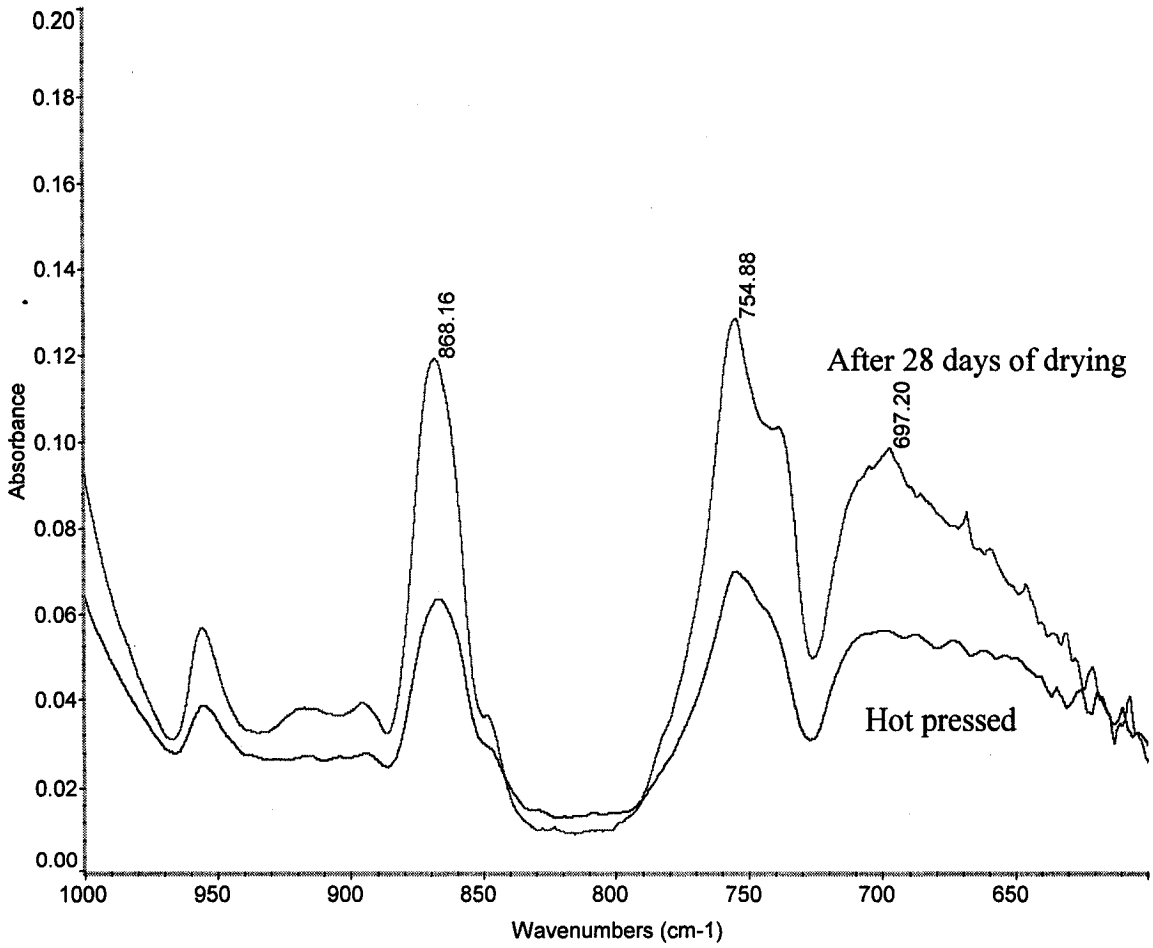


Fig. 4.3. The absorbance FT-IR spectrum of the hot pressed and solution cast dried L 9000 poly (L, D-lactide) films.

Comparison between the FT-IR spectra of the hot pressed samples and those of the solution cast films after 28 days of drying under ambient conditions revealed no presence of the solvent (Fig. 4.3). As expected the FT-IR spectra of the freshly cast poly (D-lactide) film is not distinguishable from the FT-IR spectra of the poly (L-lactide) (Fig. 4.4). Taking into account previous research results and the FT-IR data it can be concluded that in matter of several days residual solvent content becomes very low even under ambient conditions. It should be noted that despite the fact that no solvent traces

were found on FT-IR spectra small amounts of residual solvent can strongly influence the properties of the solution cast film.

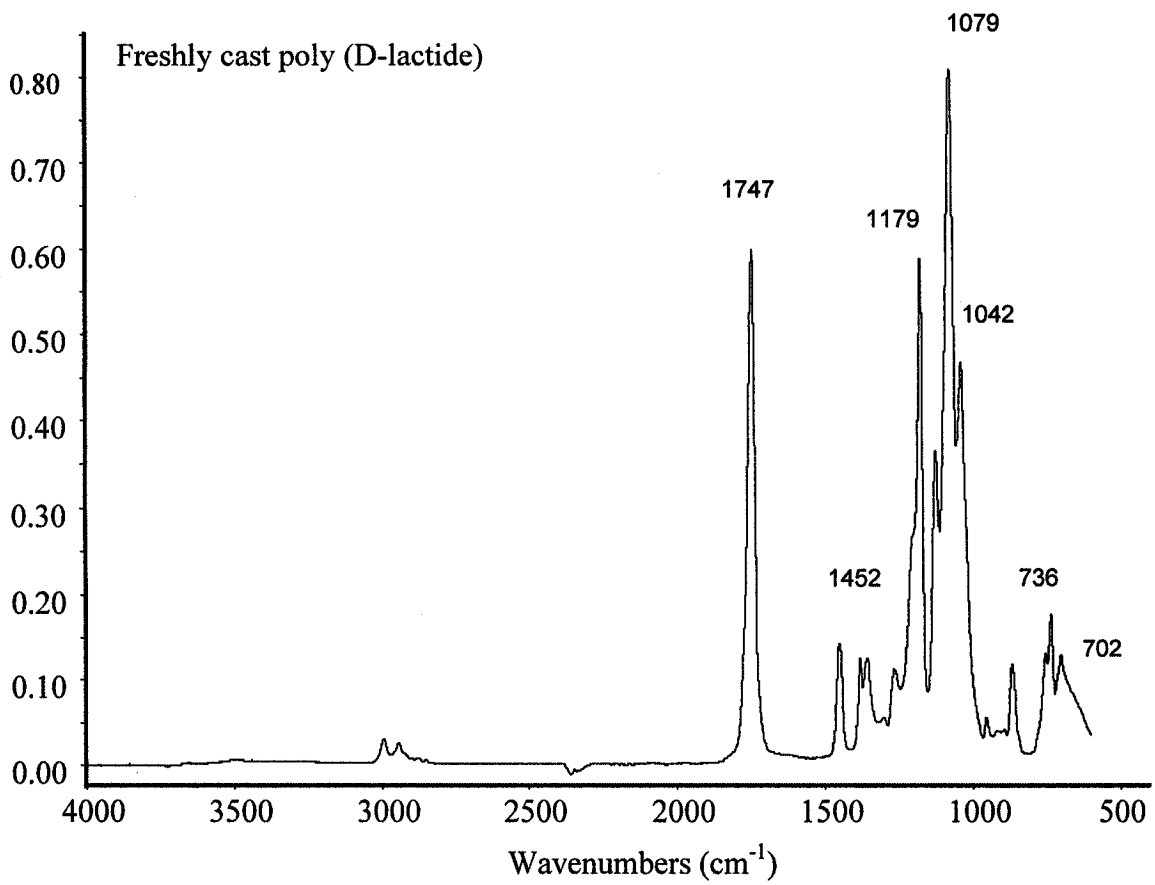


Fig. 4.4. The absorbance FT-IR spectrum of the freshly solution cast Purasorb PD poly (D-lactide) film.

### 4.2. Isothermal elongational measurements

Mechanical properties of polymers are strongly affected by the glass transition and can thus be used to detect the glass transition. Typically the modulus *E* decreases up to 1000 times and elongation till break can increase more than 100 times[108] upon leaving of the glassy region. In this project we use uniaxial elongation measurements at constant temperature for detecting the glass transition region. As the model for all experiments the solution cast L 9000 poly (D, L-lactide) film is used and dependence of elongational properties on temperature is compared to those of hot pressed poly (D, L-lactide) prepared from the same polymer. Presumably the glass transition temperature may depend on the preparation of the polymer samples. Since some amount of solvent remains in solution cast films even after long term drying, the influence of this residual solvent on the elongational properties of polylactide was studied. The glass transition temperature determines the lower limit for crystallization and elongational properties of polylactide were used to detect its glass transition temperature. Important issues regarding to the removal of the solvent from the solution cast polymer films also were considered.

The experimental results can be seen in Fig. 4.5. and the data for the $T_g$ determined as 90% elongation at break temperatures are given in Table 4.1. Results of the uniaxial stretching for the hot pressed poly (D, L-lactide) shows that the isothermal glass transition temperature for the bulk polymer is equal to 53.1 °C. This result correlates well with previously obtained DSC data for $T_g$ taking into account the kinetic nature of the glass transition phenomena. The higher data spread can be explained by significantly less uniformity of the hot pressed polymer film.

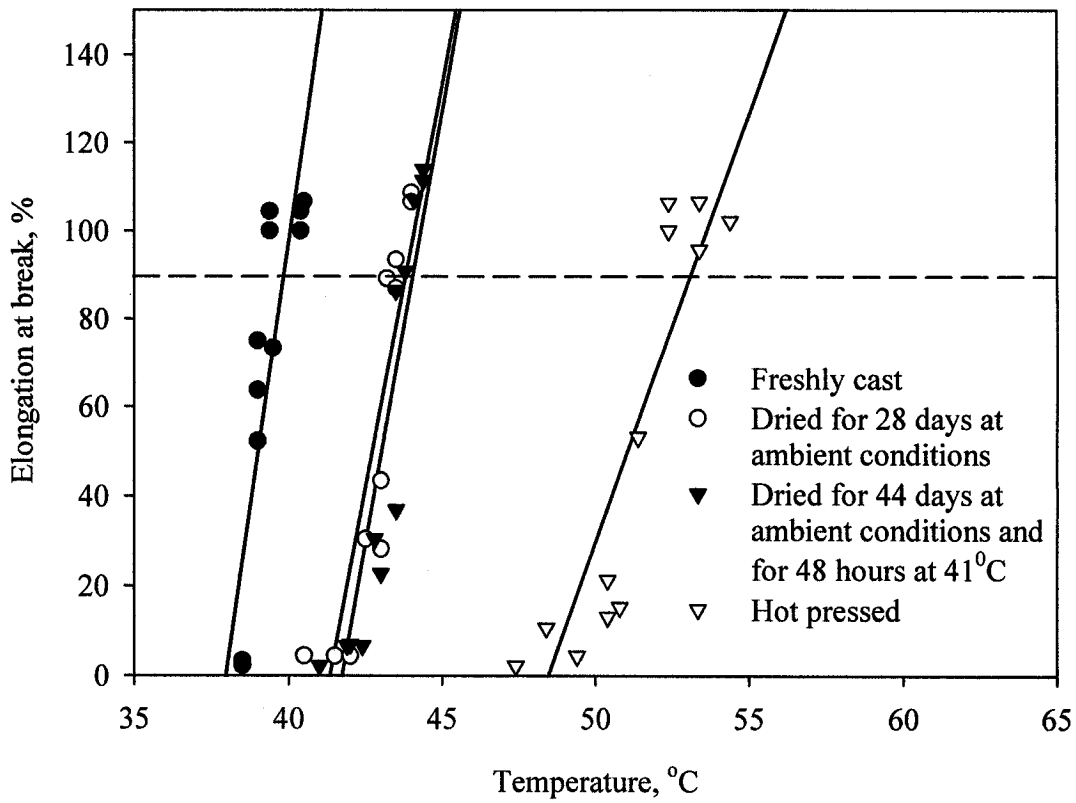


Fig. 4.5. Results of the isothermal uniaxial stretching of the L9000 poly (D, L-lactide). The dashed horizontal line represents 90% elongation.

Data from experiment 1 obviously indicate that residual dichloromethane acts as plasticizer in poly (D, L-lactide) and decreases the glass transition temperature. In experiments this decrease is found to be 3.8 °C from 43.7 °C to 39.9 °C. It should be noticed that rate at which dichloromethane volatilizes from polymers is high even at ambient conditions therefore it is very difficult to obtain results that would quantitatively express plasticizing effect of the dichloromethane on poly (D, L-lactide). Nevertheless results clearly indicate existence of this effect. Taking into account FT-IR analyses results it should be concluded that even trace amounts of the residual solvent can

significantly decrease the glass transition temperature in polylactide. It can be expected that annealing at higher temperature will increase glass transition temperature.

Table 4.1. Results of the isothermal uniaxial stretching of the L9000 poly (D, L-lactide).

| Experiment | 90 % elongation temperature (°C) |
|---|---|
| Hot pressed sample | 53.1 |
| Experiment 1 | 39.9 |
| Experiment 2 | 43.7 |
| Experiment 3 | 44.0 |

From the FT-IR analysis it was established that the samples used in experiment 2 contained residual solvent in amounts that can not be detected. Surprisingly this sample demonstrated significantly lower Tg than the hot pressed sample with the difference exceeding 9 °C.

In order to observe possible deviations from this anomalous low glass transition temperature, the polymer sample in experiment 3 was dried at ambient conditions for extra 18 days and was subjected to 48 hour drying at 41 °C. Experiment 3 results show that glass transition temperature of solution cast poly (D, L-lactide) stabilized on 44.0 °C and did not change significantly as compared to experiment 2. Difference in glass transition temperature for samples in experiment 2 and 3 is approximately 0.3 °C and possibly explained by the inaccuracy in measurements.

From the isothermal stretching results it can be seen that the data are significantly scattered. This phenomenon is concerned with a peculiar feature of mechanical stretching. In the region very close to the glass transition, stresses exerted on the sample to stretch it can be high and any slight sample defects and uneven thickness can cause premature breakage even if the sample did not reach its overall breaking point.

### 4.3. Residual solvent influence on glass transition as observed by DSC

DSC data are presented in Table 4.2 and Fig.4.6. The obtained results confirm the lowering of the glass transition temperature in solution cast poly (D, L-lactide) films as compared to the hot pressed polymer.

DSC data also confirm this glass transition temperature shift. It can be seen that according to the DSC data, the difference is approximately 8 K. Especially interesting is that the cold crystallization extremum is shifted in the same direction and by the same amount. This fact confirms that in solution cast films, the concentration of the nucleation sites is much higher than in bulk polymers.

All of the DSC results and the isothermal elongational measurements are in good agreement. Even trace amounts of solvent that can not be determined by FT-IR significantly influence the polymer chain mobility and thus decrease the glass transition temperature of polylactide.

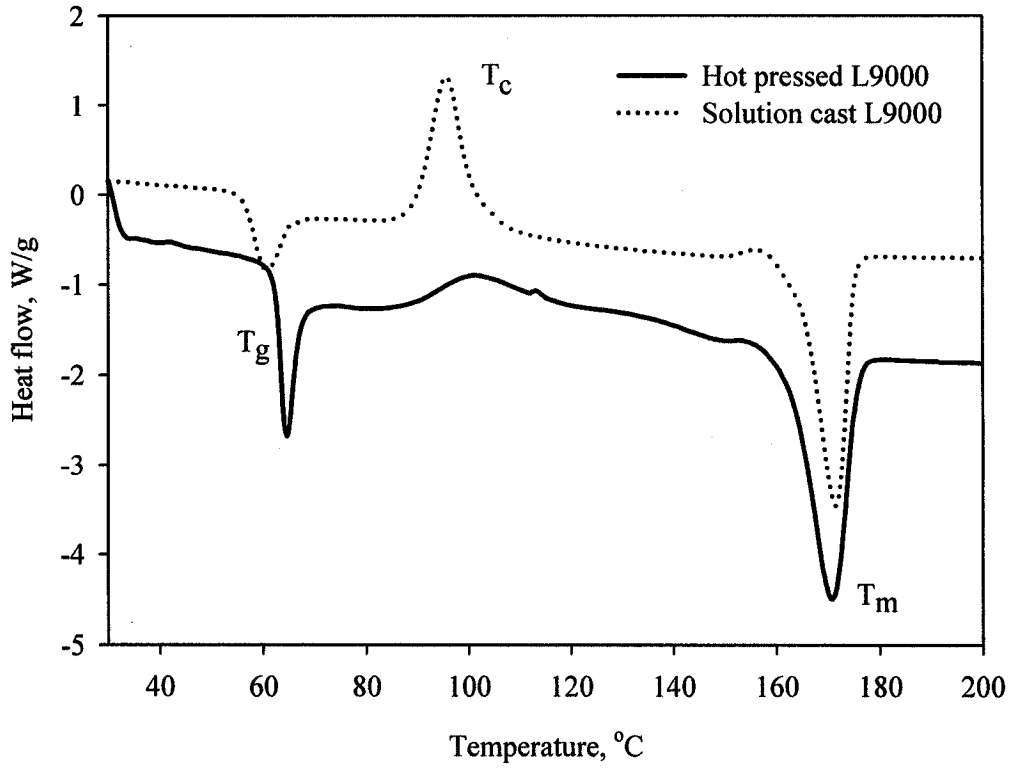


Fig. 4.6. Comparative DSC curves for hot pressed and solution cast poly (D, L-lactide). Only the heating experiment is shown. $T_g$, $T_c$, $T_m$ represent glass transition, cold crystallization and melting peaks respectively.

Table 4.2. Properties of poly (D, L-lactide) obtained from DSC data.

| Polymer | Glass transition temperature, $T_g$, °C | Cold crystallization maximum, $T_c$, °C | Melting point, $T_m$, °C |
|---|---|---|---|
| Hot pressed | 63.52 | 101.54 | 171.67 |
| Solution cast after 36 days drying (experiment 2) | 55.90 | 93.62 | 171.13 |

It is very interesting that the cold crystallization peak is also shifted by approximately 8 K. This can be explained by the fact that the residual solvent acts as a nucleating agent. The area under the cold crystallization peak for the solution cast film is also bigger than for the hot pressed sample, therefore the overall crystallinity that it is reached in the DSC experiments is higher for this sample.

### 4.4. Influence of the experimental scan rate on the observed glass transition temperature of polylactide

The theory of the kinetic nature of the glass transition temperature is supported by experimental data for the L 9000 polylactide. On Fig. 4.7 combined data for different temperature scan rates are presented. Data for the 20 K/min and 2 K/ min scan rates are taken from the Biomer data sheet for L 9000 polylactide[105]. Data for the 5 K/min scan rate is obtained from our DSC analysis and the isothermal glass transition temperature (0 K/min) is obtained from the elongational experiments.

With increasing scan rate, the observed glass transition temperature increases, in good agreement with the modern glass transition theory. The experimental data can be interpolated by a power law equation, correlating well with other experimental studies[35]. For our data power law equation can be expressed as:

$$q = 0.0624 * T_g^{4.217} \qquad [4.1]$$

where $q$ is the cooling/heating rate, in K/min.

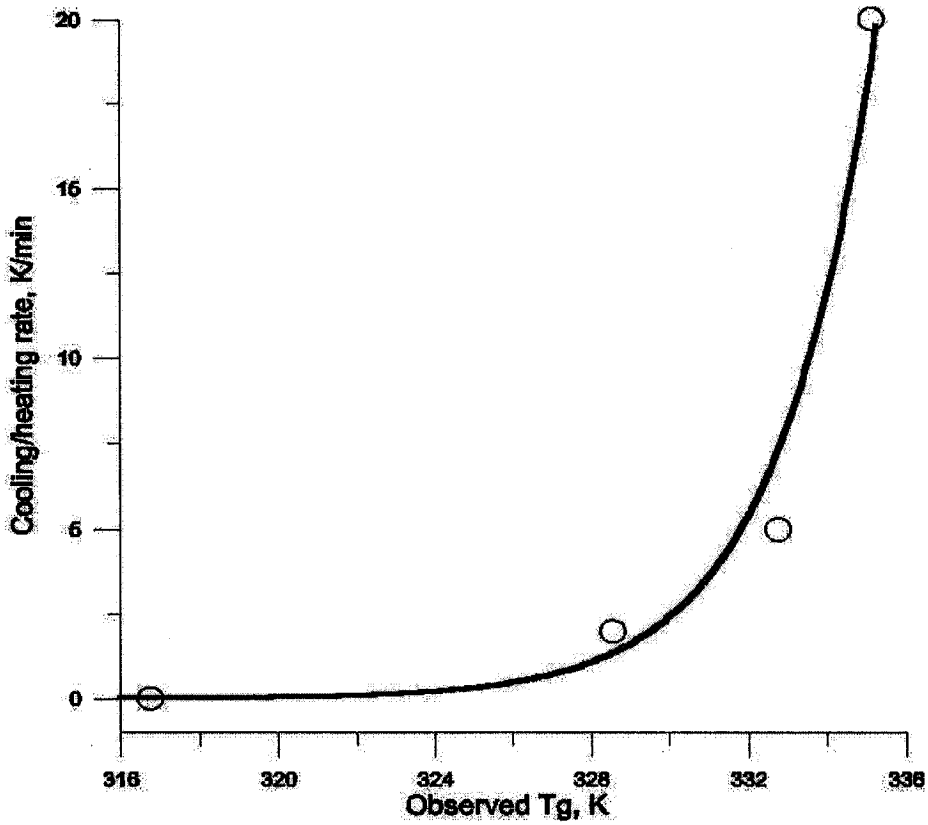


Fig. 4.7. Combined data for the glass transition temperature of L 9000 polylactide.

## 4.5. Crystallization behavior of the polylactide blends of different compositions observed by DSC

It was found that bulk polylactides show very low cold crystallizability during DSC experiments (Fig. 4.8). Supposedly it can be explained by the very low initial nucleation centers present in bulk polymers. After melting and fast cooling, polylactide can be crystallized during DSC experiments yielding a highly crystalline polymer. Note the absence of cold crystallization for solution cast polylactide films annealed for long time (Fig. 4.9).

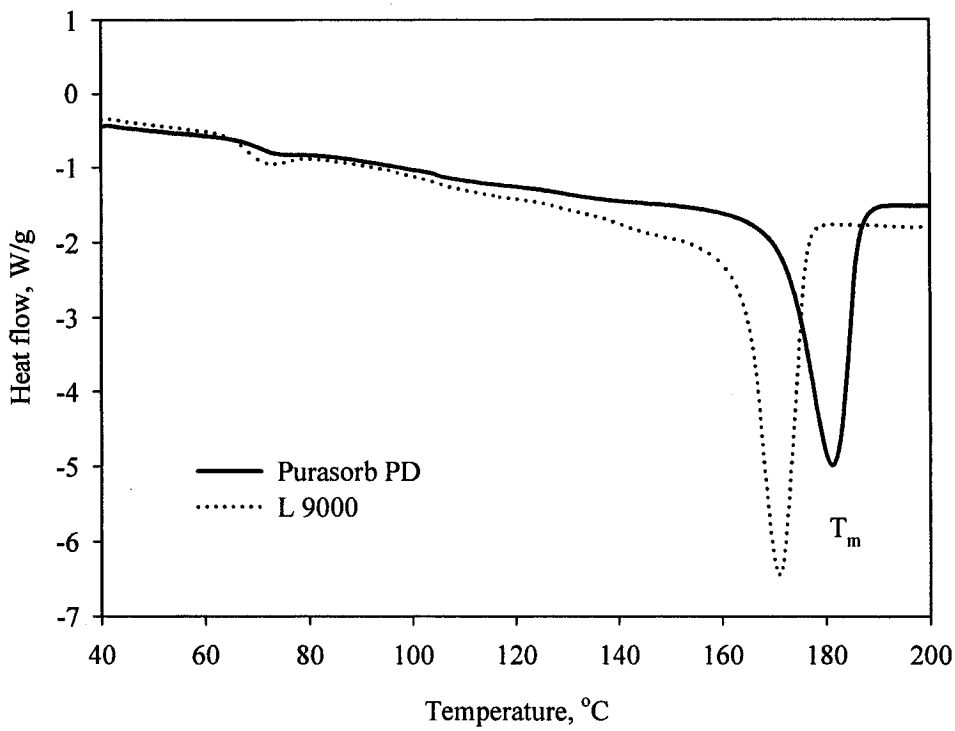


Fig. 4.8. DSC curves of the bulk polylactides. The first heating run is shown.

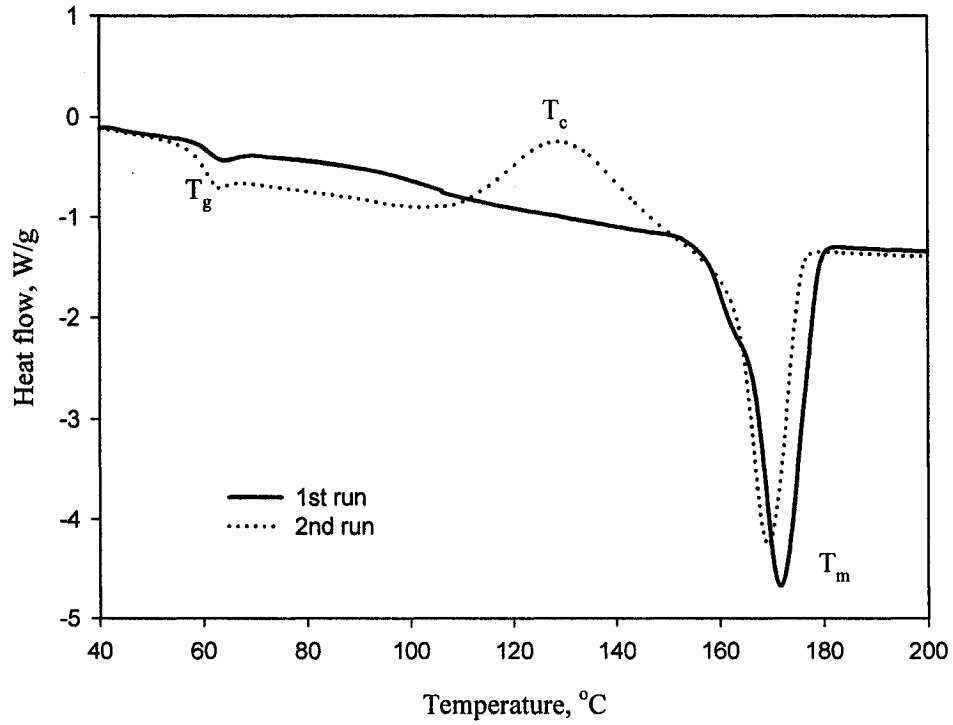


Fig. 4.9. DSC curves for the solution cast L9000 annealed at 140 °C for 100 minutes, prior to analysis.

A series of DSC analyses were made on blends containing 2 % and 5 % Purasorb PD polylactide in L 9000. In order to study the influence of the D-lactide on the crystallization behavior, all analyses were performed on solution cast films. In both the first and second runs the blends containing D-polylactide show a small peak at about 210 – 220 °C that does not exist for pure L 9000 (Fig. 4.10 and 4.11). The area under this peak increases as the D-polylactide content increases. These peaks observed in the range of stereocomplex melting point confirm the presence of the stereocomplex. It can be concluded that even a low D-polylactide content can be enough for stereocomplexation to occur in solution cast polylactide blends.

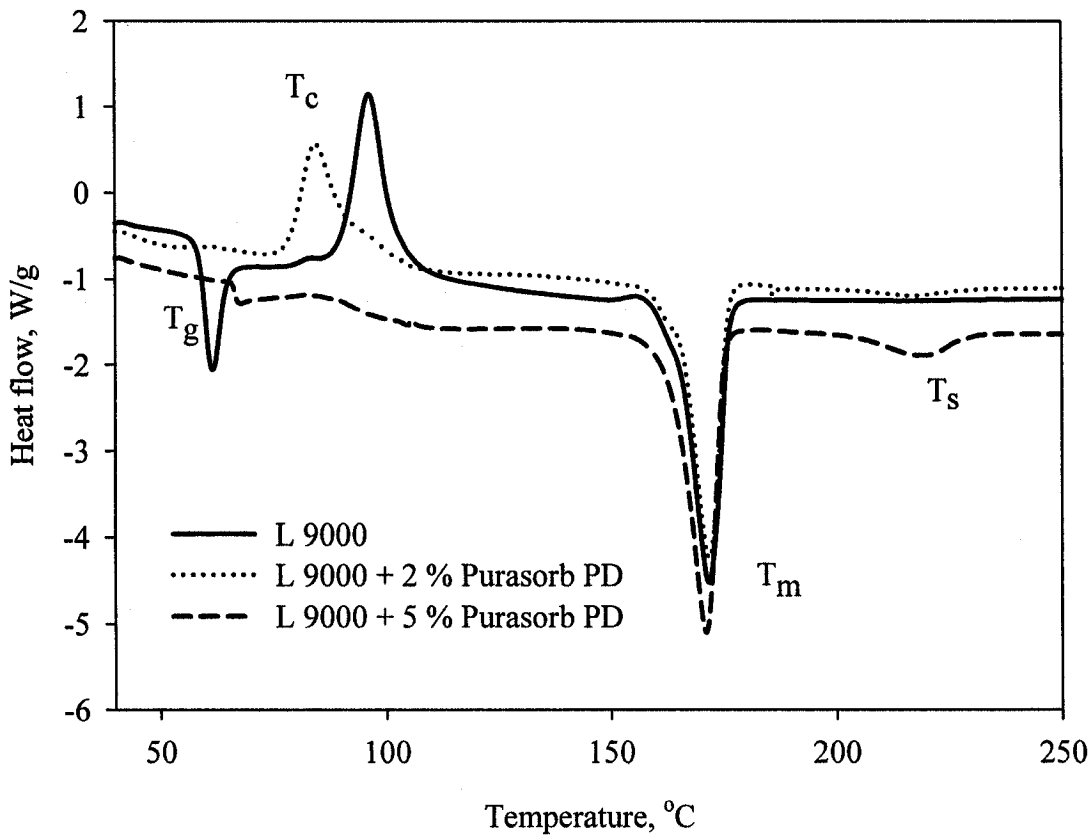


Fig. 4.10. The first run DSC curves for the blends of L- and D- polylactides with the different D-lactide content. $T_s$ represents the stereocomplex melting peak.

The addition of the D-lactide strongly influences the crystallization behavior of polylactide blends. In Fig. 4.10 the cold crystallization peak shifts to lower temperatures and simultaneously crystallization is suppressed with increasing D-lactide content. This Tc shift and cold crystallization suppression were observed only in first runs and are thus related to the solution cast polylactide morphology. The basic thermodynamic characteristics of the polylactide blends are summarized in Table 4.3. It can be concluded that the amount of the stereocomplex formed during crystallization of the blends is not proportional to the amount of the D-polylactide in blend. Since for stereocomplexation both enantiomers in equal amounts are needed, the D-polylactide enriched blend yields much more stereocomplex during the crystallization.

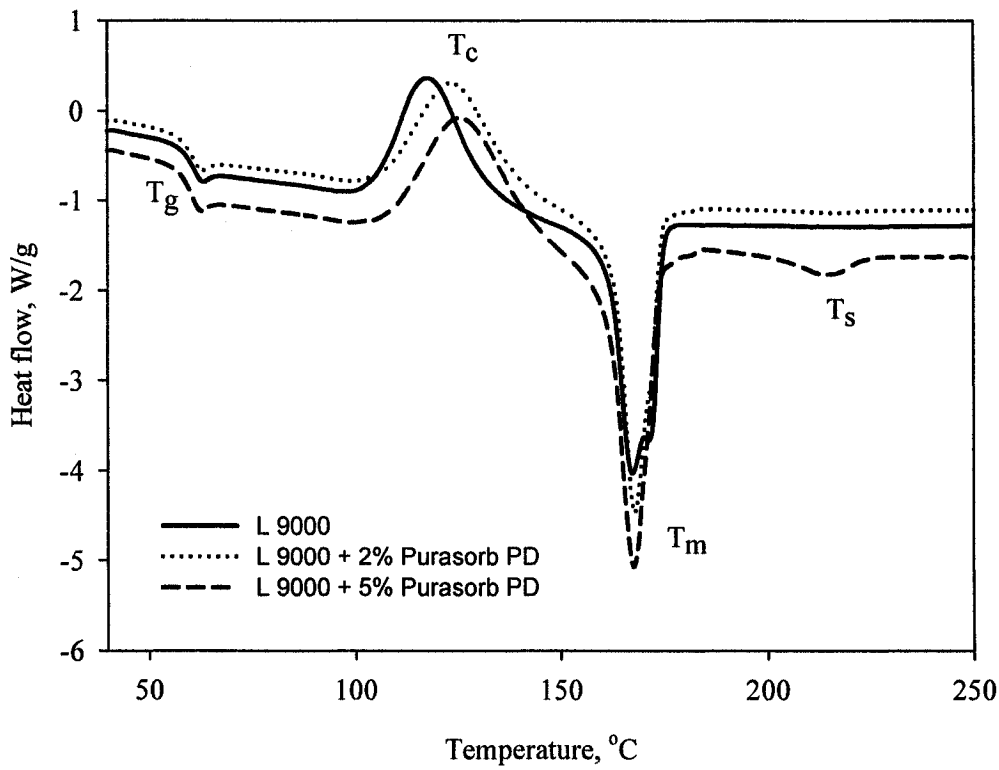


Fig. 4.11. Second run DSC curves for the blends of L- and D- polylactides with varying D-lactide content.

Table 4.3. Thermodynamic characteristics of the L 9000 and Purasorb PD polylactides blends.

| | First run | | | Second run | | |
|---|---|---|---|---|---|---|
| | L 9000 | L 9000 + 2 % PD | L 9000 + 10 % PD | L 9000 | L 9000 + 2% PD | L 9000 + 10 % PD |
| Glass transition, Tg, °C | 60.1 | – | – | 61.1 | 60.8 | 60.8 |
| Cold crystallization maximum, Tc, °C | 96.4 | 84.6 | 80.9 | 118.0 | 123.9 | 126.4 |
| Heat of crystallization, kJ/g | 26.3 | 19.3 | 9.2 | 33.3 | 30.3 | 28.0 |
| Melting point, Tm, °C | 171.7 | 171.8 | 171.7 | 167.4 | 168.0 | 167.7 |
| Melting heat, kJ/g | 35.4 | 30.8 | 29.3 | 37.8 | 36.0 | 31.3 |
| Stereocomplex melting point, Ts, °C | – | 217.0 | 217.4 | – | 216.7 | 213.9 |
| Heat of stereocomplex melting, kJ/g | – | 1.68 | 5.5 | – | 0.78 | 3.8 |

The following explanation for this behavior is offered:

1. The small addition (i.e. the blend with 2 wt. % D-polylactide in Fig. 4.10) of the D-polylactide causes the formation of numerous stereocomplex crystallites but their amount is insufficient for the formation of the three-dimensional network. Separate stereocomplex crystallites act as heterogeneous nucleating agents shifting the cold crystallization peak but the rate of crystallization is almost not affected.

2. In the blend with higher D-polylactide content (i.e. the blend with 5 % D-polylactide in Fig. 4.10) the amount of the formed stereocomplex is enough for the formations of a three-dimensional network therefore the crystallization maximum shifts even more and the crystallization rate is dramatically depressed due to a decrease in the chain mobility.

3. In the second run (Fig. 4.11) for all three cases, the crystallization rate is almost the same and the crystallization maximums are shifted only slightly, but these shifts are in the opposite direction as compared to the first run. This effect can be explained as follows: during the fast cooling of the melt after the first run the polymer remains almost amorphous and crystallization proceeds equally for all blends through self-nucleation (i.e. stereocomplex and orthorhombic crystals are formed). The little difference in cold crystallization maximums can be explained by the significantly higher molecular weight of the added D-polylactide.

### 4.6. Crystallization behavior of solution cast polylactide films and elimination of excess nucleation

The solution cast film typically has very high concentration of nucleation sites which is much higher than that for the bulk polymer. It is thought that the high nucleation in cast films is caused by the residual solvent. Polar solvents demonstrate especially high nucleation activity. During cold crystallization, these nucleation sites become areas of spherulite growth and in a very short period of time crystallization stops due to constraints (Fig. 4.12a and 4.12b)). This provides evidence for our previous explanation

of the significant shift of the cold crystallization peak as compared to the hot pressed and bulk material (Fig. 4.6 and 4.8). Also this limits the crystallization time until which spherulite growth can be observed. Excess nucleation can be eliminated by film melting prior to experiments. The heating and cooling for the premelting were performed using the same technique as used for the crystallization studies, to prevent crystallization during cooling. After melting for a short time, the concentration of nuclei decreases many times allowing longer times for spherulite growth (Fig. 4.12c and 4.12d)).

It was experimentally established that heating for 3 minutes at a temperatures 10 °C higher than the melting point is enough to erase completely the thermal history of the polymer. This short time melting would not affect polylactide chain integrity even in absence of the inert atmosphere during melting as established by Huettenberger[105]. It should be noted that heating to temperatures up to 250 °C causes some polylactide decomposition and a decrease of the melting point (Table 4.3).

In the range of temperatures from 100 °C to 160 °C the nucleation concentration is almost constant and decreases only slightly as temperature increases. Calculations of the nucleation concentration in polylactide crystallized at different temperatures before and after premelting showed that this procedure allows a decrease in concentration of nuclei by more than 5 times. It was estimated that in the solution cast film an average nucleation concentration was $9.44*10^{16} \pm 1.16*10^{16}$ $m^{-3}$ while after a short time melting, the nucleation concentration decreases to $1.78*10^{16} \pm 0.35*10^{16}$ $m^{-3}$.

It should be also noted that premelting does not decrease significantly the nucleation concentration in temperature range below 100 °C since in the regime I polylactide shows very high intrinsic nucleation concentration and nuclei formed by the

residual solvent contribute only a small portion of the overall nucleation. Numerous experiments revealed no significant decrease of the nucleation concentration after premelting when polylactide was crystallized at low temperatures as compared to untreated cast polylactide. Because of this it is extremely difficult to perform any measurements of crystallite growth rates in the low temperature range.

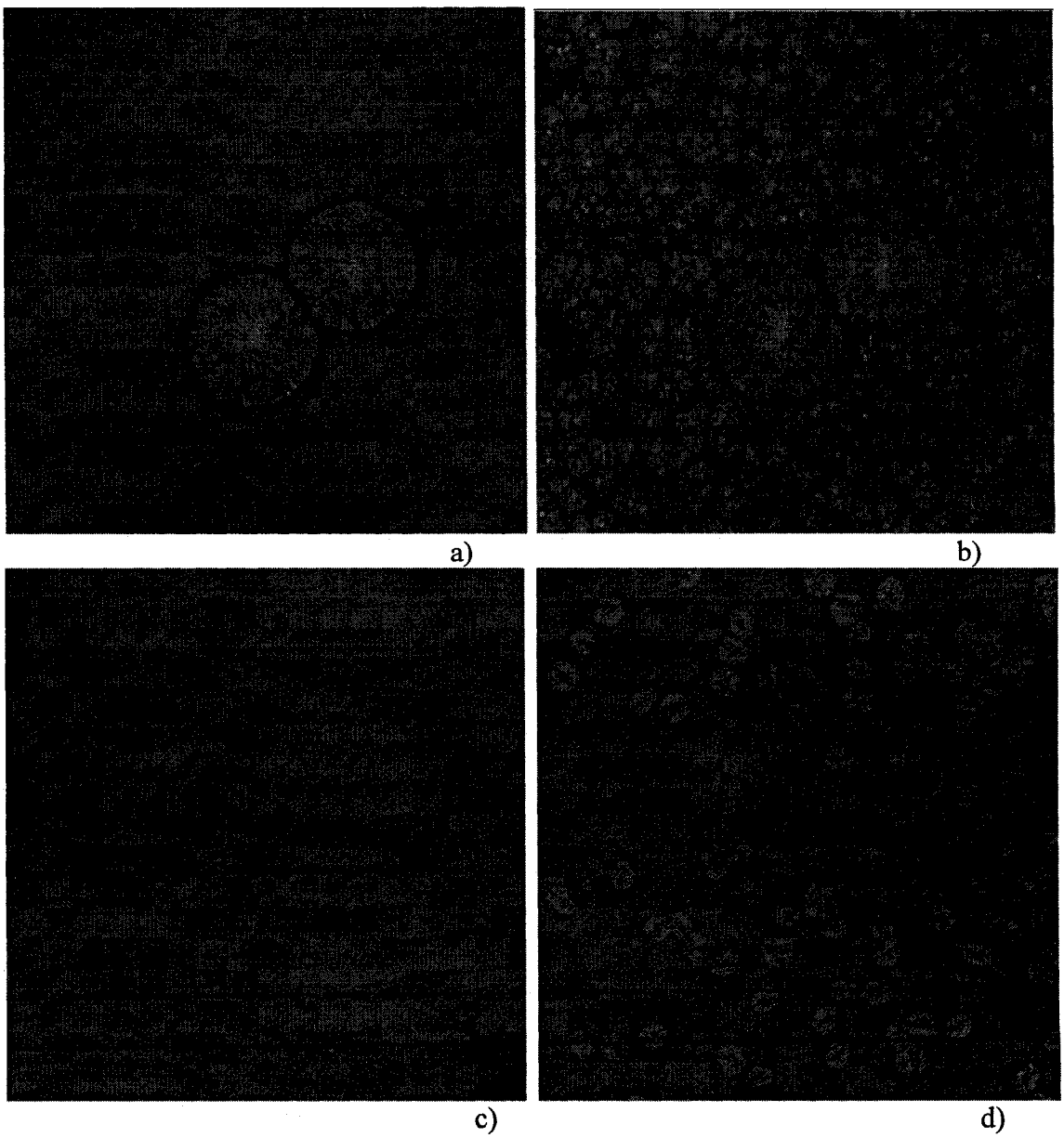


Fig. 4.12. Solution cast film (a) and crystallized for 2 min at 110 °C (b). Premelted film (c) and crystallized for 2 min at 110 °C (d). AFM height images, 100 μm scans.

## 4.7. Verification of the validity of the repeated heating/cooling technique for the studies of crystallization growth rate

Since the sample under investigation is subjected to several fast cooling and heating cycles it is important to verify the reliability of the isothermal assumption. For this purpose, one of the samples of polylactide film was repeatedly heated to 120 °C and cooled and AFM imaging was performed after each cooling cycle (Fig. 4.13 (a), (b), (c)). The second sample was annealed at 120 °C for 4 minutes, the same total annealing time experienced by the first sample. As a result the first sample was subjected to three heating/cooling cycles and the second one experienced only one cycle. Obviously the difference in morphology and spherulite growth between two samples shows the effect of the two additional heating/cooling cycles. Measurements of the first generation spherulites yielded an average size of 32.53 ±0.93 μm and 31.22 ±1.22 μm for the first and second samples respectively. This corresponds about 4 % deviation, therefore it can be concluded that the experimental conditions used in this study can be considered to be isothermal. At 120 °C crystallization proceeds very fast and for the majority of the experiments this deviation should be even less, since crystallization rates are lower.

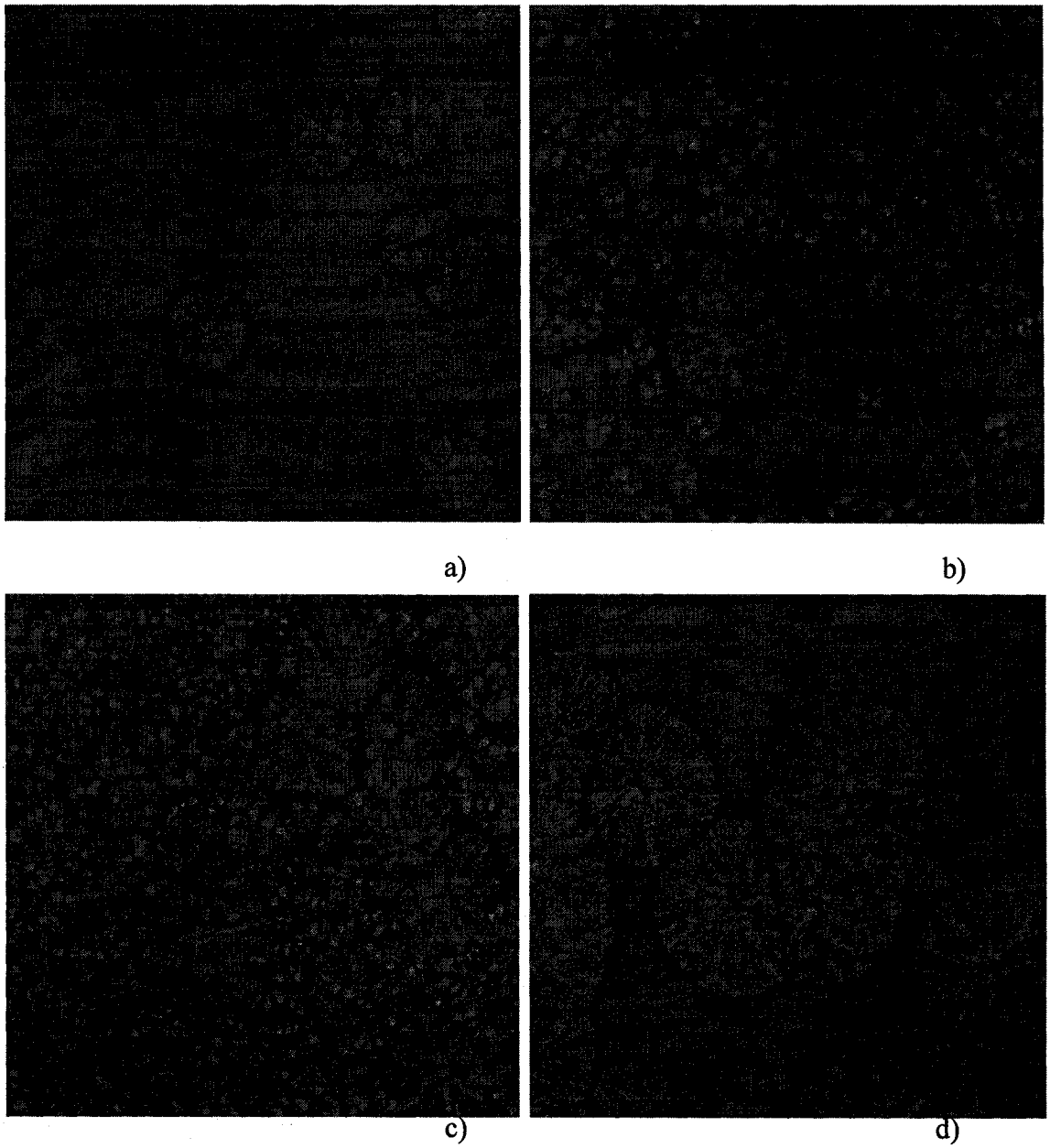


Fig. 4.13. Developments of the crystalline morphology in L 9000 + 10 % Purasorb PD polylactide blend at 120 °C. The sample was repeatedly crystallized for 2 min (a), 3 min (b) and 4 min (c). The reference sample (d) was crystallized for 4 min continuosly. AFM height images are shown. All images represent 100 μm scans.

It is also interesting to note that the crystalline morphology of these two samples is significantly different. While the second sample crystallizes in the form of spherulites of very narrow size distribution, the first sample demonstrates secondary nucleation which commences in the beginning of each heating cycle. As a result, the first sample contains spherulites having three different sizes. The most credible explanation to this phenomenon is that polylactide undergoes very fast nucleation at lower temperatures during heating and cooling cycles. Since the heating and cooling time is very short, it is enough only for the formation of the nucleation sites which start to form new spherulites at the beginning of the next heating cycle. This phenomenon was also observed in many other experiments.

### 4.8. Isothermal crystallization behavior of L 9000 and Purasorb PD polylactide blends

Isothermal crystallization behavior was studied in pure L 9000 and in blends of L 9000 polylactide with 2% and 10% of Purasorb PD. The annealing times were chosen according to crystalline structure growth rate from 2 to 96 minutes. The maximum time for measurements is defined by the growth rate and the nucleation concentration. When a growing crystalline structure meets a neighboring crystallite, normal growth ceases and the constrained spherulites develop straight borders. For each sample at least 16 unconstrained spherulite sizes were measured. For all samples studied, the spherulite size was directly proportional to annealing time with an intersection very close to the origin (Fig. 4.14, 4.15, 4.16). This indicates that nucleation sites in polylactides have a very short incubation time which could not be detected in this type of experiments.

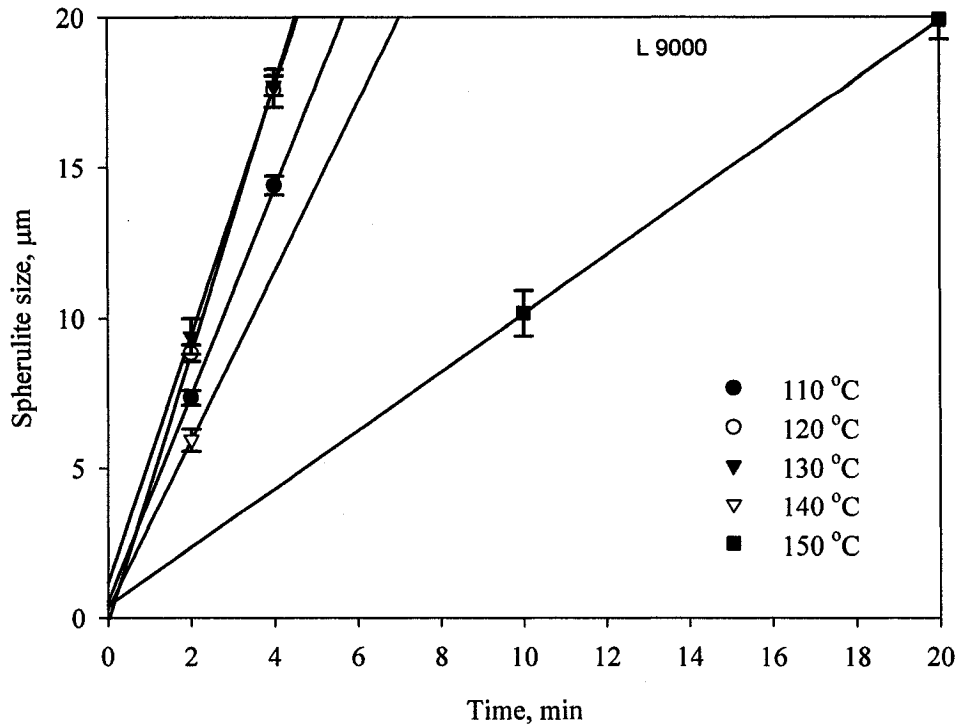


Fig. 4.14. L 9000 polylactide spherulite growth at different temperatures.

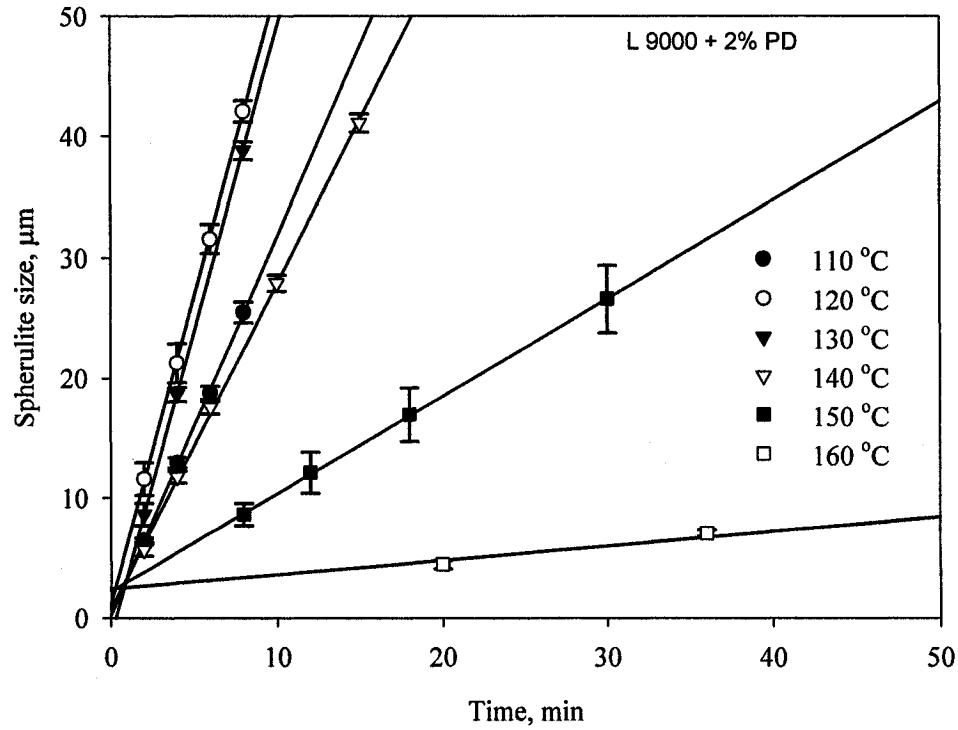


Fig. 4.15. L 9000 + 2 % Purasorb PD polylactide blend spherulite growth at different temperatures.

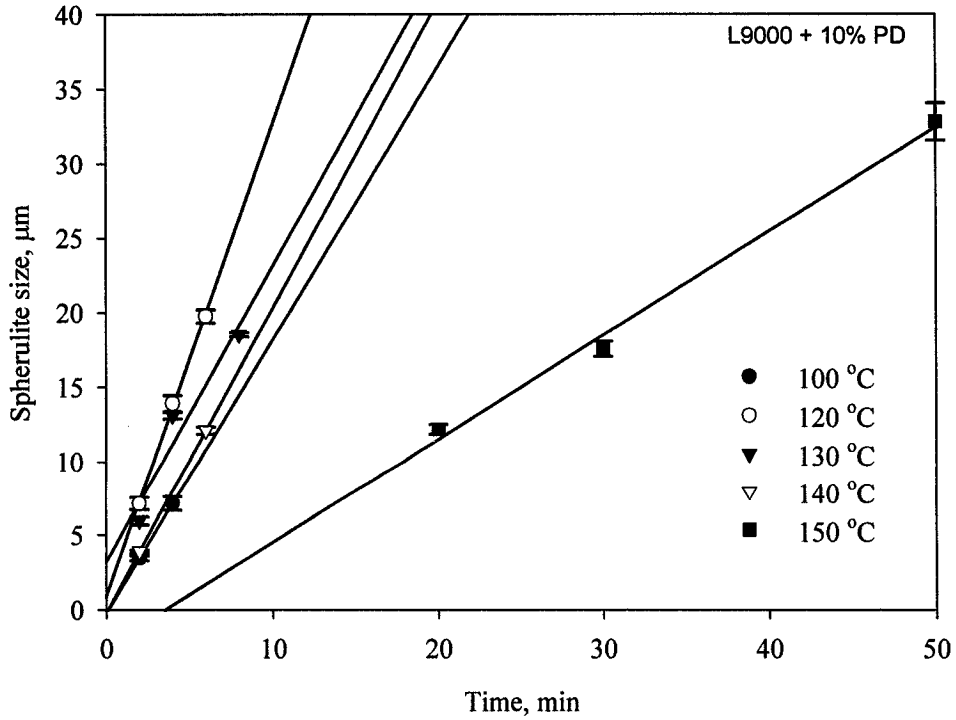


Fig. 4.16. L 9000 + 10 % Purasorb PD polylactide blend spherulite growth at different temperatures.

The standard deviation of the measurements was small and rarely exceeded 3%. In Fig. 4.14, 4.15, 4.16, 4.18, 4.19 some lines were omitted due to scaling considerations. Complete data, including standard deviations of the measurements can be found in Appendix II. The slope of these lines gives the spherulite growth rate at each temperature. These results are presented in Table 4.4 and dependences of the spherulite growth rate on temperature for all three samples are shown in Fig. 4.17. All three graphs have the distinctive "bell-shaped" appearance characteristic to the overwhelming majority of polymers. It shows that the crystallization of L 9000 polylactide and its blends with

Purasorb PD at each temperature are governed only by one of the growth regimes and thus can be described by Equation [2.19].

It was expected that L 9000 polylactide blends would show not only lower overall crystallization rate but also lower spherulite growth rate with increasing D-polylactide amount. Two factors should decrease the spherulite growth rate in these blends: first, is stereocomplexation and second is higher molecular weight of the Purasorb PD. Surprisingly, the blend with 2 % of D-polylactide showed significantly higher maximum spherulite growth rate than the pure L 9000 polylactide while the sample with 10 % Purasorb PD showed significantly lower growth rate in all range of temperatures. The nature of this effect is yet to be explained. The maximum spherulite growth rate for pure L 9000 is reached at 122.1 °C and for the blends containing 2 % and 10 % this maximum is at 125.2 °C and 120.1 °C respectively.

Table 4.4. Isothermal spherulite growth rates for the blends of L 9000 polylactide and Purasorb PD.

| Temperature, °C | Spherulite growth rates, μm/min | | |
|---|---|---|---|
| | L 9000 | L 9000 + 2 % PD | L 9000 + 10 % PD |
| 100 | 2.628 | 2.356 | 1.835 |
| 110 | 3.430 | 3.146 | 2.456 |
| 120 | 4.483 | 5.088 | 3.165 |
| 130 | 4.128 | 5.034 | 2.358 |
| 140 | 2.806 | 2.705 | 1.625 |
| 150 | 0.975 | 0.814 | 0.699 |
| 160 | 0.152 | 0.120 | 0.062 |

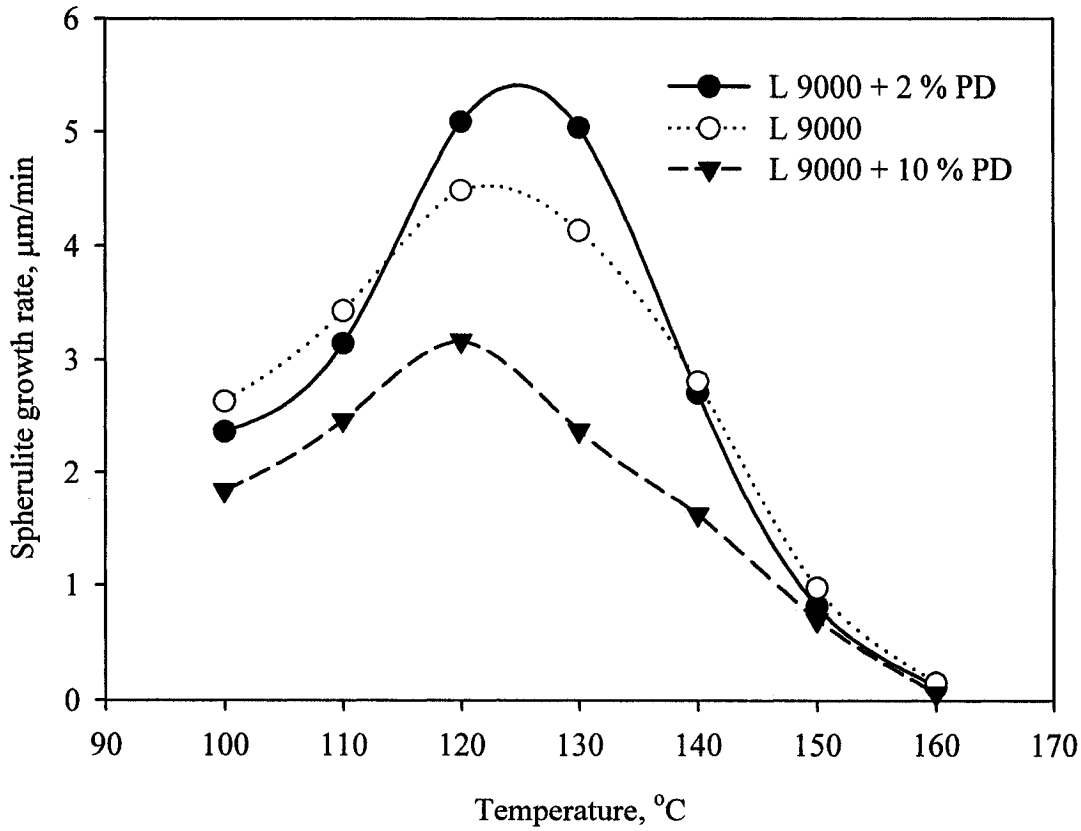


Fig. 4.17. Isothermal spherulite growth rates for the blends of L 9000 polylactide and Purasorb PD.

### 4.9. Crystallization behavior of Purasorb PL and Purasorb PD polylactide blends

The crystallization behavior of Purasorb PL and that of its blends with Purasorb PD is especially interesting because both of these polymers consist solely of enantiomers of the same kind and have equal molecular weight. In this study, spherulite growth rates at different temperatures of the pure Purasorb PL and its blend with 10 % of Purasorb PD have been studied. The results of the measurements of the spherulite size

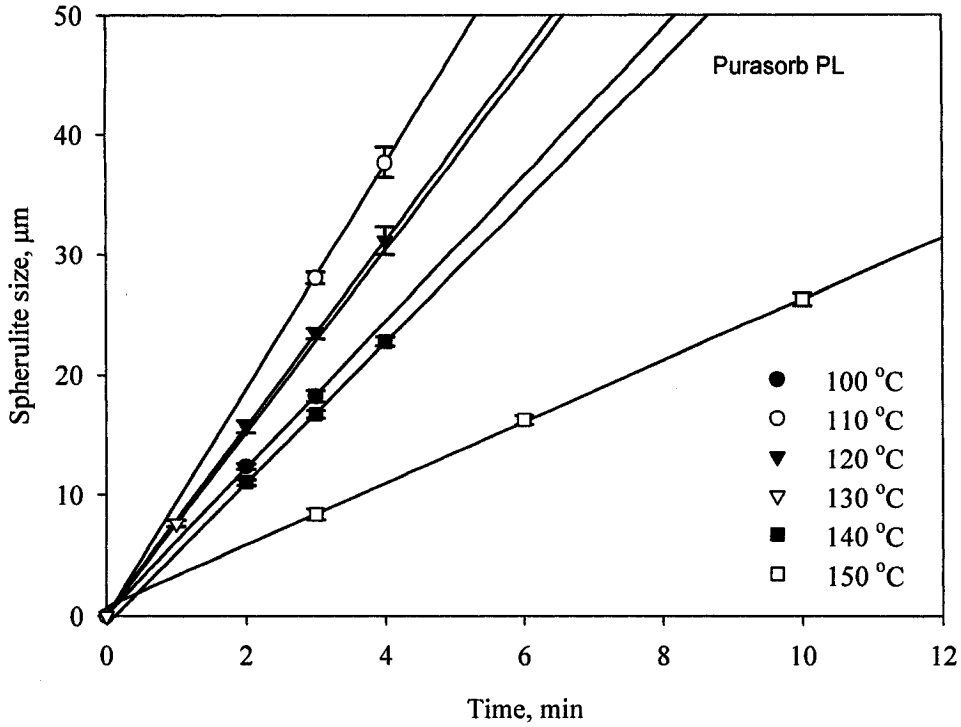


Fig. 4.18. Purasorb PL polylactide spherulite growth at different temperatures.

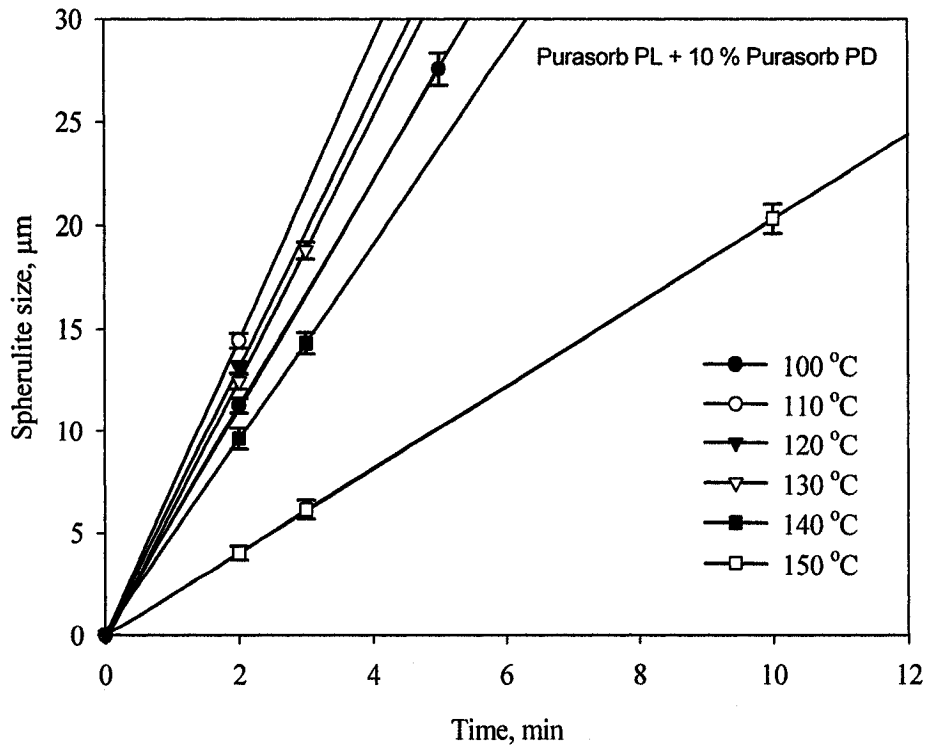


Fig. 4.19. Purasorb PL + 10 % Purasorb PD polylactide blend spherulite growth at different temperatures.

over time under isothermal conditions are given in Fig.4.18 and 4.19. Data for the spherulite growth rate are given in Table 4.5. and graphically presented in Fig. 4.20.

Table 4.5. Isothermal spherulite growth rates for the blends of Purasorb PL and Purasorb PD.

| Temperature, °C | Spherulite growth rates, μm/min | |
|---|---|---|
| | Purasorb PL | Purasorb PL + 10% Purasorb PD |
| 100 | 6.178 | 5.526 |
| 110 | 9.349 | 7.558 |
| 120 | 7.7709 | 6.564 |
| 130 | 7.6045 | 6.3605 |
| 140 | 5.8525 | 4.718 |
| 150 | 2.5602 | 2.025 |

It was found that for the both samples, the shape of the spherulite growth rate curves were significantly different from the "bell" shape and have two unequal extremums. It is especially interesting that shapes for both samples are similar with the spherulite growth rate for the blend being 20 – 30 % lower than that for the pure Purasorb PL. This observation supports the experimental results by M. Di Lorenzo[71] (Fig. 2.7) obtained for a pure L-polylactide with a lower molecular weight of about 100 000. This crystallization behavior had never previously been observed in pure polymers. In this study it was found that global spherulite growth rate maximum is at about 111 ° C and the second local maximum is at about 129 ° C for both samples.

Typically the spherulite growth rate decreases with increasing molecular weight. This is explained by decreasing polymer chain mobility with increasing lenth. In our experiments, it was found that Purasorb PL with a molecular weight almost twice higher than that of L 9000 polylactide showed spherulite growth rate almost two times higher. There is also a difference in the polymer chain structure and it is possible that the small 2 % D-lactide repeat unit content in the L 9000 polylactide causes this decrease of the spherulite growth rate. The randomly arranged D-lactide repeat units create steric impediments during crystallization thus decreasing the spherulite growth rate.

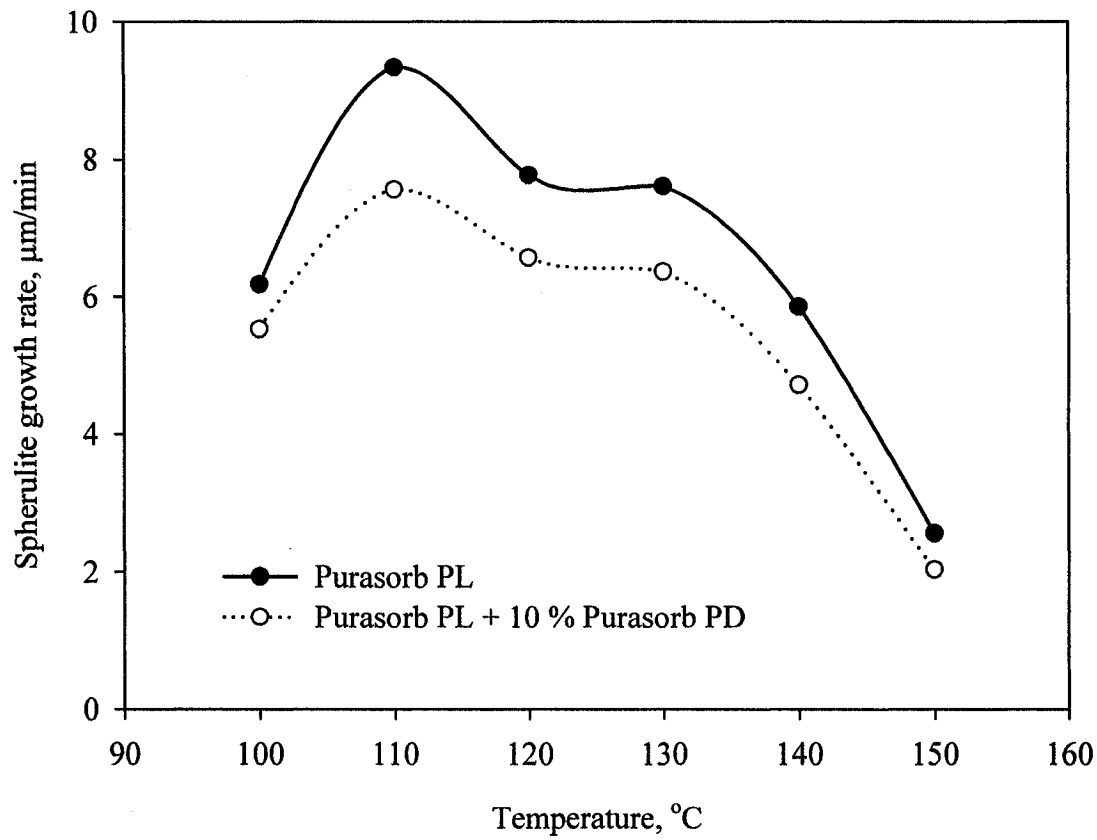


Fig. 4.20. Isothermal spherulite growth rates for the blends of Purasorb PL and Purasorb PD.

## 4.10. Crystalline morphology of polylactide: Three regions of crystallization

Like many polymers polylactide shows three distinctive regimes of crystallization morphology. The theoretical aspects of the crystallization morphology have been discussed in Chapter 2.6. The crystalline morphologies of the polylactides and their blends are similar. The only significant difference is that the three crystallization regimes have different temperature limits. In this study, the polylactide blend of L 9000 + 2 % Purasorb PD has been used.

*Regime I.* This is a low temperature regime with an upper temperature limit of about 90 °C. In this regime the nucleation concentration is extremely high and crystallization starts in the form of the numerous lamellae (Fig. 4.21).

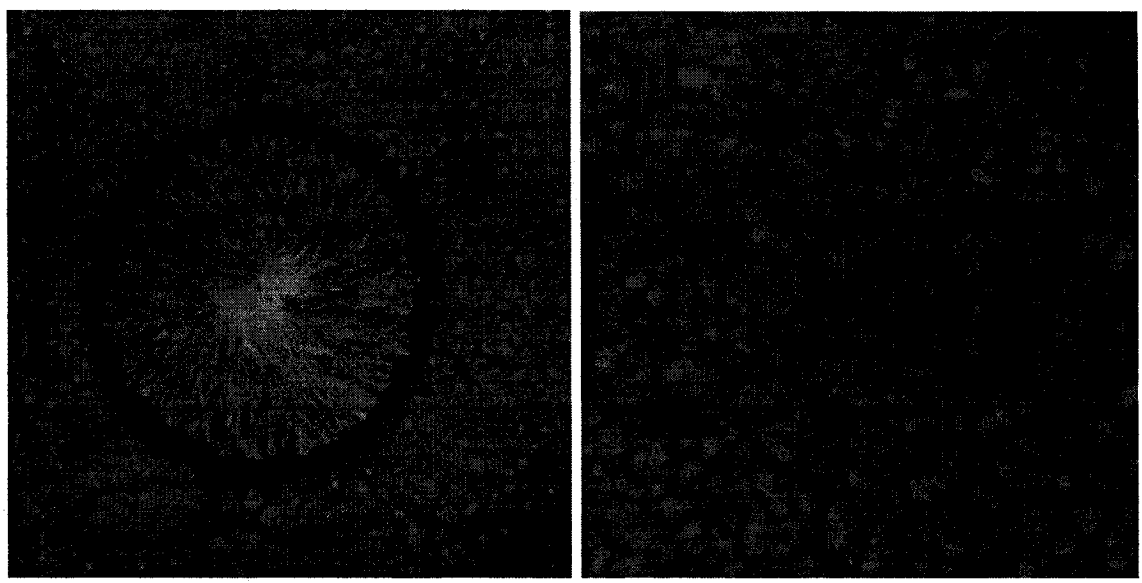

a) b)

Fig. 4.21. a) The crystalline morphology of the solution cast polylactide annealed at 80 °C for 4 min. 100 μm AFM height image is shown. b) The crystalline morphology of the same sample after 15 min of annealing. 20 μm AFM height image is shown.

The crystallization rate is low and the lamellae do not form any distinctive crystalline aggregates. Because of this it is very difficult to perform any measurements of the crystalline structures' growth rate in region I (Fig. 4.21 (b)). It should be noted that despite the fact that the lamellae growth rate in regime I is low, due to the very high nucleation the overall crystallization rate is the highest of all temperatures. This fact is also supported by the DSC analysis which shows that the highest crystallization rate is in the range of 85 -95 °C (Fig. 4.6).

*The transition region* between regime I and regime II is shown in Fig. 4.22. In this regime, polylactide starts to form distinctive crystalline structures in the form of the "sheafs". Simultaneously, the growth rate increases and the nucleation concentration decreases dramatically.

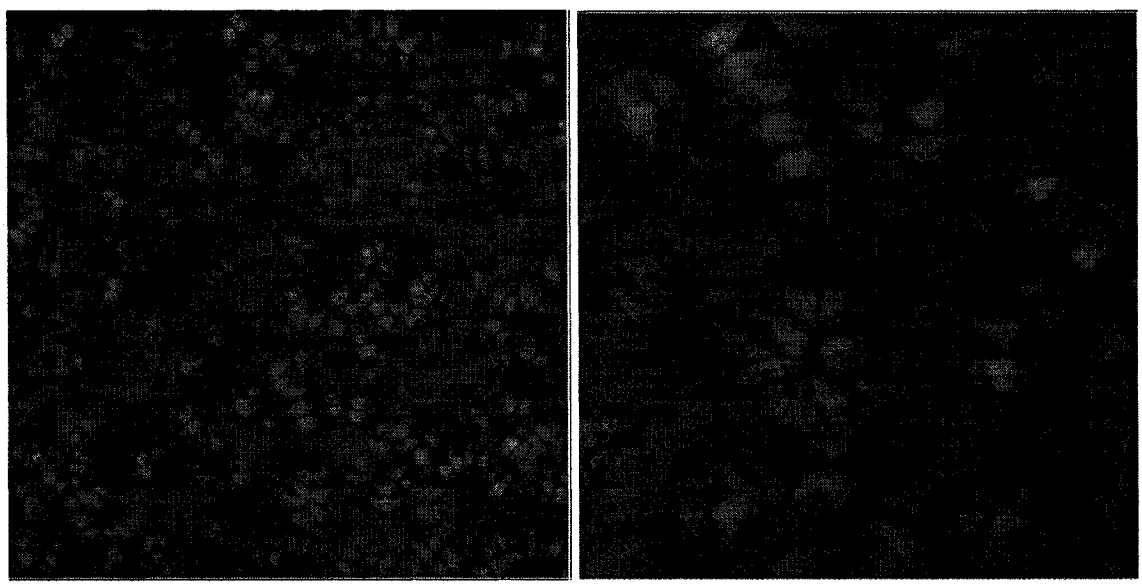

a) b)

Fig. 4.22. The crystalline morphology of the solution cast polylactide annealed at 90 °C for 4 min. 100 μm AFM height image is shown (a). The 20 μm AFM height image of the same sample (b).

*Regime II* starts from approximately 90 °C and lasts up to 140 °C. This is the regime in which crystallization occurs in the form of perfect spherulites and the spherulite growth rate is the highest (Fig. 4.23). The nucleation concentration reaches its minimum and remains almost constant until the melting point. In region II, the spherulite growth rate can be measured with very high precision. Since the spherulite growth in regime II starts from single lamellae, the spherulite acquires a perfectly round shape after a certain time of growth (compare the spherulite shapes on Fig. 4.23 (a) and Fig. 4.23 (b)). Note the secondary nucleation phenomena in Fig. 4.23 (b) caused by the second cooling/heating cycle after 4 minutes of the crystallization. The size of the spherulites formed after the secondary nucleation is half of the size of the spherulites formed during the initial nucleation.

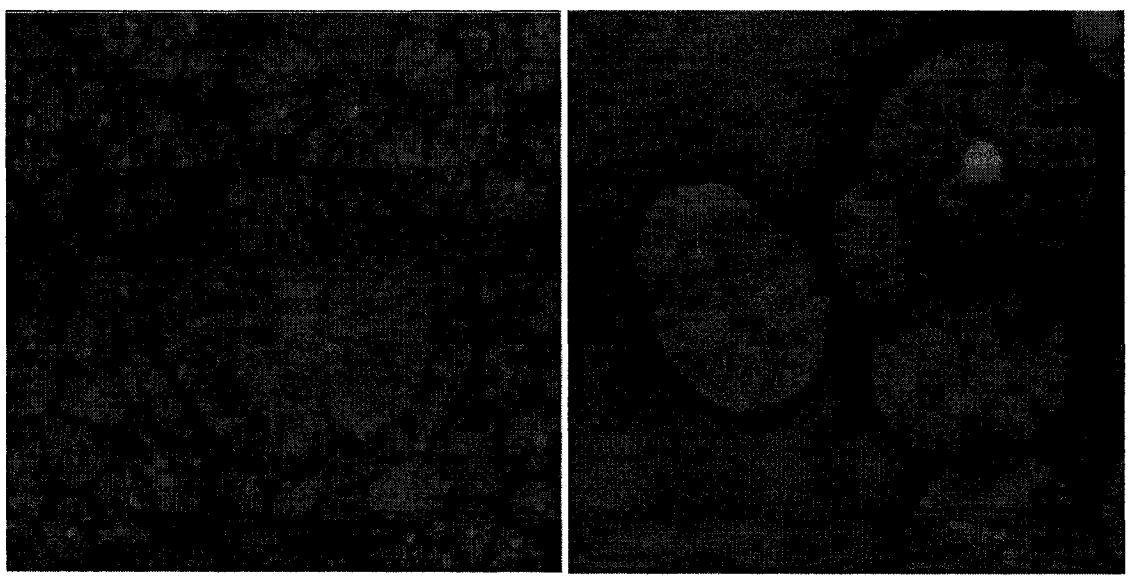

a) b)

Fig. 4.23. a) The crystalline morphology of the solution cast polylactide annealed at 120 °C for 4 min. 50 μm AFM height image is shown. b) The crystalline morphology of polylactide annealed at 130 °C for 8 min. 100 μm AFM height image is shown.

*Regime III* is the high temperature crystallization regime starting from 140 °C and lasting up to the melting point. In this regime, the crystallization morphology changes dramatically, turning from spherulites to axialites (Fig. 4.24). The nucleation concentration remains almost unchanged as compared to regime II, but the crystallite growth rate gradually decreases. It is clear that crystallization proceeds by wedging out of the new lamellae from the crystallization center rather than branching from random points of the growing lamella which prevails in the regime II. Even after a long growing time, the crystalline structures in regime III remain in the shape of a "sheaf" having planar symmetry. With increasing temperature the axialites becomes more symmetrical (compare axialites shapes in Fig. 4.24 (a) and Fig. 4.24 (b)).

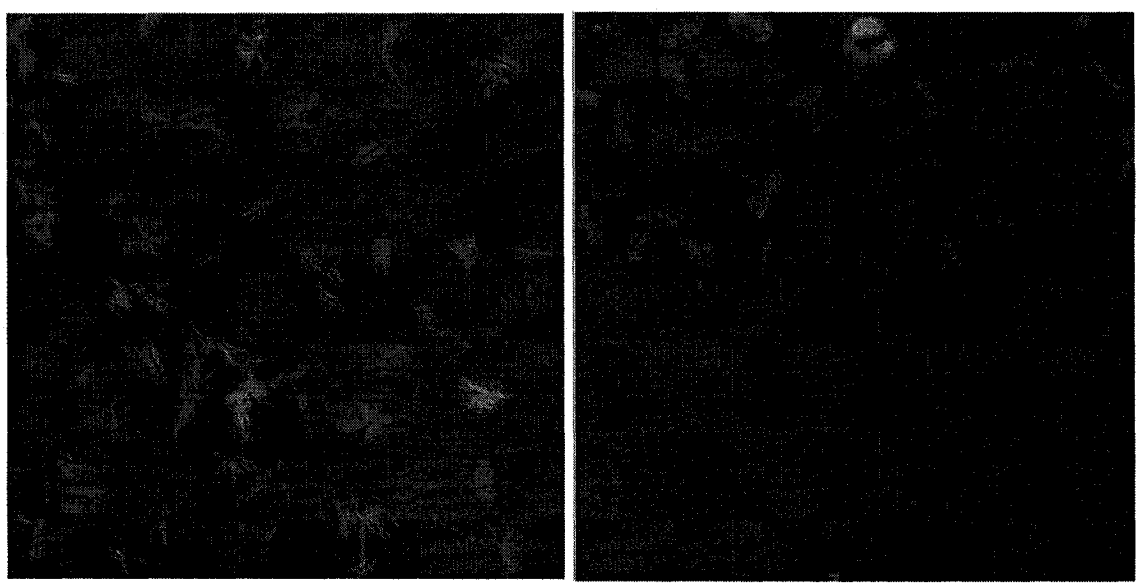

a) b)

Fig. 4.24. a) The crystalline morphology of the solution cast polylactide annealed at 150 °C for 10 min. 100 μm AFM height image is shown. b)The crystalline morphology of polylactide annealed at 160 °C for 60 min. 100 μm AFM height image is shown.

### 4.11. Spherulite growth kinetics analysis

Experimental data of spherulite growth rate of polylactide blends were analyzed using the Hoffman-Lauritzen equation [2.19] rearranged in the following way:

$$\ln G + \frac{U^*}{R(T_c - T_\infty)} = \ln G_0 - \frac{K_g}{T_c \Delta T f} \qquad [4.2]$$

It should be noted that the parameter $T_m^0$ in the supercooling equation ($\Delta T = T_m^0 - T_c$) and other equations is an equilibrium melting temperature defined as the melting temperature of an extended chain crystal. $T°m$ is usually determined by extrapolation of the Hoffman–Weeks or the Gibbs–Thomson plots[109]. For polylactides this parameter is equal to 270 °C[53]. For the data fitting, $U^*$ = 4500 J/mol and $C$ = 30 °C were used[57]. All other parameters of this equation were introduced in Chapter 2.4. The $K_g$ parameter here is a term connected with the energy needed for the formation of nuclei of critical size defined as:

$$K_g = \frac{nb_0 \sigma \sigma_e T_m^0}{\Delta H k} \qquad [4.3]$$

The parameter $n$ indicates the crystallization regime of the polylactides and changes as regime changes. Kinetic analysis for the L 9000 polylactide and its blends with Purasorb PD are given in Fig. 4.25, 4.26, 4.27, 4.28, 4.29, 4.30 and Table 4.6.

The experimental data can be described by three lines corresponding to three regimes of the crystallization kinetics. The width of regime II is about 20 °C for all three samples. As expected there are few differences in the crystallization kinetics of L 9000 polylactide and its blend with 2 % of Purasorb PD. For the blend with 10% Purasorb PD lower border of regime II shifts down by about 5 degrees. The $K_g$ parameter value, the

slope in graphs such as Fig. 4.25, in regime II varies in accordance with growth rate, while in regime III, $K_g$ gradually decreases with increase of the D-polylactide content. The $K_g$ value found from kinetic analyses are close to those reported in the literature, $K_g(II)$ = 185000 $K^{-2}$[57]. Our analysis supports the observation that the transition temperature between regimes II and III depends on molecular weight and increases with molecular weight. C. Silvestre et al[110] determined the transition temperature to be equal to 115 °C for polylactide with Mw = 60 000 and M. Di Lorenzo[57] found it to be equal to 120 °C for polylactides with Mw = 101 000. This transition temperature was about 126 °C for L 9000 polylactide, which has a Mw = 220 000 therefore correlating with previous studies.

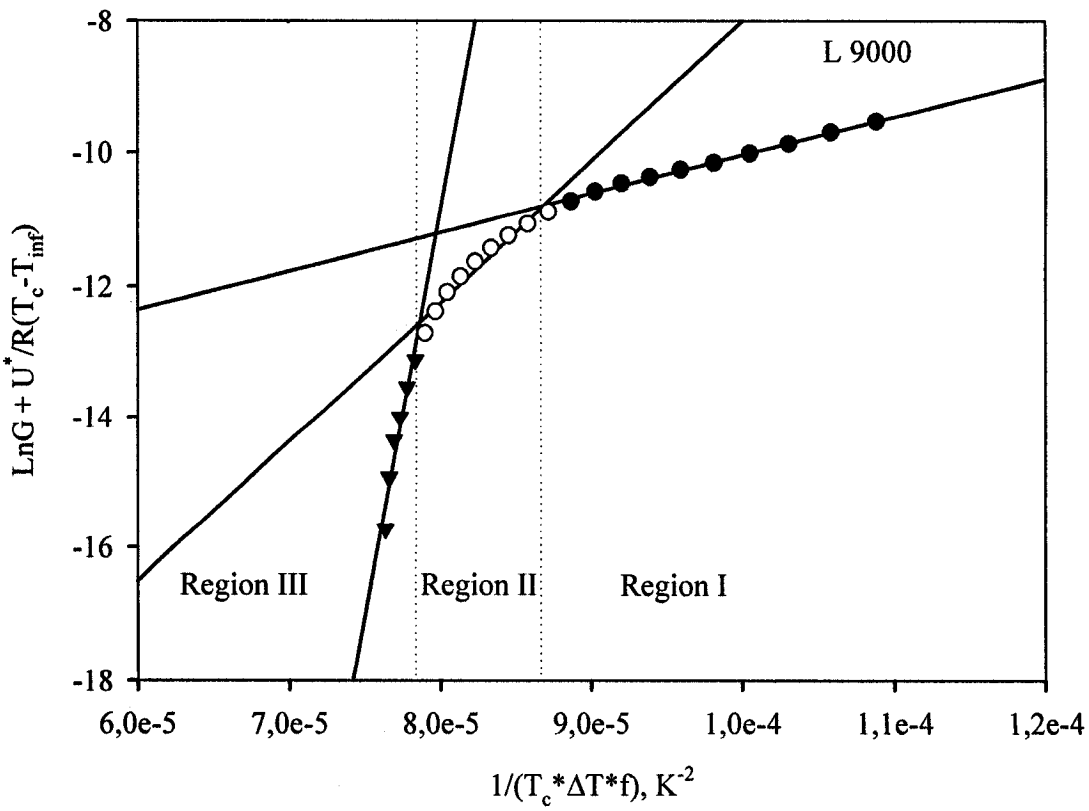


Fig. 4.25. Kinetic analysis of growth rate of L 9000 polylactide.

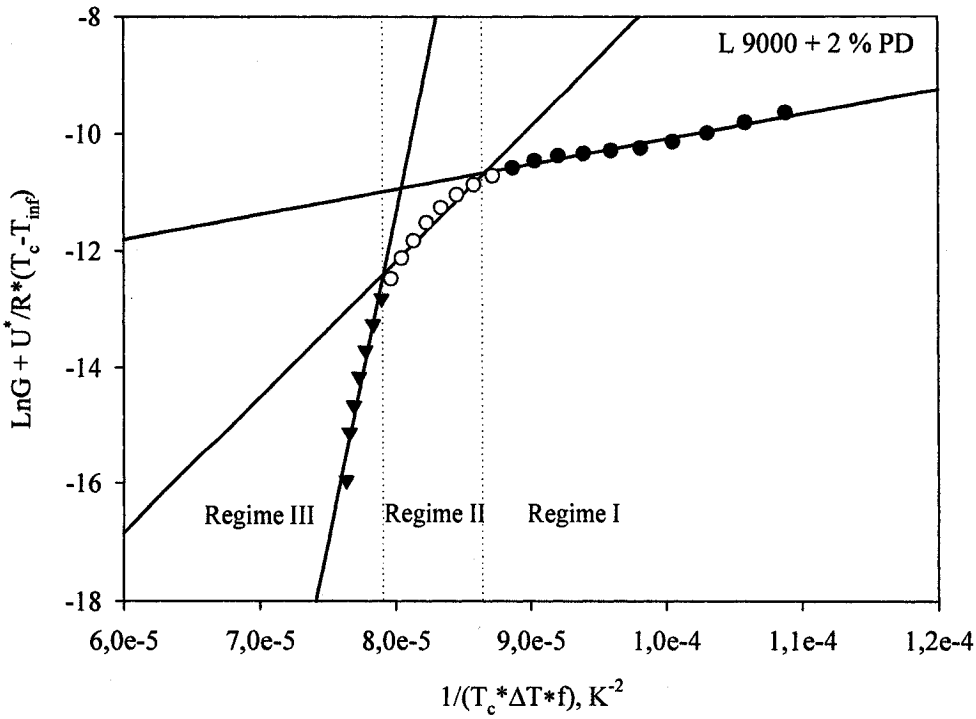


Fig. 4.26. Kinetic analysis of growth rate of L 9000 + 2 % Purasorb PD polylactide blend.

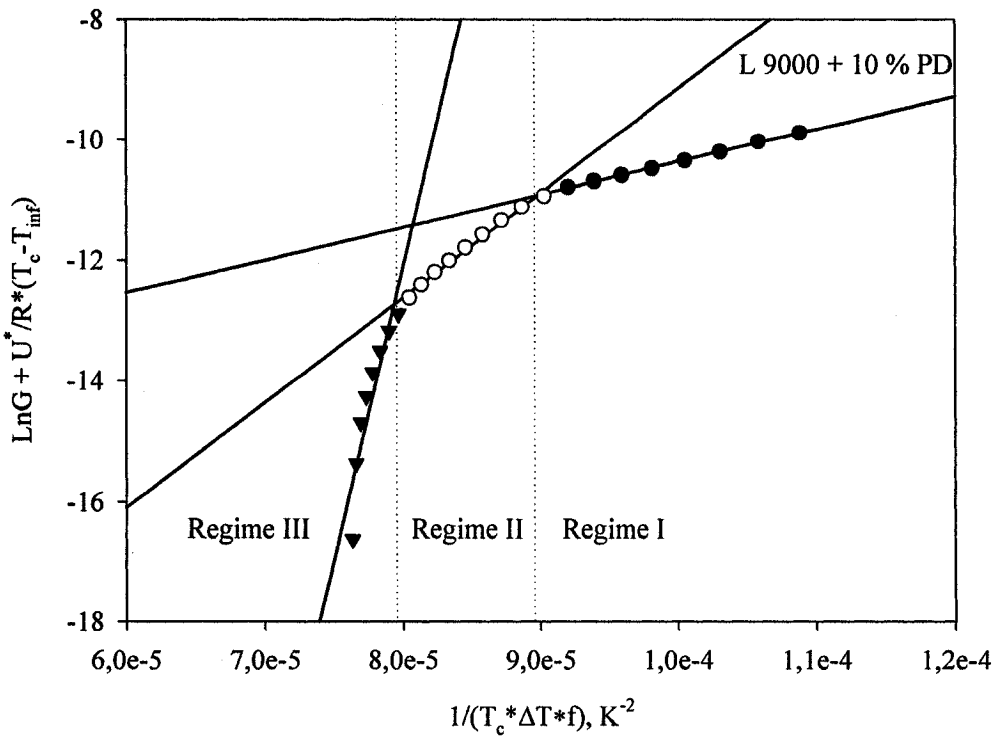


Fig. 4.27. Kinetic analysis of growth rate of L 9000 + 10 % Purasorb PD polylactide blend.

Table 4.6. Crystallization regimes and critical energy for the formation of the nuclei for L 9000 polylactide and its blends with Purasorb PD.

| | Regime I | | Regime II | | Regime III | |
|---|---|---|---|---|---|---|
| | Range , °C | $K_g$, $K^{-2}$ | Range , °C | $K_g$, $K^{-2}$ | Range , °C | $K_g$, $K^{-2}$ |
| L 9000 | < 125.5 | 57700 | 125.5 – 146.3 | 212065 | >146.3 | 1227800 |
| L 9000 + 2 % PD | < 126.0 | 42900 | 126.0 – 144.4 | 231500 | >144.4 | 1114800 |
| L 9000 + 10 % PD | < 120.7 | 54300 | 120.7 – 143.5 | 173300 | >143.5 | 965200 |

The kinetic analysis for the Purasorb PL polylactide and its blend with Purasorb PD are given in Fig. 4.28, 4.29 and Table 4.7.

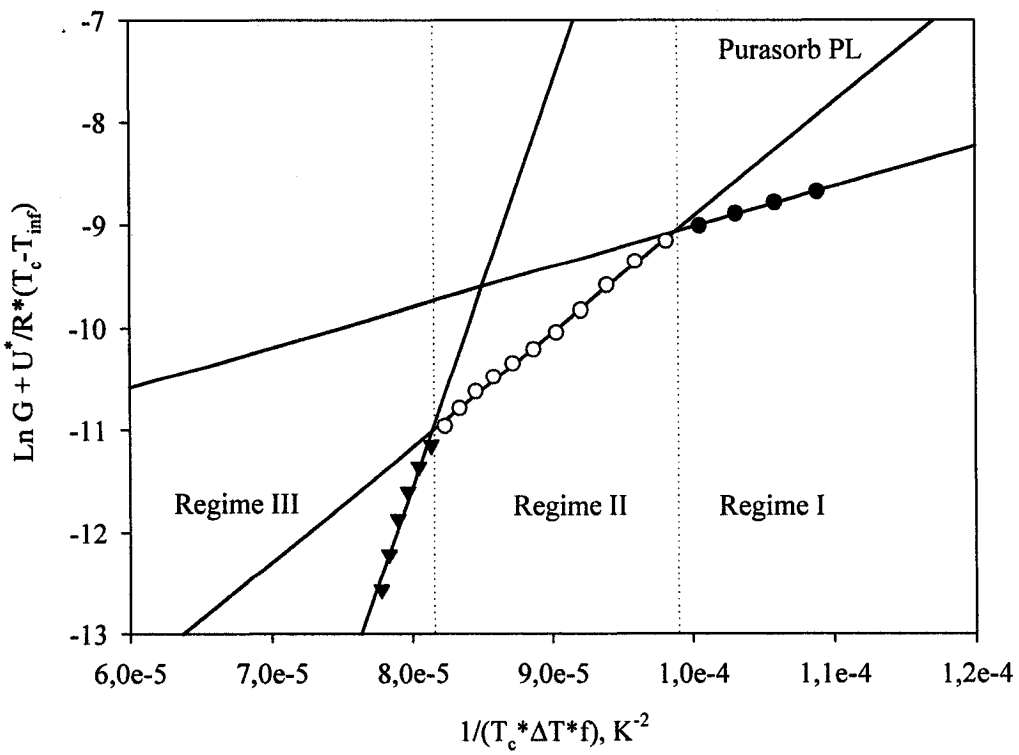


Fig. 4.28. Kinetic analysis of growth rate of Purasorb PL polylactide.

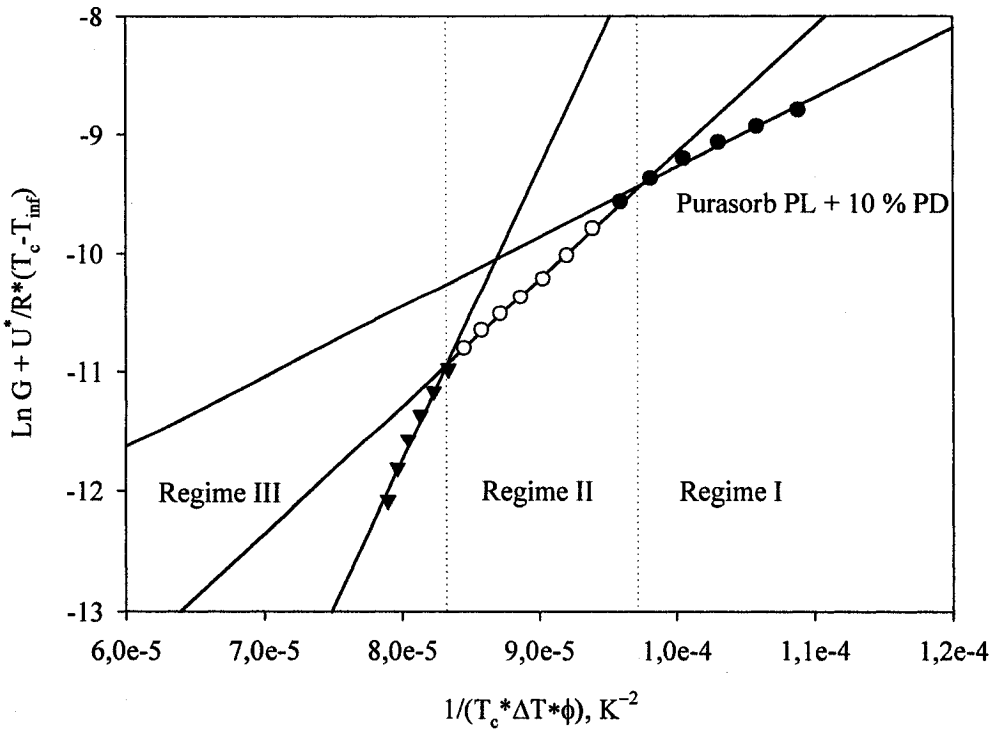


Fig. 4.29. Kinetic analysis of growth rate of Purasorb PL + 10 % Purasorb PD polylactides blends.

Table 4.7. Crystallization regimes and critical energy for the formation of the nuclei for Purasorb PL polylactide and its blends with Purasorb PD.

| | Regime I | | Regime II | | Regime III | |
|---|---|---|---|---|---|---|
| | Range , °C | $K_g$, $K^{-2}$ | Range , °C | $K_g$, $K^{-2}$ | Range , °C | $K_g$, $K^{-2}$ |
| Purasorb PL | < 109.4 | 39300 | 109.4 – 137.3 | 112400 | >137.3 | 393400 |
| Purasorb PL + 10 % PD | < 110.7 | 58900 | 110.7 – 132.7 | 106500 | >132.7 | 245900 |

As compared to L 9000, Purasorb PL has a wider Regime II, with a breadth of 22 – 28 °C and the transition temperature is significantly lower than expected. This gives an explanation to the fact that the maximum growth rate for the Purasorb PL is reached at lower temperatures than for the L 9000 polylactide. The $K_g$ values are two times lower for regimes II and about 4 times lower for regime III for the Purasorb PL as compared to the L 9000 polylactide. This unproportionally lower $K_g$ explains the unusually high growth rate at high temperatures for the Purasorb PL and its blend with Purasorb PD.

## 5. Conclusions

In this study, the crystallization behavior and morphology of solution cast polylactides containing different amounts of D-polylactide content were studied. The experiments showed that more than a month long drying under ambient conditions do not remove all residual solvent. It was found that even small amounts of the residual solvent significantly lower the glass transition temperature. For the detection of the isothermal glass transition temperature in films, a custom uniaxial stretching device was used. The obtained results were compared with the DSC analysis results and analysis of the kinetic behavior of the glass transition phenomena was made.

Many efforts were attempted to reveal the influence of the L-/D- polylactides stereocomplex on isothermal crystallization behavior of the polylactides using the Atomic Force Microscopy and DSC. It was found that while L 9000 polylactide and its blends with Purasorb PD polylactides show "bell" shaped spherulite growth rate temperature dependence which is typical for the majority of the polymers, Purasorb PL and its blends with Purasorb PD deviate from this pattern and show significantly higher spherulite growth rate in the high temperature region. This is caused by the nonproportional change of the nucleation activation energy Kg between regimes II and III. It was found from kinetic analysis that the Kg values for the Purasorb PL and its blends in regime III are more than 4 times less than for the L 9000 polylactide inducing easier crystallization in the region III.

Moreover, despite a higher molecular weight Purasorb PL demonstrates almost twice higher spherulite growth rate than L 9000 probably due to the absence of D-

polylactide units. This, in turn, leads to the significantly lower Kg values for the Purasorb PL and its blends with Purasorb PD as compared to those for L 9000 polylactide in regimes II and III and, respectively, to higher spherulite growth rates.

The addition of the D-polylactide to L-polylactide not only suppresses overall crystallization of the blend due to stereocomplexation but also shifts crystallization maximum to the lower temperature region. From the kinetic analysis it was found that it is caused by the lowering of the crystallization regime II transition temperature.

## 6. Contributions

The purpose of this work was to explore the possibility of studying the crystallization behavior and morphology of thin solution cast polylactide films using Atomic Force Microscopy. Since crystallization rate of the polylactide is very high custom superfast cyclic heating and cooling technique was developed to ensure isothermal annealing conditions. The validity of this technique was successfully verified.

The crystallization of wide range of L-/D-polylactide blends was studied and precise measurements of the spherulite growth rates were performed. The changes of crystalline morphology over crystallization temperature was observed and analyzed from the point of view of modern crystallization theory. A variety of different experimental techniques were also used for the polylactide blends characterization including DSC and FT-IR.

DSC analysis showed that L-/D-polylactide blends during casting form the triclinic stereocomplex with a high melting point which suppress cold crystallization of the polylactide blend. In this study, a custom technique for the measurement of isothermal glass transition temperature using elongational measurements was performed on miniature uniaxial stretching device. It was found that small amounts of the residual solvent can significantly decrease glass transition temperature of polylactide. It was also observed significantly higher nucleation of the solution cast polylactide as compared to bulk polymer and short term melting was used to eliminate excess nucleation.

Part of the research was dedicated to study of the influence D-polylactide on crystallization L-polylactide. It was experimentally proven that while blends of L 9000 polylactide with D-polylactide demonstrate typical "bell" shaped crystallization

dependence, blends of pure L-polylactide with the same D-polylactide have unusually high spherulite growth rate in regime III. For all blends addition of the D-polylactide significantly decreased spherulite growth rate. An extensive kinetic analysis was performed on experimental data, crystallization regimes region were determined and critical nuclei formation energies were determined for different blends.

## 7. Future work

One of the most promising directions of this research would be further investigation of influence of stereocomplex on crystallization behavior and morphology of polylactide. Despite the fact that stereocomplexation in polylactides is known for more than 20 years, there is very few information on stereocomplex crystallites especially on their formation and structure.

It also very interesting to continue investigation of atypical spherulite growth rate pattern of pure polylactide and its blends.

## Appendix I

### Sample alignment technique

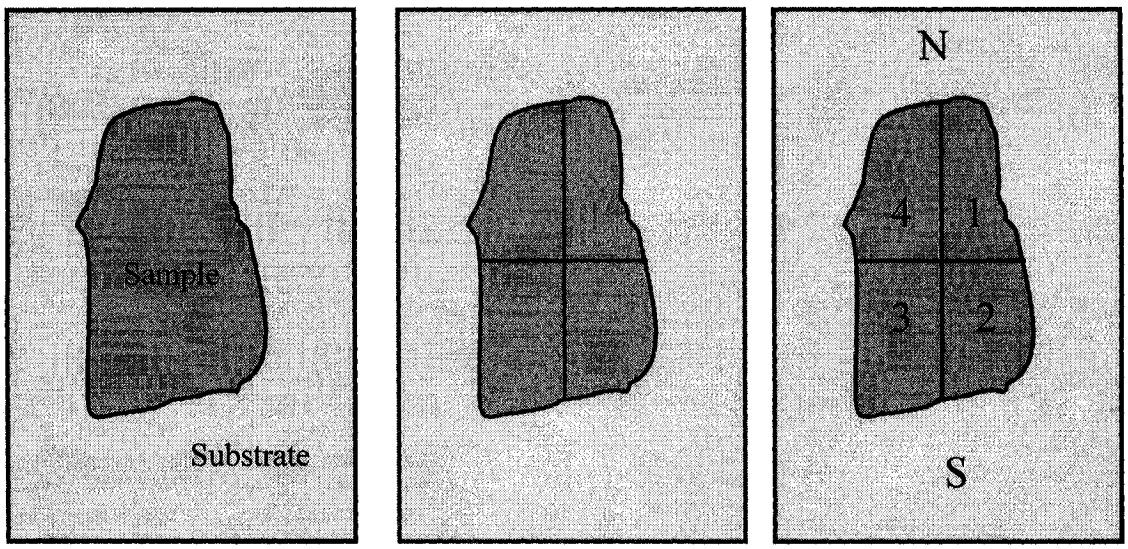


**Step 1.** Grooving **Step 2.** Marking

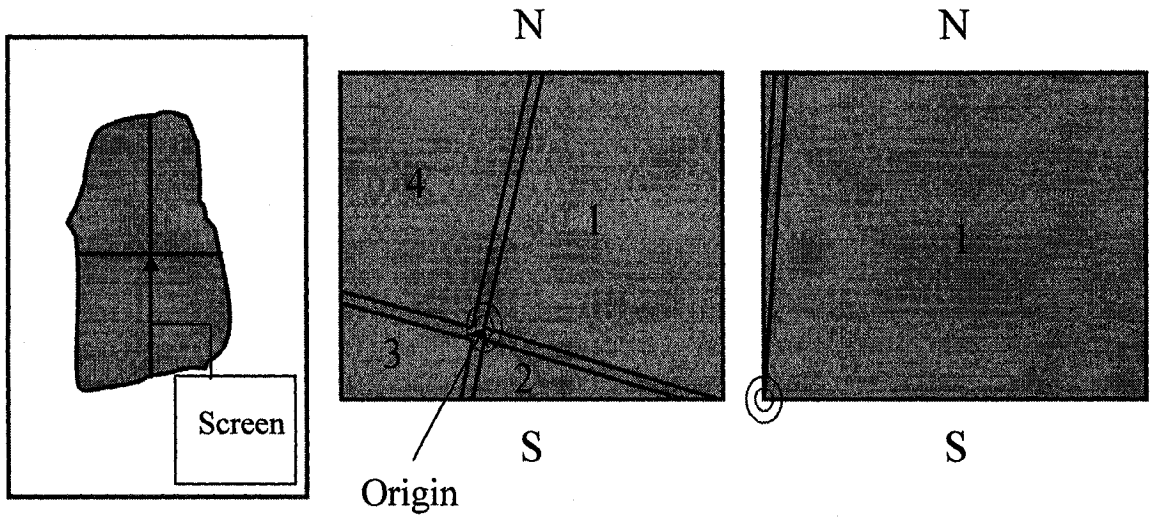


**Step 3.** The origin finding **Step 4.** Sector selection and sample alignment

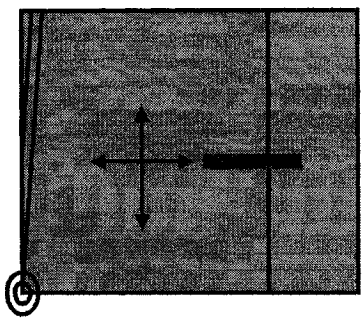

**Step 5.** Finding the research area

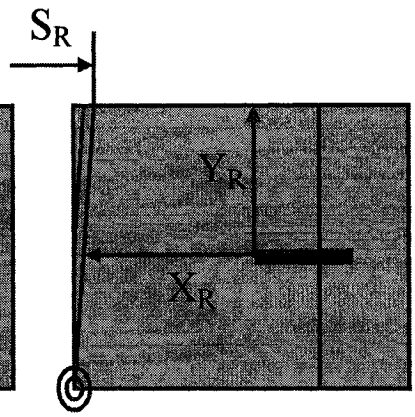


**Step 6.** Reference coordinates

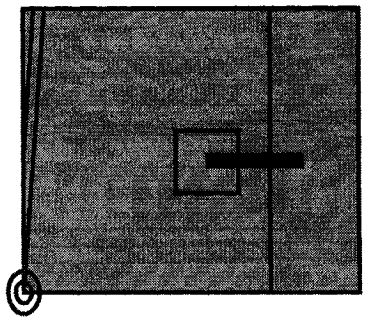

**Step 7.** Taking reference scan

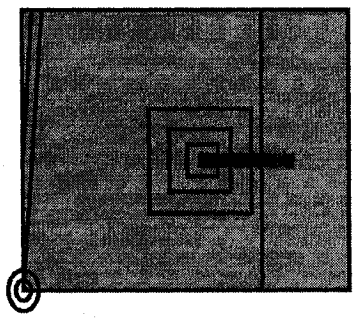

The usual research procedure

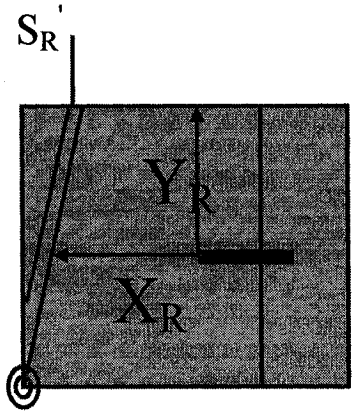


**Step 8.**
Repeat steps 3 - 6 and position cantilever using reference $X_R$ and $Y_R$
Enter scan angle correction:
$\theta = \arctan((S_R' - S_R)/195)$

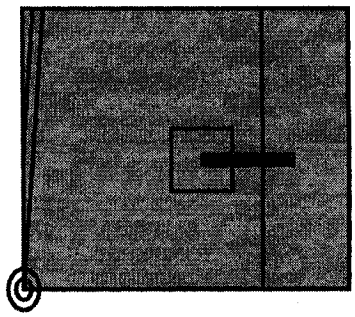

**Step 9.**
Taking of control scan

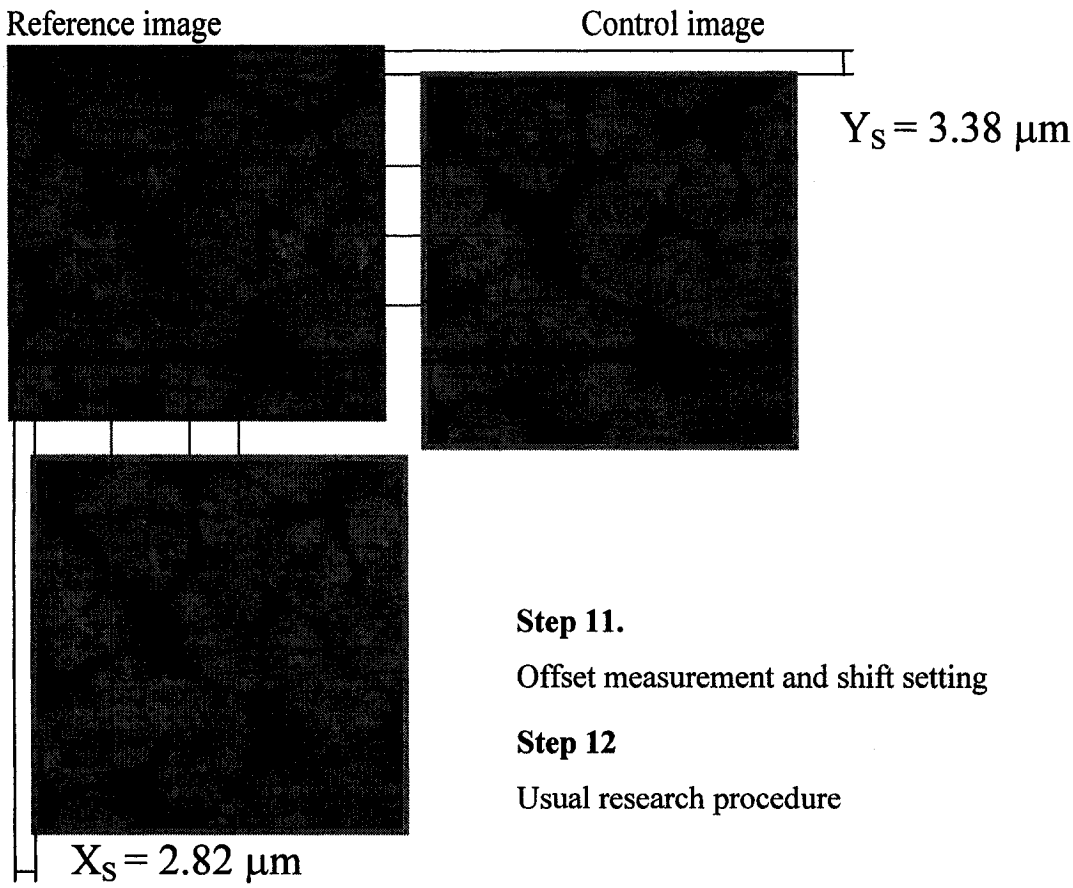


**Step 11.**

Offset measurement and shift setting

**Step 12**

Usual research procedure

## Appendix II

### Spherulite size measurement results

Table I. Spherulite size measurement results for L 9000 polylactide and its blends with Purasorb PD.

| Temperature, °C | L 9000 | | | L 9000 + 2 % Purasorb PD | | | L 9000 + 10 % Purasorb PD | | |
|---|---|---|---|---|---|---|---|---|---|
| | Time, min | Spherulite size, µm | Standard deviation, µm | Time, min | Spherulite size, µm | Standard deviation, µm | Time, min | Spherulite size, µm | Standard deviation, µm |
| 100 | 2 | 5,214 | 0,188 | 2 | 4,712 | 0,284 | 2 | 3,654 | 0,244 |
| | 4 | 10,215 | 0,256 | 4 | 9,325 | 0,336 | 4 | 7,228 | 0,321 |
| | 6 | 15,326 | 0,348 | | | | 6 | 11,015 | 0,269 |
| 110 | 2 | 7,353 | 0,250 | 4 | 12,452 | 0,329 | 2 | 5,012 | 0,258 |
| | 4 | 14,399 | 0,308 | 6 | 18,714 | 0,412 | 4 | 9,854 | 0,398 |
| | 6 | 21,074 | 0,335 | 8 | 25,114 | 0,548 | | | |
| 120 | 2 | 8,847 | 0,277 | 2 | 11,588 | 1,372 | 2 | 7,104 | 0,416 |
| | 4 | 17,643 | 0,625 | 4 | 21,289 | 1,641 | 4 | 13,899 | 0,543 |
| | 6 | 26,779 | 0,223 | 6 | 31,562 | 1,184 | 6 | 19,765 | 0,445 |
| | | | | 8 | 42,081 | 0,873 | | | |
| 130 | 2 | 9,402 | 0,593 | 2 | 8,633 | 0,930 | 2 | 5,933 | 0,274 |
| | 4 | 17,740 | 0,312 | 4 | 18,646 | 0,580 | 4 | 13,086 | 0,213 |
| | 6 | 25,917 | 0,418 | 8 | 38,823 | 0,721 | 8 | 18,504 | 0,143 |
| 140 | 2 | 5,933 | 0,370 | 2 | 5,664 | 0,497 | 2 | 3,898 | 0,109 |
| | 8 | 22,774 | 0,867 | 4 | 11,746 | 0,509 | 6 | 12,092 | 0,250 |
| | | | | 6 | 17,569 | 0,530 | | | |
| | | | | 10 | 27,929 | 0,676 | | | |
| | | | | 15 | 41,116 | 0,742 | | | |
| 150 | 10 | 10,170 | 0,744 | 8 | 8,633 | 0,930 | 20 | 12,181 | 0,339 |
| | 20 | 19,915 | 0,635 | 12 | 12,109 | 1,725 | 30 | 17,534 | 0,509 |
| | | | | 18 | 16,953 | 2,237 | 50 | 32,821 | 1,228 |
| | | | | 30 | 26,618 | 2,802 | | | |
| 160 | 30 | 4,612 | 0,185 | 20 | 4,464 | 0,352 | 36 | 2,221 | 0,325 |
| | 80 | 12,012 | 0,314 | 36 | 7,080 | 0,266 | 90 | 5,544 | 0,451 |
| | | | | 60 | 9,913 | 0,734 | 160 | 9,712 | 0,745 |
| | | | | 96 | 13,769 | 0,640 | | | |

Table II. Spherulite size measurement results for Purasorb PL polylactide and its blends with Purasorb PD.

| Temperature, °C | Purasorb PL | | | Purasorb PL + 10 % Purasorb PD | | |
|---|---|---|---|---|---|---|
| | Time, min | Spherulite size, μm | Standard deviation, μm | Time, min | Spherulite size, μm | Standard deviation, μm |
| 100 | 2 | 12,356 | 0,227 | 2 | 11,456 | 0,541 |
| | 3 | 18,451 | 0,598 | 4 | 23,124 | 0,789 |
| 110 | 3 | 28,046 | 0,465 | 2 | 14,447 | 0,360 |
| | 4 | 37,256 | 1,114 | 3 | 22,515 | 0,487 |
| 120 | 2 | 15,676 | 0,503 | 2 | 13,128 | 0,289 |
| | 3 | 23,398 | 0,444 | 3 | 20,014 | 0,895 |
| | 4 | 31,218 | 1,219 | | | |
| 130 | 1 | 7,604 | 0,260 | 2 | 12,449 | 0,367 |
| | 2 | 15,425 | 0,856 | 3 | 18,809 | 0,411 |
| 140 | 2 | 11,028 | 0,232 | 2 | 9,595 | 0,520 |
| | 3 | 16,744 | 0,317 | 3 | 14,313 | 0,509 |
| | 4 | 22,733 | 0,377 | | | |
| 150 | 3 | 8,372 | 0,429 | 2 | 4,115 | 0,421 |
| | 6 | 16,248 | 0,386 | 3 | 6,125 | 0,542 |
| | 10 | 26,311 | 0,537 | 10 | 20,025 | 0,658 |

## References


[1] R. A. Auras, B. Harte and S. Selke; Mechanical, Physical and Barrier Properties of Poly (lactic acid); Films.School of Packaging, MSU, East Lansing, MI, 48824-1223, USA.

[2] C. D. Masters, E. D. Attanasi, D. H. Root; World Petroleum Assessment and Analysis, U.S. Geological Survey National Center; Reston, VA; Oil and Gas Journal; October 13, 98-104,1998.

[3] E. T.H. Vink, K. R. Rabago, D. A. Glassner, P. R. Gruber; Applications of life cycle assessment to NatureWorks™ polylactide (PLA) production; Polymer Degradation and Stability, Vol. 80: 403–419, 2003.

[4] J. Lunt, A. L. Shafer; Polylactic Acid Polymers from Corn. Potential Applications in the Textiles Industry; Cargill Dow Polymers LLC, Minnetonka, MN 55345.

[5] G. Gallet; From fast to Slow degradation: different strategies to characterize polymer degradation by chromatographic techniques; Department of Polymer technology, Royal institute of technology, Stockholm, Sweden, 2001.

[6] Possible amendment of the structured nomenclature and the explanatory note to heading 39.07 regarding poly(lactic acid) (proposal by the US Administration); World Custom Organisation, Harmonized system review sub-committee, Brussels, 26 June 2003.

[7] L.H.Sperling ; Introduction to Polymer Science, D. Wiley and sons, New York, 1998.

[8] Witzke, D.R.; Introduction to Properties, Engineering, and Prospects of Polylactide Polymers, PhD Thesis, Department of Chemical Engineering, Michigan State University, East Lansing, Michigan, 32-72, 1997.

[9] R. A. Auras, B. Harte, S. Selke; Poly(Lactic Acid) Films as Food Packaging Materials ; School of Packaging, MSU, 2002.

[10] A. Toda, M. Okamura, M. Hikosaka, Y. Nakagawa; AFM observation of polyethylene single crystals: selective handedness of screw dislocations in a chair type ; Polymer, Vol. 44: 6135–6138, 2003.

[11] L. Lu, A. G. Mikos; Poly (lactic acid), Polymer data handbook, Oxford University Press, 627-633, 1999.

[12] H.K. Salzberg; Encyclopedia of Polymer Science and Technology, Vol. 11, Interscience, New York, 620-623, 1969.

[13] H. Yamane, K. Sasai; Effect of the addition of poly (D-lactic acid) on the thermal property of poly (L-lactic acid); Polymer, Vol.44; 2569-2575, 2003.

[14] H.Yamane, K. Sasai, M. Takano; Poly(D-lactic acid) as a rheological modifier of poly(L-lactic acid); Shear and biaxial extensional flow behavior ; Graduate School of Science and Technology, Kyoto Institute of Technology, Journal of Rheology, Vol. 48(3) : 599-609, 2004.

[15] H. Tsuji, Y. Tezuka et al.; Spherulite growth of l-lactide copolymers: Effect of tacticity and comonomers; Polymer, Vol. 46: 4917-4927, 2005.

[16] P.C. Painter, M.M. Coleman ; Static and Dynamic properties of the Polymeric Solid State ; D. Reidel, Boston, Chaps. 6-8, 1982.

[17] T. Okihara, M. Tsuji, A. Kawaguchi, K. Katayama, H. Tsuji, S.-H. Hyon, Y. Ikada; The frustrated structure of poly (L-lactide); Journal of Macromolecular Science Physics; B30 (1 and 2):119, 1991.

[18] T. Okihara, K. Kawaguchi, H. Tsuji, S.-H. Hyon, Y. Ikada, K. Katayama, Epitaxial crystallization and crystalline polymorphism of polylactides; K. Bull. Inst. Chem. Res., Kyoto University, 66:271, 1988.

[19] H. Tadokoro, Structure of Crystalline polymers, Wiley-Interscience, New York, 1979, Ch.5.

[20] M. Trznadel, M. Krysewski; Optical studies of regioregular poly (3-octylthiophene) s under pressure; Macromolecular. Chemical Physics, Vol. 32: 259, 1992.

[21] K. E. Hardenstine, C. J. Murphy, R. B. Jones, L. H. Sperling and G.E. Manser; Polymer applications of reneuable-resource materials ; Journal of the Applied Polymer Science, Vol. 30: 2051, 1985.

[22] E. Martuscelli; Influence of composition and molecular mass on the morphology, crystallization and melting behaviour of poly(ethylene oxide)/poly(methyl methacrylate) blends ; Polymer Engineering Science, Vol. 24: 563, 1984.

[23] Yu Long, R. Shanks, Z. Stachurski ; Kinetics of polymer crystallization, Prog. Polymer Science, Vol.20: 651-701, 1995.

[24] D. Turnbull, J. C. Fisher; Thermodynamics and crystallization in polymers; Journal of Chemical Physics, Vol. 17: 71, 1949.

[25] W. Kurz, D. Fisher ; Fundamentals of solidification, Trans Tech publications, 1984.

[26] B. Wunderlich; Trends in thermal analysis; Macromolecular Physics I, Academic press, New York, 1973.

[27] Andy Round; Introduction to Atomic Force Microscopy; H.H. Wills Physics Laboratory, University of Bristol, Bristol.

[28] J.Lauritzen, J. Hoffman; Thermodynamic analysis in polymeric systems; Journal of applied Physics, Vol. 44: 4340, 1973.

[29] J.-R. Sarasua, R. E. Prud'homme, M. Wisnewski, A. Le Borgne, N. Spassky; Crystallization and melting behavior of polylactides; Macromolecules, Vol. 31: 3895-3905, 1998.

[30] V. Ferrero, G. Coulon; Shear Banding in strained semicrystalline Polyamide 6 films as revealed by atomic force microscopy: role of the amorphous phase ; Journal of Polymer Science: Part B: Polymer Physics, Vol. 42: 687-701, 2004.

[31] G.Natta, P.Corradini, The crystal structure of 1, 2 isotactic poly-4-methyl-pentadiene-1, 3 ; European Polymer Journal, Volume 4, Issue 2, 297-298, April 1968.

[32] P. Ehrenfest; Glass-transition temperatures of compatible polymer mixtures ; Leiden Comm. Suppl. 756, 1963.

[33] Polymer processing and properties : Proceedings of the First European Meeting on Polymer Processing and Properties, Capri, June 13–16, 1983; edited by G. Astarita and L. Nicholais; published by Plenum, New York, 1984.

[34] G.W. Sherer; Relaxation in Glass and Composites, Vol. 9, JohnWiley, New York, 1986.

[35] M. Giordano, M. Russo, P. Capoluongo, A. Cusano, L. Nicolais; The effect of cooling rate on the glass transition of an amorphous polymer, Journal of Non-Crystalline Solids, Vol. 351: 515–522, 2005.

[36] H.N. Ritland; A fictitious equilibrium in polymeric systems; Journal of American Ceramic Society; Vol. 37 (8): 370, 1954.

[37] C.T. Moyniahan, A.J. Easteal, M.A. de Bolt, J. Tucker; Some aspects of equilibrium state analysis; Journal of American Ceramic Society, Vol. 59 (1–2): 12, 1976.

[38] V. Halpern, J. Bisquert; Activation energy in relaxation spectrum; Journal of Chemical Physics, Vol. 114 (21): 9512, 2001.

[39] J.H.Gibbs, E.A. Die Marcio; Equilibrium of polymeric systems; Journal of Chemical Physics, Vol.28: 373, 1958.

[40] W.A. Johnson, R.F. Mehl; Reaction kinetics in process of nucleation and growth, Trans. AIME 135, 416-458, 1939.

[41] M. Avrami; Kinetics of the multiphase polymeric systems; Journal of Chemical Physics, Vol. 7: 1103, 1939.

[42] A. Ziabicki; The mechanisms of 'neck-like' deformation in high-speed melt spinning. 2. Effects of polymer crystallization ; Applied Polymer Symposia, 6, 1, 1967.

[43] A.Y.Malkin, V.P.Beghishev and I.A.Keapin; Nucleation in heterogeneous systems; Polymer, Vol. 24: 81, 1983.

[44] L.Mandelkern; Crystallization of Polymers, McGraw-Hill, New York, 1964.

[45] E.Ergoz, J.G.Fatou and L.Mandelkern; Molecular weight effects on crystallization in binary polymer systems; Macromolecules, Vol.5:147, 1972.

[46] A. Booth and J.N. Hay; Secondary crystallization phenomena; Polymer, Vol. 12: 365, 1971.

[47] S. Chew, J.R.Griffiths and Z.H. Stachurski; Temperature effects on crystallization of immisible polymer blends; Polymer, Vol. 30: 874, 1989.

[48] S. Hoshino, E. Meinecke, J.Powers, R.S. Stain and S. Newman; Crystallization behavior of isotactic polyethylene; Journal of Polymer Science, A-3: 3041, 1965.

[49] F.C. Perez-Cardenas et al; Thermodynamics of polymer crystallization; Journal of Applied Polymer Science, Vol.43: 779, 1991.

[50] J. D. Hoffman, G. T. Davis and J. I. Lauritzen; Treatise of Solid State Chemistry, Vol.3, 1976.

[51] T. Miyata and T. Masuko; Crystallization behavior of poly (L-lactide); Polymer, Vol. 39, No 22: 5515-5521, 1998.

[52] Jitendra K. Pandey, K. Raghunatha Reddy, A. Pratheep Kumar and R.P. Singh ; An overview on the degradability of polymer nanocomposites ; Polymer Degradation and Stability, Volume 88, Issue 2, 234-250, May 2005.

[53] R. Vasanthakumari and A. Pennings; Crystallization kinetics of poly (L-lactic acid); Polymer, Vol. 24: 175, 1983.

[54] S. L. Aggarwal, L. Marker, W. L. Kollar and R. Geroch; Block polymers; Journal of Polymer Science, Vol. 4: 715, 1966.

[55] J. D. Verhoeven; Fundamentals of Physical Metallurgy, 340, Wiley, Chichester, 1975.

[56] D.C. Bassett; Principle of Polymer Morphology, Cambridge University Press, Cambridge, 1981.

[57] M. L. Di Lorenzo; Determination of spherulite growth rates of poly (L-lactic acid) using combined isothermal and non-isothermal procedures; Polymer, Vol. 42: 9441-9446, 2001.

[58] M. L. Di Lorenzo, C. Silvestre; Measurement of spherulite growth rates using tailored temperature programs, Thermochimica Acta, Vol. 396: 67-73, 2003.

[59] T.Ozawa; Kinetics of non-isothermal crystallization; Polymer, Vol.12: 150, 1971.

[60] K. Nakamura, T. Watanabe, K. Katayama, T. Amano; Non-isothermal crystallization; Journal of Applied Polymer Science, Vol. 16: 497, 1972.

[61] P. Sajkiewicz, L. Carpaneto, A. Wasiak; Application of the Ozawa model to non-isothermal crystallization of poly(ethylene terephthalate); Polymer, Vol. 42: 5365-5370, 2001.

[62] J. D. Hoffman; Crystallization kinetics in polymers; Polymer, Vol. 24: 656, 1982.

[63] W. Hoogsteen, G. ten Brinke and A. J. Pennings ; The influence of the extraction process and spinning conditions on morphology and ultimate properties of gel-spun polyethylene fibres ; Polymer, Volume 28, Issue 6, 923-928, May 1987.

[64] J. C. Mitchell; Mechanical history effects in the crystallization of cis-1,4-polybutadiene; Polymer, Volume 8, 369-379, 1967.

[65] B. Eling, S. Gogolewski, A. J. Pennings; Crystalline modifications of the polylactide; Polymer, Vol. 23:1587, 1982.

[66] J. Puiggali, Y. Ikada, H. Tsuji, L. Cartier, T. Okihara, B. Lotz; Epitaxial crystallization and crystalline polymorphism of polylactides ; Polymer, Vol. 41:8921, 2000.

[67] D. Brizzolara, H. J. Cantow, K. Diedrichs, E. Keller, A. J. Domb; Crystallization in polylactide; Macromolecules, Vol. 29:191, 1996.

[68] L. Cartier, T. Okihara, Y. Ikada, H. Tsuji, J. Puiggali, B. Lotz; Cell properties of polylactide crystalls ; Polymer, Vol. 41:8909, 2000.

[69] C. Marega, A. Marigo, V. Di Noto, R. Zannetti; Crystallization of polymers of lactic acid; Macromolecular Chemistry, Vol. 193:1599, 1992.

[70] H. Abe, Y. Kikkawa, Y. Inoue, Y. Doi; Crystallinity of polylactide blends ; Biomacromolecules, Vol. 2:1007, 2001.

[71] M. L. Di Lorenzo; Crystallization behavior of poly (L-lactic acid); European Polymer Journal, Vol. 41: 569–575, 2005.

[72] S. Iannace, L. Nicolais; Influence of crystal and amorphous phase morphology on hydrolytic degradation of PLLA subjected to different processing conditions; Journal of Applied Polymer Science, Vol. 64:911, 1997.

[73] Y. Ikada, K. Jamshidi, H. Tsuji, S.-H. Hyon; Thermal characterization of polylactides ; Macromolecules, Vol.20, 904, 1987.

[74] H. Yamane, K. Sasai; Effect of the addition of poly (D-lactic acid) on the thermal property of poly (L-lactic acid), Polymer, Vol. 44: 2569-2575, 2003.

[75] H. Tsuji, Y. Ikada; Stereocomplex formation between enantiomeric poly (lactic acid) s. XI. Mechanical properties and morphology of solution-cast films; Polymer, Vol. 40: 6699-67-08, 1999.

[76] H. Tsuji, S.-H. Hyon, Y. Ikada; Stereocomplex formation between enantiomeric Poly (lactic acid) s.3. Calorimetric studies on blend films cast from dilute solutions; Macromolecules, Vol. 24: 5651-5656, 1991.

[77] H. Urayama, T. Kanamori, K. Fukushima, Y. Kimura; Controlled crystal nucleation in the melt crystallization of poly(L-lactide) and poly(L-lactide)/poly(D-lactide) stereocomplex; Polymer, Vol. 44: 5635-5641, 2003.

[78] H. Tsuji, Y. Ikada; Stereocomplex formation between enantiomeric poly(lactic acid)s. XI. Mechanical properties and morphology of solution-cast films ; Polymer, Volume 40, Issue 24, 6699-6708, November 1999.

[79] W. Banks, M. Gordon, R. J. Roe and A. Sharples; Polymer, The crystallization of polyethylene I ; Vol. 4: 61, 1963.

[80] J. N. Hay, P. A. Fitzgerald and M. Wiles; Use of differential scanning calorimetry to study polymer crystallization kinetics; Polymer, Vol.17: 1015, 1976.

[81] K. Harnish, H. Muschik; Non-isothermal approach in DSC studies; Colloid Polymer Science, Vol. 261: 908, 1983.

[82] M. Iriarte, J. I. Iribarren, A. Etxeberria and J. J. Iruin; Crystallization and melting behaviour of poly(bisphenol A hydroxy ether)/poly(ethylene oxide) blends ; Polymer, Vol. 30: 1160, 1989.

[83] G. Binnig; Force microscopy; 4244. 7: Proc. VI Int. Conf., 1992.

[84] D. Sarid; Scanning Force Microscopy, Oxford University Press, New York, 1991.

[85] S.H.Magonov, H.-J.Cantow; Optimization of experiment in scanning force microscopy of polymers; Journal of Applied Polymer Science, Vol. 51:4, 1992.

[86] G. J. Legett, M. C. Davies, D. E. Jackson, C. J. Roberts, S. J. B. Tendler; Trends in Polymer Science, Vol. 1:115, 1993.

[87] K. L. Anderson and G. Goldbeck-Wood; Simulation of thickening growth in polymer crystallisation ; Polymer, Volume 41, Issue 25, 8849-8855, 1 December 2000.

[88] S. Schneider, X. Drujon, J. C. Wittmann and B. Lotz; Impact of nucleating agents of PVDF on the crystallization of PVDF/PMMA blends ; Polymer, Volume 42, Issue 21, 8799-8806, October 2001.

[89]D. A. Ivanov, R. Legras and A. M. Jonas; The crystallization of poly(aryl-ether-ether-ketone) (PEEK): reorganization processes during gradual reheating of cold-crystallized samples ; Polymer, Volume 41, Issue 10, 3719-3727, May 2000.

[90] V. V. Tsukruk, D. H. Reneker; Scanning probe microscopy of organic and polymeric films: from self –assembled monolayers to composite multilayers; Poymer, Vol. 36 No. 9:1791-1808, 1995

[91] W. Stocker, B. Bickmann, S. N. Magonov and H. -J. Cantow, B. Lotz and J. -C. Wittmann, M. Möller; Surface structure of polymers and their model compounds observed by atomic force microscopy ; Ultramicroscopy, Volumes 42-44, Part 2, 1141-1147, July 1992.

[92]G. Bar, S. N. Magonov and H. -J. Cantow, J. Gmeiner and M. Schwoerer; Atomic-scale imaging of anisotropic organic conductors by scanning probe techniques (STM/AFM); Ultramicroscopy, Volumes 42-44, Part 1, 644-652, July 1992.

[93] M. Matsumoto, H. Tachibana and R. Azumi ;Control of the structures and functions of Langmuir-Blodgett films using supramolecular architecture ;Materials Science and Engineering: C, Volume 4, Issue 4, , 255-261, April 1997.

[94] R. Nigmatullin, R. Lovitt, C. Wright, M. Linder, T. Nakari-Setälä and M. Gama ; Atomic force microscopy study of cellulose surface interaction controlled by cellulose binding domains ; Colloids and Surfaces B: Biointerfaces, Volume 35, Issue 2, 125-135, 15 May 2004.

[95] Hennady Shulha, Alexander Kovalev, Nikolai Myshkin and Vladimir V. Tsukruk; Some aspects of AFM nanomechanical probing of surface polymer films; European Polymer Journal, Volume 40, Issue 5, 949-956, May 2004.

[96] F. Saurenbach, D. Wollmann, B. D. Terris and A. Diaz; Bridge configuration of piezoresistive devices for scanning force microscopes; Langmuir, Vol. 8: 1199, 1992.

[97] M. G. Goh, D. Juhue, O. M. Leung, M., Y. Wang and M. A. Winnik; Light scattering and microcalorimetry studies on aqueous solutions of thermo-responsive PVCL-g-PEO copolymers; Langmuir, Vol. 9: 1319, 1993.

[98] D. Martin, J. Ojeda, J. P. Anderson and G. Pingali; AFM Conference, Natick, 1993.

[99] W. Zhao, M. H. Rafailovich, J. Sokolov, L. J. Fetters, R. Plano, M.K. Sanyal and S. K. Sinha; Neutron and X-ray reflectivity measurements of polystyrene/polybromostyrene (PS/PBrS) interfaces ; Physica B: Condensed Matter, Volume 173, Issues 1-2, 43-46, August 1991.

[100] H. G. Dikland, S. S. Sheiko, L. van der Does, M. Moller and A. Bantjes; A scanning force microscopy study on the morphology of elastomer-coagent blends ; Polymer; Vol. 34: 1400, 1993.

[101] B. K. Annis, J. Strizak, G. D. Wignall, R. G. Alamo and L. Mandelkern ; A small-angle neutron scattering study of the plastic deformation of linear polyethylene ; Polymer, Volume 37, Issue 1, 137-140, 1996.

[102] C. Mathieu, W. Stocker, A. Thierry, J. C. Wittmann and B. Lotz ; Epitaxy of isotactic poly(1-butene): new substrates, impact and attempt at recognition of helix orientation in form I′ by AFM ; Polymer, Volume 42, Issue 16, 7033-7047, July 2000 .

[103] S. N. Magonov, S. Kempf, J. Schuchhardt, G. Bar, W. Gronski and H. -J. Cantow ; Applications of scanning tunneling microscopy to organic charge transfer systems ; Synthetic Metals, Volume 42, Issues 1-2, 1815-1818, May 1991.

[104] R. M. Overney, R. Lüthi, H. Haefke, J. Frommer, E. Meyer and H. -J. GüntherodtS. Hild and J. Fuhrmann ; An atomic force microscopy study of corona-treated

polypropylene films ; Applied Surface Science, Volume 64, Issue 3, 1,197-203, March 1993.

[105] Huettenberger A.; Biomer L9000 data sheet, Biomer GmbH, Germany.

[106] C. Witschi, E. Doelker, Residual solvents in pharmaceutical products: acceptable limits, influences on physicochemical properties, analytical methods and documented values; Eur. J. Pharm. Biopharm, Vol. 43, 215-242, 1997.

[107] J. Newman, C. J. Nunn. Solvent retention in organic coatings. Prog. Org. Coatings; Vol. 3, 221-243, 1975.

[108] L. H. Sperling, Polymer physics, Whiley and Son, 1992.

[109] S. Hocquet, M. Dosière, M. H. J. Koch; Equilibrium Melting Temperature of Poly(trimethylene terephthalate); Laboratoire de Physicochimie des Polymères, Université de Mons-Hainaut, Mons (Belgique).

[110] C. Silvestre, M.L. Di Lorenzo, E. Di Pace; Crystallization of the polyolefins, NY, Marcel Dekker, 2000.